MESOZOIC TECTONIC INVERSION IN THE NEUQUÉN BASIN

OF WEST-CENTRAL ARGENTINA

A Dissertation

by

GABRIEL ORLANDO GRIMALDI CASTRO

Submitted to the Office of Graduate Studies of
Texas A&M University
in partial fulfillment of the requirements for the degree of

DOCTOR OF PHILOSOPHY

December 2005

Major Subject: Geology

MESOZOIC TECTONIC INVERSION IN THE NEUQUÉN BASIN

OF WEST-CENTRAL ARGENTINA

A Dissertation

by

GABRIEL ORLANDO GRIMALDI CASTRO

Submitted to the Office of Graduate Studies of
Texas A&M University
in partial fulfillment of the requirements for the degree of

DOCTOR OF PHILOSOPHY

Approved by:

Chair of Committee,	Steven L. Dorobek
Committee Members,	Philip D. Rabinowitz
	Niall C. Slowey
	Brian J. Willis
	David V. Wiltschko
Head of Department,	Richard L. Carlson

December 2005

Major Subject: Geology

ABSTRACT

Mesozoic Tectonic Inversion in the Neuquén Basin

of West-Central Argentina. (December 2005)

Gabriel Orlando Grimaldi Castro, B.S., Universidad Nacional de Córdoba, Argentina;

M.S., Texas A&M University

Chair of Advisory Committee: Dr. Steven L. Dorobek

Mesozoic tectonic inversion in the Neuquén Basin of west-central Argentina produced two main fault systems: (1) deep faults that affected basement and syn-rift strata where preexisting faults were selectively reactivated during inversion based on their length and (2) shallow faults that affected post-rift and syn-inversion strata. Normal faults formed at high angle to the reactivated half-graben bounding fault as a result of hangingwall expansion and internal deformation as it accommodated to the shape of the curved footwall during oblique inversion. Contraction during inversion was initially accommodated by folding and internal deformation of syn-rift sedimentary wedges, followed by displacement along half-graben bounding faults. We suspect that late during inversion the weight of the overburden inhibited additional fault displacement and folding became the shortening-accommodating mechanism.

A Middle Jurassic inversion event produced synchronous uplift of inversion structures across the central Neuquén Basin. Later inversion events (during Late Jurassic, Early Cretaceous, and Late Cretaceous time) produced an "inversion front" that

advanced north of the Huincul Arch. Synchroneity of fault reactivation during the Callovian inversion event may be related to efficient stress transmission north of the Huincul Arch, probably due to easy reactivation of low-dip listric fault segments. This required little strain accumulation along "proximal" inversion structures before shortening was transferred to more distal structures. Later inversion events found harder-to-reactivate fault segments, resulting in proximal structures undergoing significant inversion before transferring shortening.

The time between the end of rifting and the different inversion events may have affected inversion. Lithosphere was probably thermally weakened at the onset of the initial Callovian inversion phase, allowing stress transmission over a large distance from the Huincul Arch and causing synchronous inversion across the basin. Later inversion affected a colder and more viscous lithosphere. Significant strain needed to accumulate along proximal inversion structures before shortening was transferred to more distal parts of the basin.

Timing of inversion events along the central Neuquén Basin suggest a mega-regional control by right-lateral displacement motion along the Gastre Fault Zone, an intracontinental megashear zone thought to have been active prior to and during the opening of the South Atlantic Ocean.

DEDICATION

To Silvia, Micaela, and Camila, for their endless love and support

ACKNOWLEDGEMENTS

I thank Dr. Wayne Ahr for his encouragement, for delicious conversations, and for generously taking the time and effort to lead two great and extremely enriching field trips.

I want to thank my fellow students at the Department of Geology and Geophysics, most especially, Pablo Cervantes, for his warm friendship and encouragement during times of slight disorientation. Thanks also to Pablo Buenafama, Mitchell Graff, Takamasa Kanaya, Hesham El-Sobky, Matt Fey, Martin Finn, Aaron Adams, Katie Poole, Isaac Perez, Rafael Almeida, Khryste Wright, María Corazón Santa Ana, Fernando Rodríguez, and Sergio Olave for the constructive discussions and for making my stay at Texas A&M a very pleasant time.

Orlando and Malena, my parents, had a lot to do with me and my family making the decision "not to give up my dream". I will always appreciate their encouragement and unconditional support.

Finally, I thank my wife, Silvia, and my two lovely daughters, Micaela and Camila, for their enormous patience, constant encouragement, and for putting a smile on my face every time I think of them.

TABLE OF CONTENTS

LIST OF FIGURES

CHAPTER I

INTRODUCTION

Basin inversion is defined as the compressional or transpressional deformation of a former extensional basin (Williams et al., 1989). This style of intracontinental deformation has been recognized on every continent that has been explored for hydrocarbons (Harding, 1985; Dellapé and Hegedus, 1995; Homovc et al., 1995; Lowell, 1995; Manceda and Figueroa, 1995; Morley, 1995; Peroni et al., 1995; Thomas and Coward, 1995; Uliana et al., 1995; Welsink et al., 1995; Beauchamp et al., 1996).

The geometry of inversion structures may make them suitable as structural traps for petroleum accumulations. In addition, inversion tectonics can have important effects on other aspects of petroleum systems. For example, inversion causes uplift of a basin, with consequent effects on burial history and oil generation and maturation, porosity evolution, fracture development, migration pathways, and alteration of fault sealing properties (Coward, 1994). Inversion tectonics can also have significant effects on the structural and stratigraphic evolution of an area, and must be carefully considered during regional restoration of structural cross sections, shortening estimations, assumptions about the nature of structures at depth, subsidence patterns, and analysis of syn-inversion sedimentation (Coward, 1994; McClay, 1995).

The following chapters comprise an integrated study of inversion tectonics that developed in a foreland setting. Different scales of observation, ranging from the study

---

This dissertation follows the style and format of the American Association of Petroleum Geologists Bulletin.

of syn-inversion hangingwall internal deformation to plate-scale implications, are combined to present a comprehensive analysis inversion tectonics.

Chapter II contains a three-dimensional seismic characterization of Mesozoic inversion structures in the Central Neuquén Basin. The main topics of this chapter are the documentation of the complex fault framework that characterizes inversion structures and the analysis of its kinematic implications. Emphasis is given to lateral along-strike relationships, which are generally overlooked in 2D seismic-based studies. The study shows that two main fault systems developed during inversion. A deep fault system affecting basement and syn-rift strata underwent selective reactivation during inversion based mainly on differences in horizontal fault length. A shallow syn-inversion fault system developed in association with internal hangingwall deformation during oblique inversion. Structural restorations of different stratigraphic levels show a multi-stage inversion process that alternatively involves reactivation of the main half-graben bounding fault and internal faulting and folding of syn-rift sedimentary wedges.

In Chapter III we examine spatial and temporal patterns of Mesozoic inversion occurrence and propagation across the central Neuquén Basin. Five main inversion structures were identified and their timing of deformation established using stratigraphic indicators. Results show two main stages of inversion propagation north of the Huincul Arch. A Middle Jurassic event resulted in synchronous uplift of inversion structures across the basin. Later inversion events from Late Jurassic to Late Cretaceous time are characterized by northward propagation of an inversion front that produces diachronous uplift of inversion anticlines. Different inversion propagation patterns between Callovian

and later inversion events may be related with the mechanical behavior of different segments of reverse-reactivated faults and with temporal variations in the rheology of the lithosphere. These variations may have affected the efficiency with which stress was transmitted north of the Huincul Arch and therefore controlled the timing of uplift of inversion structures across the Northern Sub-basin.

In Chapter IV we present an analysis of plate-scale implications of Huincul Arch-related deformation and associated tectonic inversion in the central Neuquén Basin. An integration of published literature with observations from this study suggests that the evolution of the Huincul Arch is tied to widespread continental extension that preceded the opening of the South Atlantic Ocean.

This study adds important insights into the complex nature of inversion tectonics and foreland deformation in southern South America. Results from this study have implications for the tectono-stratigraphic evolution of other segments of the southern Andean foreland or in other retroarc foreland settings.

The detailed geometric and kinematic characterization of inversion structures in the Northern Sub-basin expands our knowledge about factors influencing timing and styles of tectonic inversion in a non-collisional retro-arc foreland setting. It also provides a framework for the prediction of fractured zones by defining areas subjected to maximum strain.

Assessment of tectonic controls on sedimentation in the Northern Sub-basin during Mesozoic time contributes to the development of predictive models for sedimentary facies distribution and petroleum systems configuration. Integration of

basin-scale structural and stratigraphic analysis with mega-regional published

interpretations contributes to our understanding of the Mesozoic tectono-stratigraphic

evolution of southern South America.

CHAPTER II

THREE-DIMENSIONAL SEISMIC CHARACTERIZATION OF MESOZOIC INVERSION STRUCTURES IN THE CENTRAL NEUQUÉN BASIN, ARGENTINA

INTRODUCTION

Inversion structures form when normal faults formed during an earlier stage of crustal extension undergo reverse displacement during later compressional deformation (Hayward and Graham, 1989; Coward, 1994; Sibson, 1995). Basin inversion is often recognized where dip-slip reversal of half-graben bounding faults produces uplift of syn- and post-rift sequences (Brun and Nalpas, 1996; Buiter and Pfiffner, 2003). Inverted parts of basins are turned inside out to become positive features (Hayward and Graham, 1989; Buchanan and McClay, 1991).

Several factors affect the occurrence and style of inversion structures: (1) capability of fault reactivation (Sibson, 1985; Etheridge, 1986; Sibson, 1995); (2) fault geometry (Buchanan and McClay, 1991, 1992), pre-inversion geometry of the basin (Butler, 1989), (3) thermal state of the lithosphere at the time of inversion (Sandiford, 1999; Nielsen and Hansen, 2000; Sandiford et al., 2003), and (4) plate-tectonic setting (Kluth and Coney, 1981; Ziegler et al., 1998; Marshak et al., 2000). The interplay of these factors produces complex structural styles, areal distribution, and timing of inversion structures, as recognized in natural examples (Kluth and Coney, 1981; McClay, 1989; Ziegler, 1989; Homovc et al., 1995; Manceda and Figueroa, 1995; Uliana et al., 1995; Marshak et al., 2000; Beauchamp, 2004; Chambers et al., 2004).

An inverted half-graben is the simplest inversion structure (Figure 2.1). This requires two discrete deformational episodes: an extensional phase followed by a contractional phase (Williams et al., 1989; Mitra, 1993). Geometries of resulting structures and stratigraphic relationships can be used to analyze the kinematics and timing of inversion. Most previous studies of basin inversion have used 2D seismic sections or laterally-continuous outcrops to characterize inversion styles and to estimate rates and amount of inversion (Hayward and Graham, 1989; Williams et al., 1989; Mitra, 1993). Pre-, syn-, and post-rift strata can acquire diagnostic geometries during inversion that allow the definition of a "null point" (or "null line" in three dimensions; Turner and Williams, 2004), which separates fault segments showing opposite displacement. These segments can be used to calculate an inversion ratio (Figure 2.1; Williams, 1989).

The development of an inverted half-graben typically involves the reactivation and potential propagation of pre-existing extensional faults into post-rift strata. Contraction is accommodated by reverse displacement along these faults, the development of new faults, and folding of pre- and syn-inversion strata (cf. Koopman et al., 1987).

Despite the importance of inversion-related deformation relative to the development of petroleum system, the nature of three-dimensional inversion structures is poorly documented and understood. The aim of this study was to characterize, in full 3D, structural and stratigraphic relationships associated with tectonic inversion structures that formed in a retroarc foreland setting. A 3D seismic and borehole dataset over a series of Mesozoic inversion structures in the Neuquén Basin of west-central Argentina
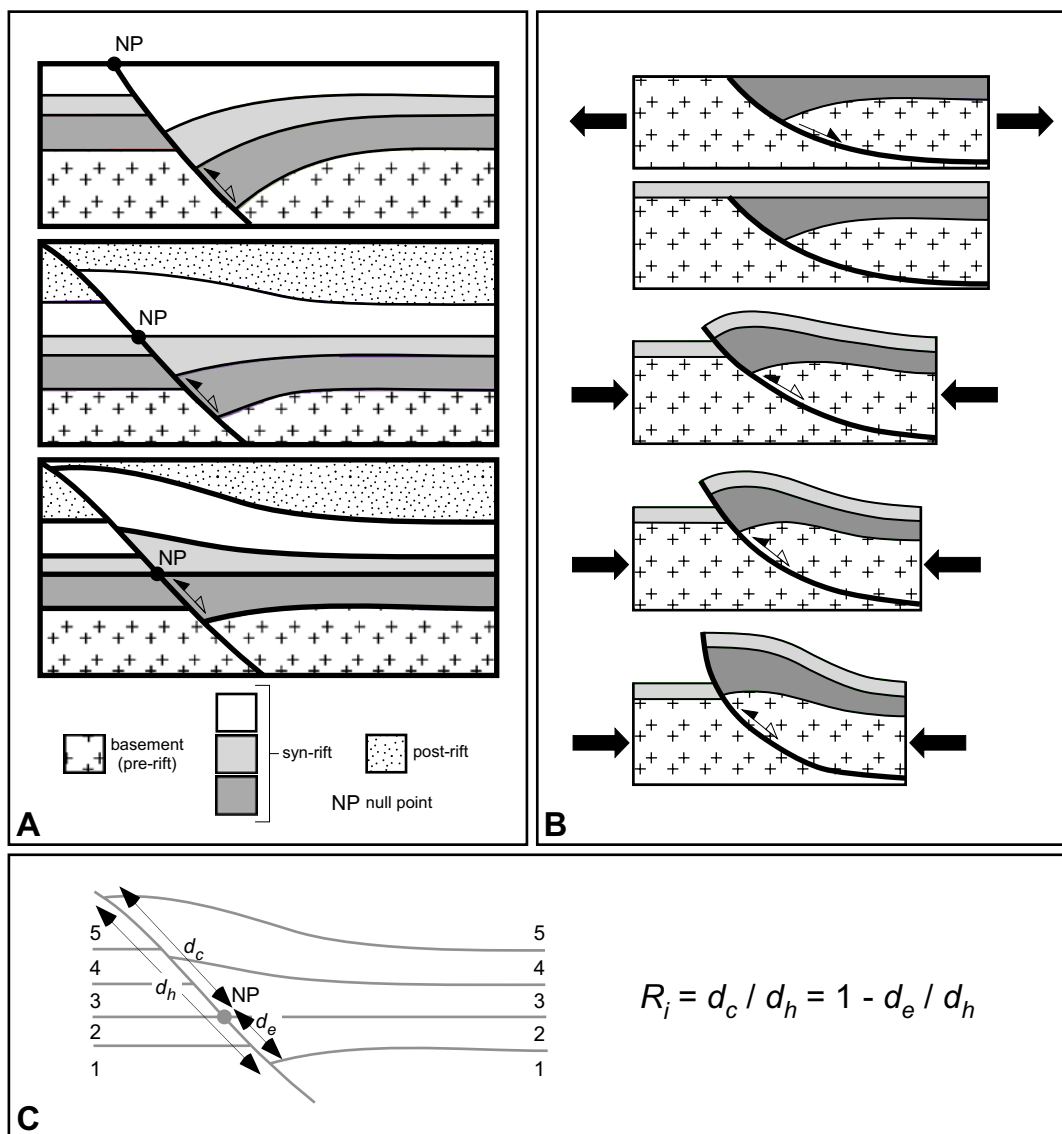
Figure 2.1. Conceptual model and key terms for a classical half-graben inversion structure. (A) Sequential diagrams showing the contractional inversion of an extensional fault. The null point (NP) moves progressively downward through the syn-rift sequence with increased inversion (after Williams et al., 1989). (B) Generalized cross-sections of a half-graben undergoing total inversion and developing a fault-propagation fold in the post-rift strata (modified from Bailey et al., 2002). (C) Terms of the inversion ratio (R_i) equation. d_h is the thickness of the syn-rift section parallel to the fault; d_c is the thickness of the partial syn-rift section in contraction; d_e is the thickness of the partial syn-rift section that is below the null point.

Within the figure:

Legend: basement (pre-rift); syn-rift; post-rift; NP null point

$$R_i = d_c\,/\,d_h = 1 - d_e\,/\,d_h$$

was analyzed. High-resolution time-structure maps, 3D visualization, and seismic-attribute analysis (variance, time-dip, and amplitude) allowed the documentation of structural styles, fault linkage and propagation patterns, fold development, and syn-inversion growth stratal patterns. The detailed seismic mapping that was a major part of this study provides perhaps one of the most detailed and thorough structural characterizations of several inversion structures and hopefully adds important insights into the complex nature of inversion.

Fold-related growth strata have been studied extensively in outcrop, seismic, and borehole datasets, with most studies aimed at describing the effects of tectonics on stratigraphic development and sediment dispersal patterns associated with contractional structures (Burbank et al., 1996; Bernal and Hardy, 2002; Champel et al., 2002; van der Beek et al., 2002; Bernal et al., 2004; Shaw et al., 2004). Syn-tectonic growth strata have been used to unravel the kinematics and folding mechanisms of various fault-related folds, including inversion structures (Riba, 1976; Suppe et al., 1992; Ford et al., 1997; Poblet et al., 1997; Storti and Poblet, 1997; Casas-Sainz et al., 2002; Echavarría and Allmendinger, 2002; Salvini and Storti, 2002; Strayer et al., 2004). Examination of inversion structures and analog-model experiments indicate that these structures differ from other types of antiformal features in that additional structural elements and deformational processes (e.g., backthrusts, shortcut faults, buttressing, and internal sediment compaction) also affect growth stratal patterns. The resulting stratal geometries can, therefore, be different from those associated with typical fault-propagation or fault-

bend folds. The three-dimensional aspects of syn-inversion growth strata also have not been studied in detail.

Analog models of inversion provide insight into the kinematics and geometries of inversion under controlled conditions. These studies typically investigate two-dimensional (cross-sectional) aspects of structural development as influenced by footwall geometry (McClay, 1989; Buchanan and McClay, 1991, 1992; Yamada and McClay, 2004), the mechanical properties of basin-filling sediments (Buchanan and McClay, 1991, 1992; Brun and Nalpas, 1996), angularity between later compressional and previous extensional stress directions (Brun and Nalpas, 1996; Dubois et al., 2002), and amounts of extension and shortening (Buchanan and McClay, 1991, 1992; Keller and McClay, 1995; Brun and Nalpas, 1996; Yamada and McClay, 2004). Most detailed descriptions of inverted half-grabens come from scaled analogs, and some of the documented structural styles and kinematic implications are commonly used as templates for seismic interpretation of inverted basins.

Later studies utilized sandbox analog models to reproduce structural features associated with dip-slip inversion (Figure 2.2; McClay, 1989; Buchanan and McClay, 1991, 1992; Mitra and Islam, 1994; Eisenstadt and Withjack, 1995; McClay, 1995). Other analog modeling studies have taken a pseudo 3-D approach by investigating structural development during inversion in both cross-sectional and plan views. Keller and McClay (1995) describe fault-linkage patterns on the surface of an initially extended sandbox when subjected to coaxial contraction and showed that the extensional fault fabric strongly influences inversion geometry. They also argued that transfer zones
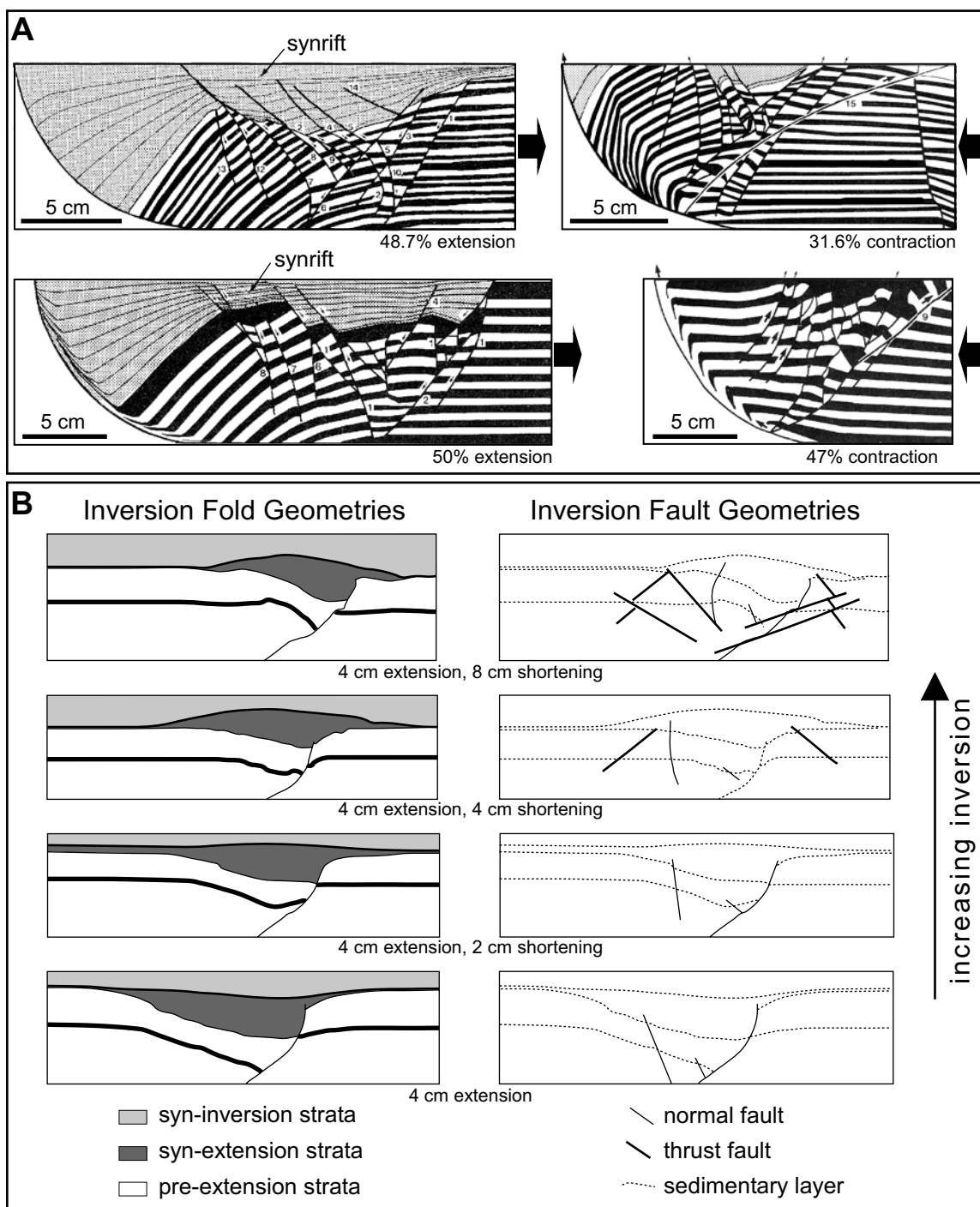
Figure 2.2. Analog model experiments that investigated 2D aspects of structural development associated with inversion. Structural relationships are observed along vertical cross-sections through the scaled models. (A) Geometric and structural relationships in an inverted half-graben above a listric fault with homogeneous sand (above) and interlayered sand and clay fill (below) (after McClay, 1989). (B) Deformation in an inverted half-graben with different amounts of shortening (after Eisenstadt and Withjack, 1995).

between adjacent extensional faults were reactivated during inversion (Figure 2.3).

Eisenstadt and Withjack (1995) documented variations in fault and fold localization and

development as a function of the amount of shortening (Figure 2.3). They showed the

limitations of quantitative and qualitative techniques (e.g., inversion ratio and

resemblance of extensional or contractional structures) for estimating the magnitude of

inversion. Other workers have constructed scaled models to evaluate the relationship

between normal fault reactivation and the angle between the extension and shortening

directions (Nalpas et al., 1995; Brun and Nalpas, 1996; Dubois et al., 2002). These

studies found that fault reactivation is related to the extension-contraction obliquity, as

expected from theoretical models. The amount of overburden, however, may also

influence which faults are preferentially reactivated, a thicker basin fill favoring the

locking-up of some pre-existing faults (Figure 2.4).

Yamada and McClay recently investigated the structural relationships associated

with inversion of 3-dimensional (i.e., curved in map view) listric faults (Yamada and

McClay, 2003a, b; Yamada and McClay, 2004). Their analog models are intended to

reproduce stratal and structural geometries associated with changes in fault strike and

hangingwall transfer of material parallel to the fault trace. Their work shows that fault

shape greatly influences structural development. Where extension and inversion are

coaxial, inversion anticlines have axial traces that mimic the plan-view shape of the

extensional bounding fault (Figure 2.5). In addition, the 3-D inversion thrust architecture

is controlled by the geometry of the main fault and locations of maximum inversion-

related uplift and syn-rift subsidence are coincident (Yamada and McClay, 2004).
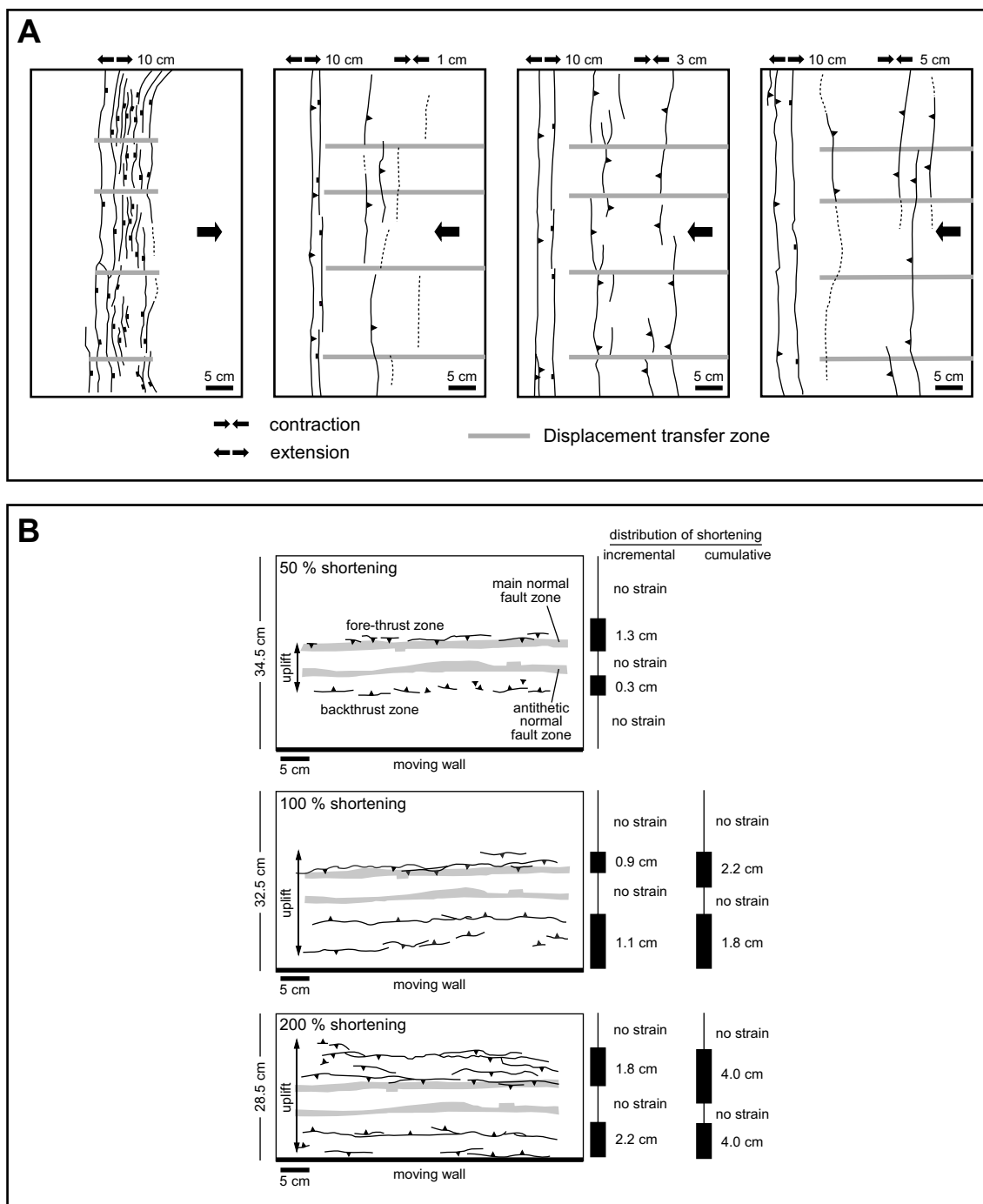
Figure 2.3. Analog model experiments that investigated lateral structural relationships associated with inversion structures. (A) Lateral relationships between accommodation zones during extension and inversion (modified from Keller and McClay, 1995); (B) Plan view of progressive development of structural features under different amounts of shortening following extension (after Eisenstadt and Withjack, 1995).
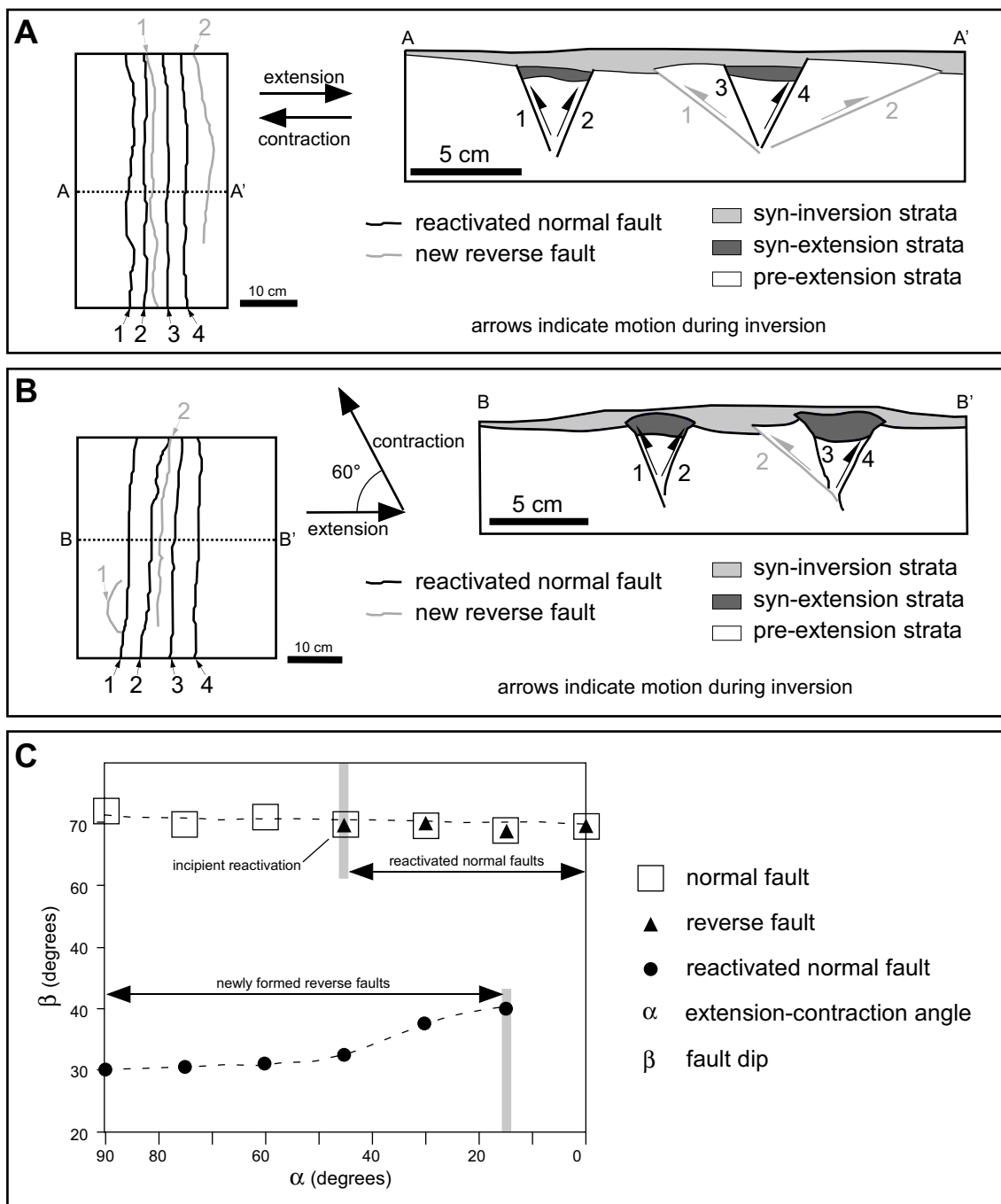
Figure 2.4. Analog model experiments that investigated 2D aspects of structural development associated with non-coaxial extension and shortening. Structural relationships are observed along vertical cross-sections through scaled models of symmetrical grabens. (A) Fault development during inversion where extension and shortening are coaxial; (B) Fault development during inversion where shortening is oblique to original extension direction (after Dubois et al., 2002); (C) Dip variations of normal and reverse faults as a function of angle between tensile and compressive directions in an entirely brittle system (after Brun and Nalpas, 1996).
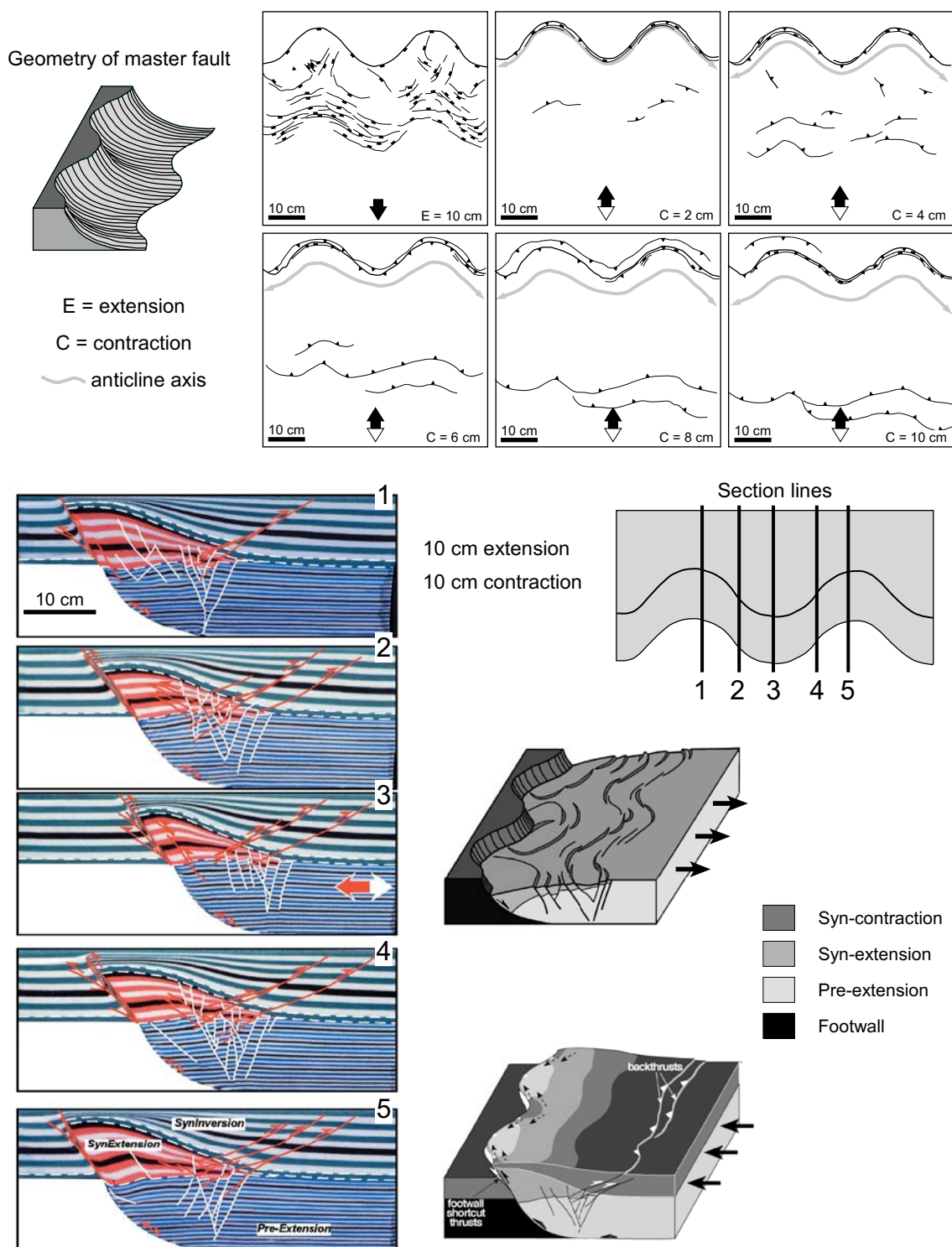
Figure 2.5. Analog model experiments that investigated lateral structural relationships associated with three-dimensional inversion structures. Experimental result and conceptual model for the influence of fault geometry on structural development during inversion (after Yamada and McClay, 2003).

Numerical methods have also been used to model kinematic and thermo-mechanical aspects of half-graben inversion (Nielsen and Hansen, 2000; Vanbrabant et al., 2002; Buiter and Pfiffner, 2003). These models allow the evaluation of stress distribution, fault mechanical properties, lithosphere rheology, erosion, and heat flow effects on basin inversion. Inversion tectonics may also be useful for investigating the thermal and mechanical structure of the lithosphere at the time of inversion (Sandiford, 1999; Nielsen and Hansen, 2000).

The North Sea is a "classic" location for natural examples of inverted half grabens (Badley et al., 1989; Cartwright, 1989; Hayward and Graham, 1989; Nalpas et al., 1995; Thomas and Coward, 1995). Although published studies from the North Sea provide basin-scale descriptions of inversion patterns, few document in detail structural and stratigraphic complexities of individual inversion structures. Basin inversion also has been described in other regions like the Alps (Gillcrist et al., 1987; Butler, 1989; Coward et al., 1991), Alpine Foreland (Gillcrist et al., 1987; Ziegler, 1987; Ziegler et al., 1995; Cristallini et al., 1997; Kley and Monaldi, 2002), Atlas Mountains (Beauchamp et al., 1996; Beauchamp et al., 1997), Ancestral Rockies (Kluth, 1991, 1994; Marshak et al., 2000), Andean Foreland (Dellapé and Hegedus, 1995; Homovc et al., 1995; Manceda and Figueroa, 1995; Uliana et al., 1995; Welsink et al., 1995), and South China Sea (Letouzey et al., 1990; Olson, 2001; Chambers et al., 2004) but, again, detailed descriptions of the complex structural and stratigraphic relationships are rarely provided. Most detailed studies of inversion are outcrop-based, where limited exposure prevents a full three-dimensional analysis of the fault framework and syn-inversion growth strata.

3-D seismic data may allow more complete investigation of basin inversion. Masaferro et al. (2003) investigated the geometry and kinematics of an inversion structure in the Central Andean Foreland using a 3D seismic survey. Detailed documentation of the complex fault framework and construction of isochron maps for growth strata investigation was possible with the 3D seismic coverage over the structures.

GEOLOGIC SETTING

The Neuquén Basin extends from 33° to 41° S and from 67° to about 72°W across the Andean foreland of Argentina and neighboring Chile (Figure 2.6). The tectonic history of the basin is characterized by two major evolutionary stages: (1) Late Triassic – Early Cretaceous backarc extension followed by (2) a Late Cretaceous – Recent retroarc foreland setting (Dewey, 1988; Legarreta and Uliana, 1991; Uliana and Legarreta, 1993; Vergani et al., 1995; Franzese and Spalletti, 2001; Franzese et al., 2003). The main Triassic normal fault trends that developed during extension are oriented NE-SW and ENE-WSW in the southern portion of the basin (Figure 2.7A; Ramos, 1978; Vergani et al., 1995). This area is tectonically dominated by the Huincul Arch, an E-W right-lateral shear zone characterized by transpressive uplift that was active from Early Jurassic to Late Cretaceous time (Orchuela et al., 1981; Ploszkiewicz et al., 1984; Tankard et al., 1995; Vergani et al., 1995). The Huincul Arch divides the
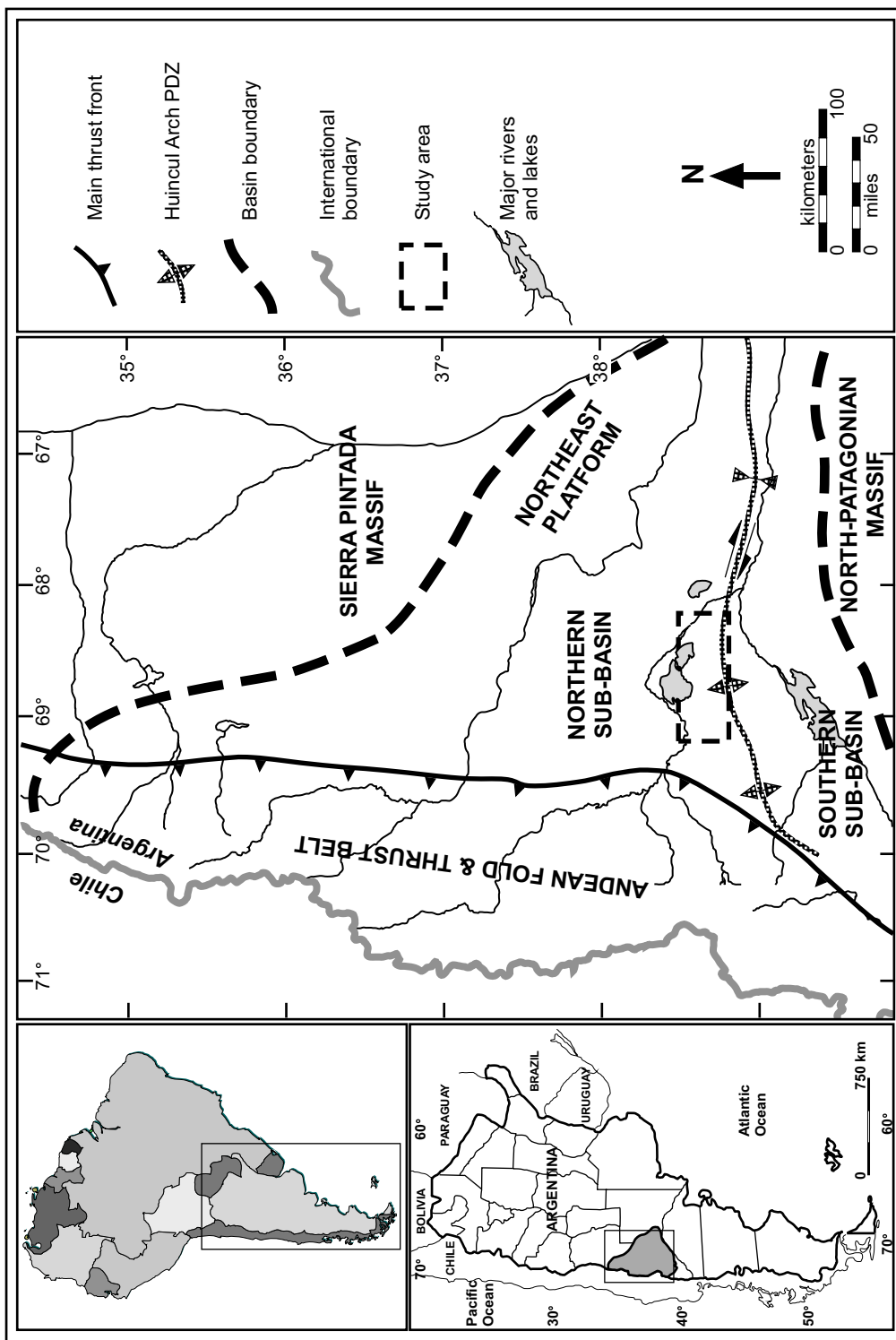
Figure 2.6. Generalized tectonic map of the Neuquén Basin showing main provinces and structural elements.
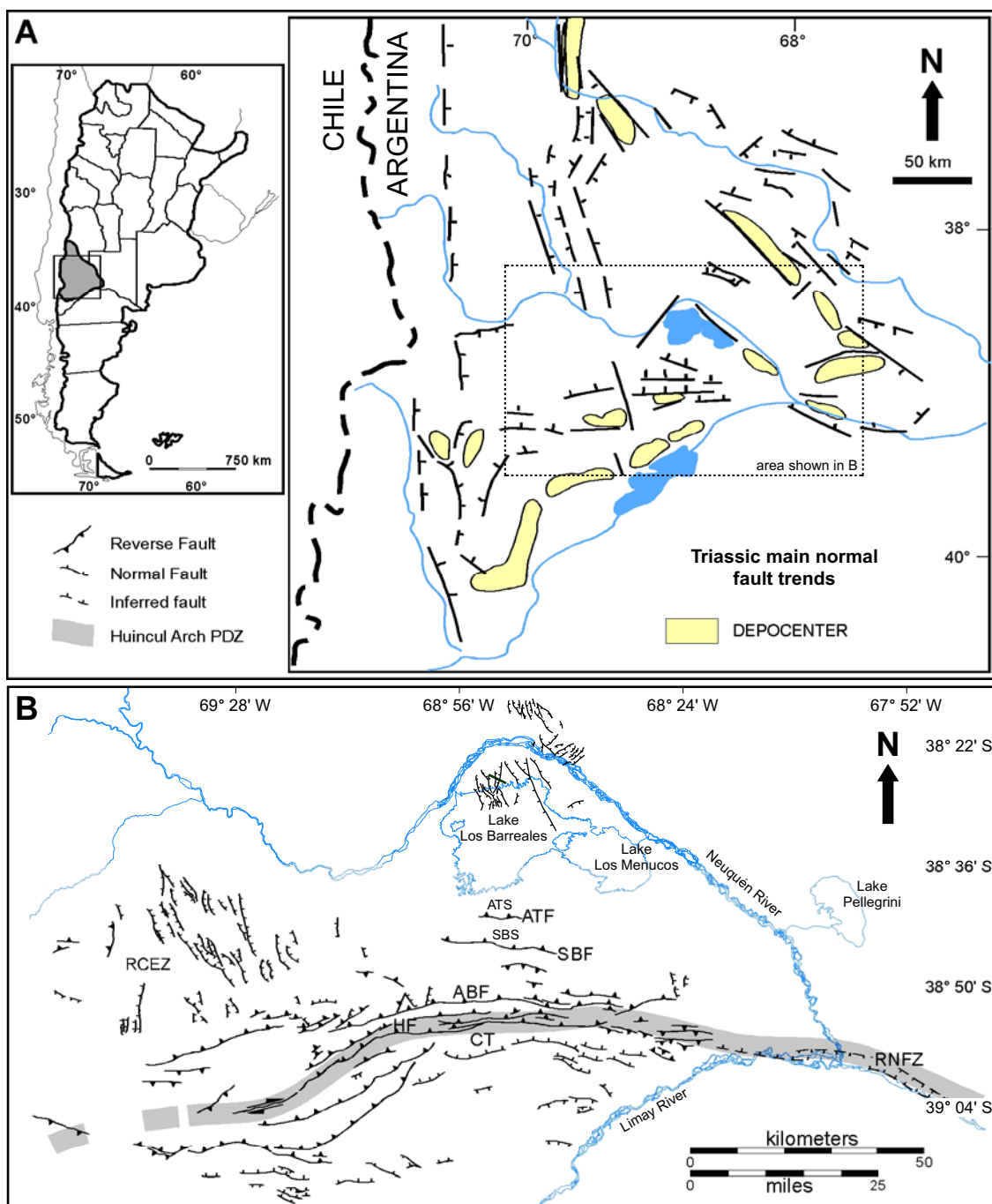
Figure 2.7. Structural configuration of the Neuquén Basin. (A) Extensional fault systems formed during Late Triassic time (after Vergani et al., 1995). (B) Main structural elements of the Huincul Arch and surrounding areas of the Neuquén Basin after Mesozoic transpression. Based on Maretto and Lara (2002), Orchuela et al. (1981), Pángaro and Bruveris (1999), Ploszkiewicz et al. (1984), and Vergani et al. (1995). HF: Huincul Fault, ABF: Aguada Baguales Fault, ATF: Aguada Toledo Fault, ATS: Aguada Toledo Structure, CT: Challacó Trough, SBF: Sierra Barrosa Fault, SBS: Sierra Barrosa Structure, RCEZ: Ramón Castro Extension Zone, RNFZ: Río Negro Fault Zone. The Huincul Arch is the approximately 10-km wide deformation zone indicated by the shaded line.

Neuquén Basin into two main depocenters, known as the Northern and Southern Sub-basins.

The area investigated during this study covers the Northern Sub-basin along the northern flank of the Huincul deformation zone (Figures 2.6, 2.7B). In this region, Late Triassic half-grabens were tectonically inverted during transpressional deformation along a restraining bend in the Huincul Arch principal displacement zone (Ploszkiewicz et al., 1984; Vergani et al., 1995; Cruz et al., 2002). Compressional stress that caused the inversion of rift depocenters likely had a general N-S orientation. The most conspicuous inversion structures in the study area are the Sierra Barrosa (SBS) and Aguada Toledo (ATS) structures, which are the main focus of this study.

Pre-rift basement rocks beneath the Neuquén Basin consist of a complex of early Paleozoic metamorphic and igneous rocks, with a thin interval of Carboniferous strata. Pre-rift basement is overlain by up to 7 km of Mesozoic-Cenozoic strata (Figure 2.8; Vergani et al., 1995). Syn-rift strata include the "pre-Cuyo" and lowest "Cuyo" groups, which consist mostly of siliciclastic facies that were deposited in alluvial fan, fluvial, and lacustrine environments (Legarreta and Gulisano, 1989; Urien and Zambrano, 1994) with a significant pyroclastic component.

The post-rift succession was deposited during three main transgressive-regressive cycles: 1) the Toarcian-Bathonian middle to upper Cuyo Group; 2) the Callovian-Oxfordian Lotena Group; and 3) the Kimmeridgian-Albian Mendoza and Rayoso Groups; (Digregorio, 1972; Digregorio and Uliana, 1980; Gulisano and Pando, 1981; Hinterwimmer and Jáuregui, 1985; Legarreta and Gulisano, 1989; Urien and Zambrano,
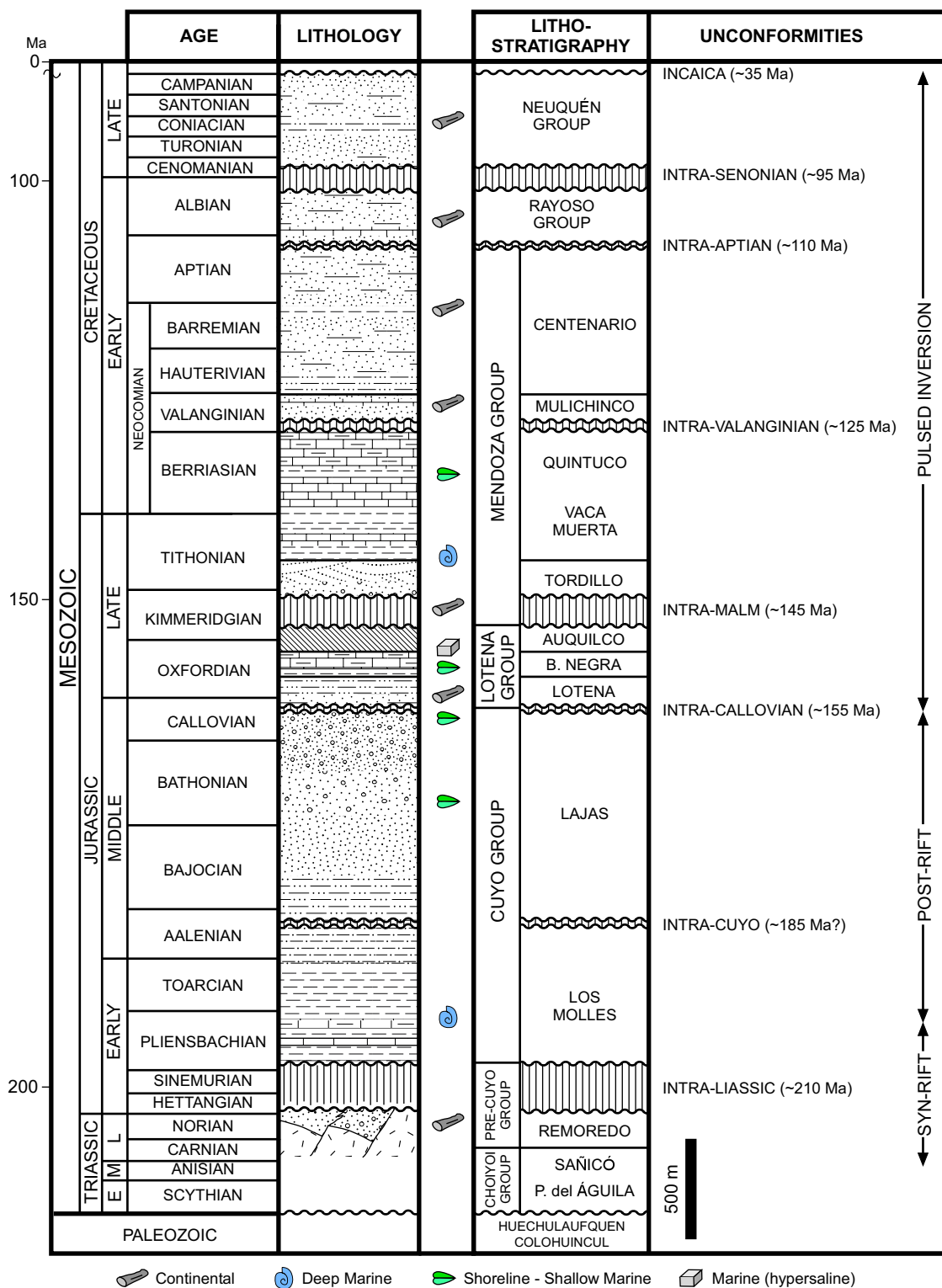
Figure 2.8. Composite stratigraphic column of the Northern Sub-basin (Neuquén Basin). After Urien and Zambrano (1994), Vergani et al. (1995), Veiga (2002), and Cobbold and Rossello (2003).

1994). Continental deposits of the Late Cretaceous (Cenomainan-Campanian) Neuquén Group cap the section in the study area. These post-rift sedimentary units are bounded by five major unconformities of variable areal extent and duration throughout the central Neuquén Basin. These unconformities, in ascending order are referred to as the Intra-Liassic, Intra-Callovian, Intra-Malm, and intra-Valanginian, and Intra-Senonian (Figure 2.8). The Intra-Liassic unconformity caps the syn-rift sedimentation and is associated with uplift and erosion previous to the first Cuyo transgression. The Intra-Callovian unconformity marks the first significant tectonic event along the Huincul Arch, which resulted in initial inversion across the study area. The Intra-Malm unconformity is associated with the strongest inversion event in the area. The Intra-Valanginian and Intra-Senonian unconformities are the result of less intense tectonic events along the Huincul Arch, which resulted in uplift and erosion of Lower and Upper Cretaceous strata, respectively. Subordinate breaks in the stratigraphic record are observed locally as intra-formational unconformities and reflect local response to tectonic deformation.

DATA AND METHODS

An extensive seismic and borehole dataset was made available to Texas A&M University by Repsol-YPF of Argentina. The seismic dataset consists of four, partially-overlapping, 3D seismic-reflection surveys that cover an area of about 1,500 km^2 in the southern portion of the Northern Sub-basin along the northern flank of the Huincul Arch shear zone (Figure 2.9).
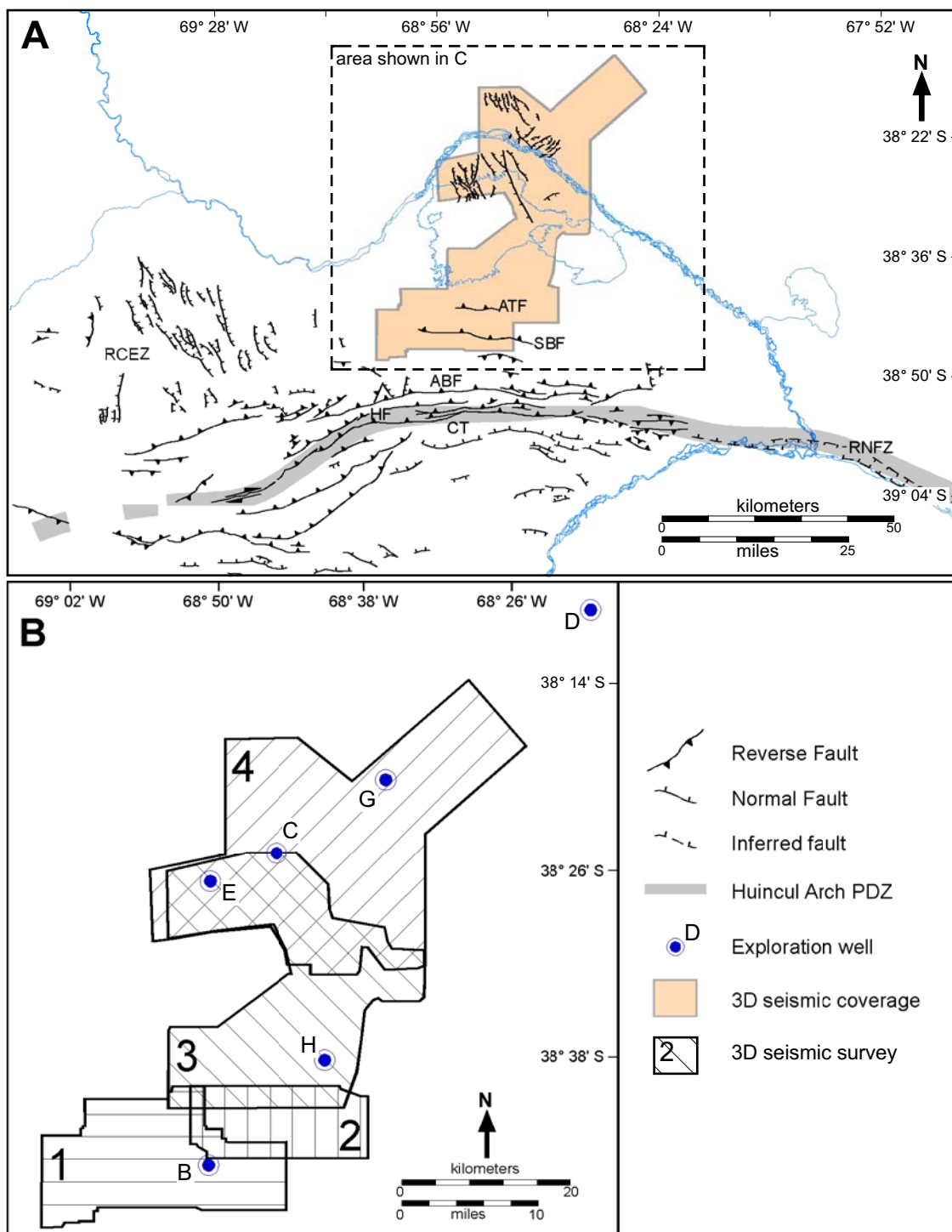
Figure 2.9. Borehole and seismic dataset used in this study. (A) Location of the dataset relative to Neuquén Basin's main structural elements. (B) Numbers and relative position of the four partially-overlapping 3-D surveys analyzed. See Figure 2.7 for name references.

3D amplitude volumes have a horizontal resolution from 15 m (Survey 1) to 30 m (Surveys 2 to 4). Vertical resolution is determined by the frequency content and interval velocities, which are similar for all surveys but vary significantly for different stratigraphic intervals. An extraction of frequency spectra for a small seismic sub-volume of Survey 1 allowed the estimation of vertical resolutions at different depths, which are considered representative of the entire dataset (Figure 2.10). Using the extracted frequencies and interval velocities from Well B, a vertical resolution of 27 m was estimated for the sand-rich strata of the Upper Mendoza Group (Centenario Formation; 500-900 ms TWT). Vertical resolution decreases for the carbonate- and marl-rich lower Mendoza Group (Quintuco and Vaca Muerta Formations; 900-1200 ms TWT), with an estimate of 47 m. Resolution again increases to 38 m for the interbedded sands and shales of the Lotena and Cuyo Groups (1200-2000 ms TWT), whereas the lowest values are observed in the lowest Cuyo and Pre-Cuyo intervals (52 m; 2000-2600 ms).

Borehole data consist of log curves (digital or paper versions of spontaneous potential, gamma-ray, sonic, and resistivity curves) and mud-logging reports from five exploratory wells that partially penetrated the Lower Jurassic section. None of the wells within the 3D surveys penetrated the entire Mesozoic section, although the deepest well (Well E) reached 4798 m below the surface. This represents about 85% of the entire stratigraphic thickness in this part of the basin. Well D, located about 2 km NE of the area covered by 3D seismic, reaches early syn-rift strata and was used as a reference for mapping deep stratigraphic levels (Lower Cuyo and Pre-Cuyo strata) (Figures 2.8, 2.9).
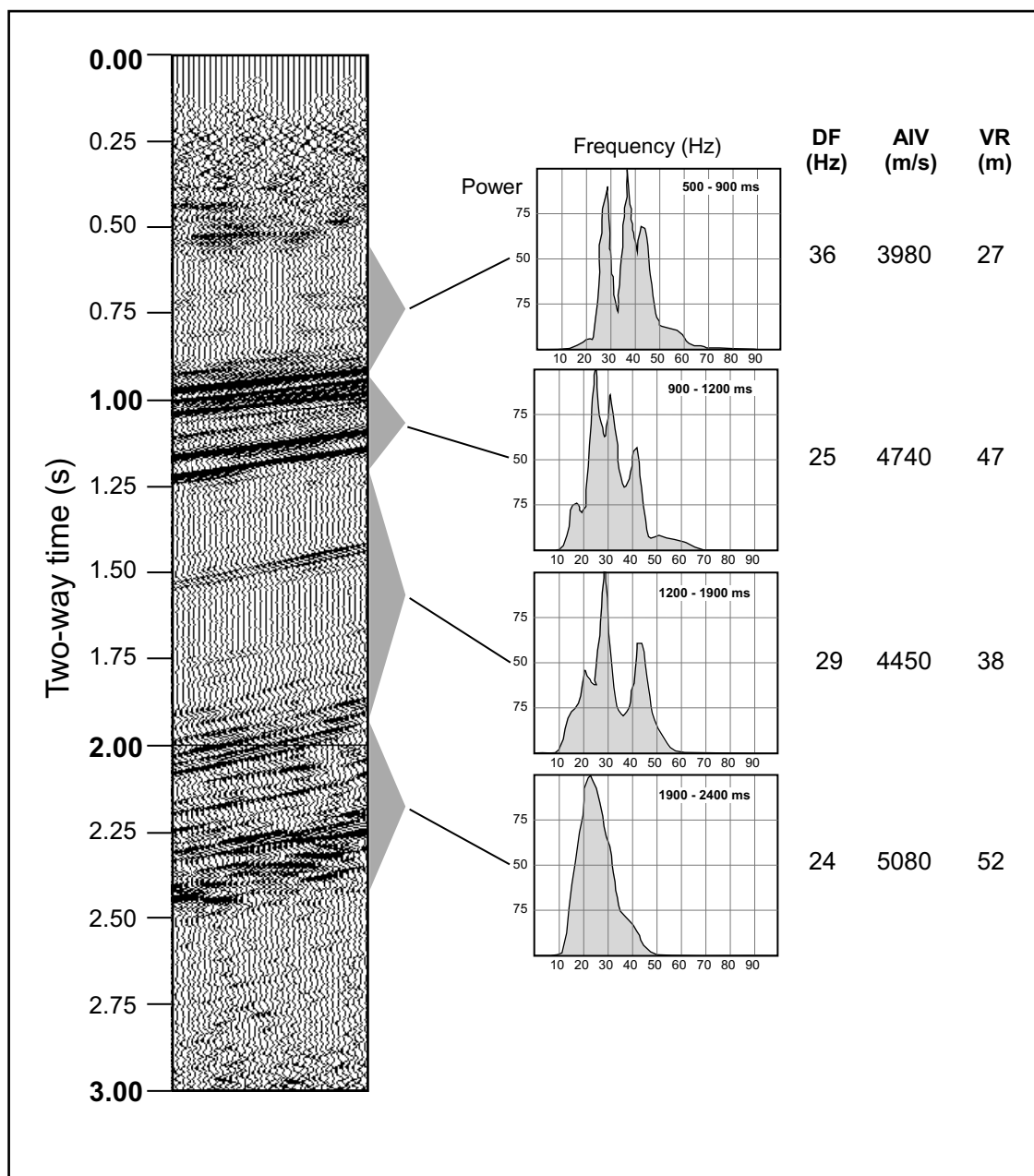
Figure 2.10. Estimation of vertical resolution for a sub-volume of seismic survey 1 (10 by 10 traces). Frequency spectra for different time-intervals are shown. DF = Dominant Frequency; AIV = Average Interval Velocity; VR = Vertical Resolution. Vertical resolution is estimated as 1/4 of the wavelength of the dominant frequency. Average interval velocities were obtained from well B sonic log.

Repsol-YPF also provided access to proprietary reports on the regional Mesozoic stratigraphy of the area.

All seismic data, log curves, and stratigraphic markers were loaded onto a Unix workstation from 8 mm magnetic tapes. GeoQuest™ GeoFrame™ 4.0.3 by Schlumberger™ was used to interpret and visualize the data. Detailed seismic mapping was done using IESX™ and BaseMap Plus™ seismic interpretation and gridding modules. WellEdit™ and WellPix™ were used to analyze, edit and correlate log curves. Coherency volumes of all 3D surveys were generated using Variance Cube™. The coherency volumes were computed using a time-window of 80 ms, inline and crossline ranges of 3 traces and the "×" operator, which uses all eight traces surrounding the center trace to calculate the coherency. The generated volumes, when combined with amplitude sections, enhanced the imaging of faults and facilitated fault mapping (Figure 2.11). Additional seismic-attribute volumes were generated to aid in stratigraphic interpretation (e.g., instantaneous frequency and instantaneous phase attributes).

Available checkshot surveys were used to calibrate the sonic logs and generate synthetic seismograms. This was achieved using the Synthetics™ module in the GeoFrame™ suite. Pseudo-checkshots were created in cases where a checkshot from a nearby well was not usable due to significant structural and stratigraphic differences. In these cases, known reflections were assigned a depth, which was known from well logs or lithology profiles.

Checkshot surveys were available for wells C, E, and H, which are within seismic surveys 3 and 4 (Figure 2.9). After sonic log editing, calibration, and
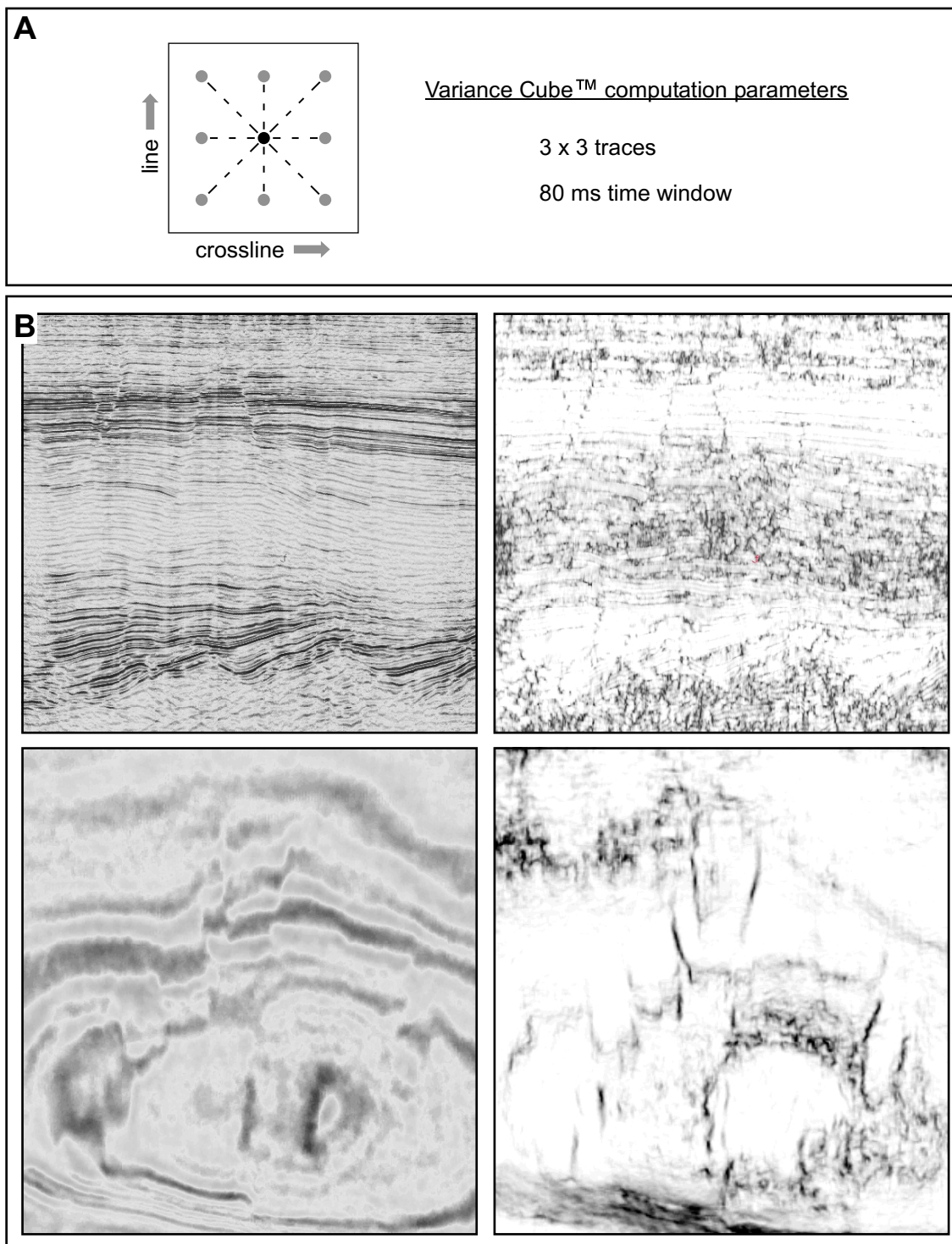
Figure 2.11. Variance Cube™ computation parameters and results. (A) Trace correlation geometry. (B) Amplitude (left) and coherency (right) versions of a vertical seismic section and time slice from Surveys 2 and 1, respectively, showing the increase in fault imaging quality for the coherence volume.

construction of synthetic seismograms (Figure 2.12), markers for key stratigraphic levels were then posted on the seismic data and mapped across the surveys. The wavelet used to compute the seismograms was statistically extracted from a seismic sub-volume around each well (20 x 20 traces and time interval enclosing the main units mapped), using zero phase, normal polarity, and a Ricker type wavelet. Seismic correlation was then used to extend the interpretation to adjacent surveys without well control (i.e., Survey 2). In the case of Survey 1, only partial data for well B was released (i.e., no checkshot survey), and therefore the sonic log, calibrated with a pseudo-checkshot, was used to generate the time-to-depth curve (Figure 2.12).

Three-dimensional visualization was done using GeoViz™. Structural restorations were performed using a 2DMove™ by Midland Valley™. Selected vertical seismic profiles and interpreted cross-sections were converted to depth using the domain-conversion function in 2DMove™. This is performed by constructing a velocity model consisting of layer geometries, assigning a seismic velocity at the top of each layer, and using a rate of change in velocity with depth within each layer. Interval velocities used in the model were obtained from acoustic logs and checkshot surveys.

Ages of key stratigraphic surfaces were obtained from proprietary biostrati-graphic reports and published literature from the Neuquén Basin. Poor data resolution and lack of continuous reflections did not allow adequate extensive mapping of the top of basement and syn-rift internal stratigraphic levels, which in turn prevented construction of regional syn-rift time-thickness maps.
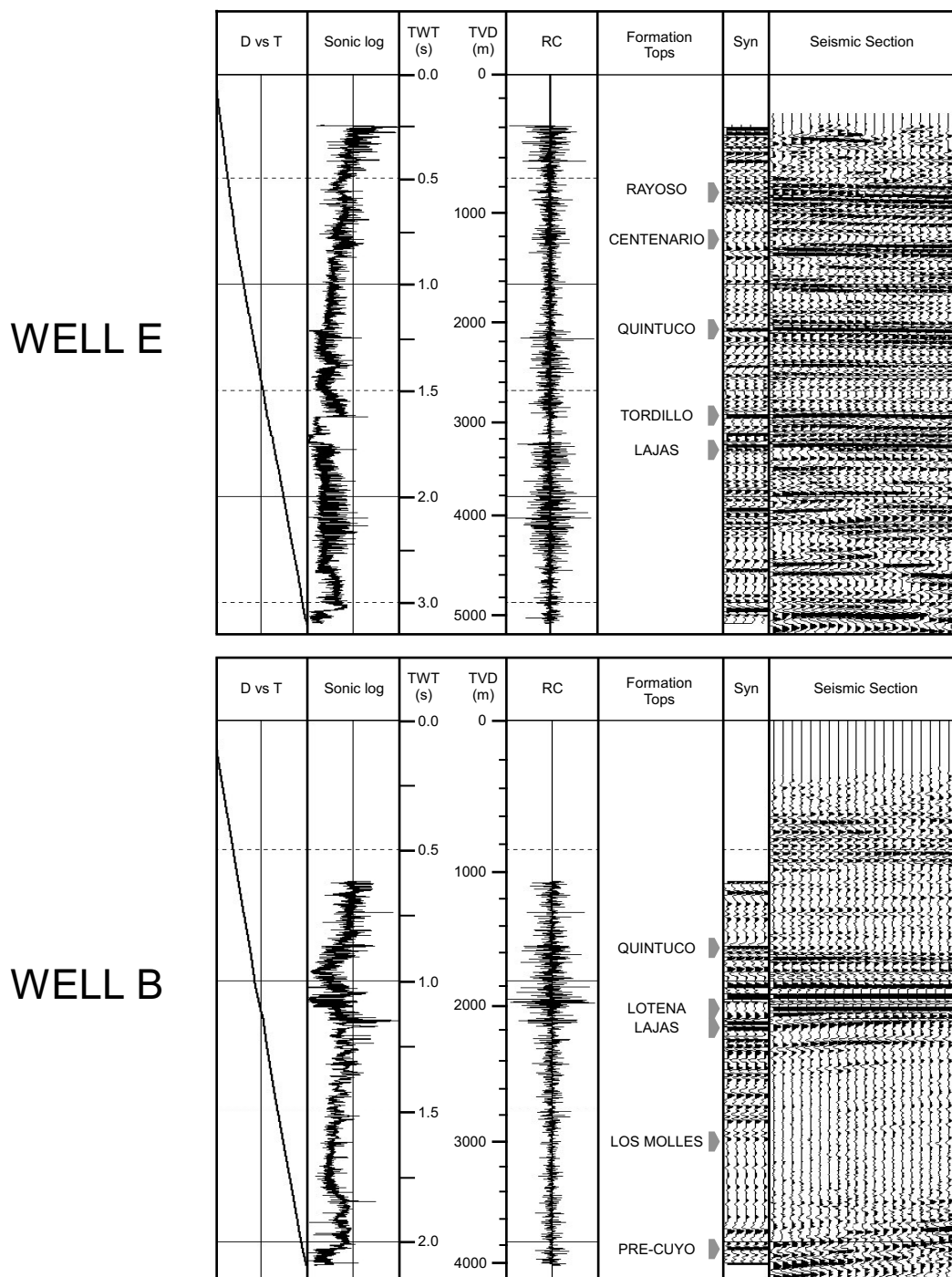
Figure 2.12. Synthetic seismogram generation panels for wells E and B and representative seismic section from well locations. See Figure 2.9 for well locations. D vs T = Depth vs time curve; TVD = True Vertical Depth; TWT = Two-way time; RC= Reflection Coefficients; Syn = Synthetic Seismogram.

RESULTS

Seismic-stratigraphic relationships

Structural and stratigraphic mapping across the area of 3D seismic coverage shows that the most prominent inversion structures in the area are the Sierra Barrosa and Aguada Toledo structures, which are covered by Surveys 1 and 2 (Figure 2.9). These structures record important tectonic events that occurred during Late Triassic to Late Cretaceous time, which predates the main phases of the Andean orogeny. The interpreted tectono-stratigraphic framework for these structures was combined with seismic-facies analyses to identify five main tectono-stratigraphic units for the Sierra Barrosa and Aguada Toledo structures (Figure 2.13): pre-rift basement, syn-rift, post-rift, syn-inversion 1, and syn-inversion 2.

Basement is seismically identified by its relatively reflection-free to chaotic seismic character. It was not penetrated by wells in the study area and therefore was mapped based on geometrical relationships and seismic-facies recognition. The top of basement horizon is generally characterized as a discontinuous positive reflection.

Syn-rift strata (Pre-Cuyo to Lowest Cuyo strata) are imaged as wedge-shaped intervals characterized by a complex seismic signature, where divergent continuous reflections are intermixed with chaotic to almost reflection-free packages that are bounded by faults or onlap against basement. The upper portion of the syn-rift interval is imaged as continuous reflections corresponding to basal strata of the Los Molles Formation. In outcrop, basal syn-rift strata consist of intermixed volcanic and coarse
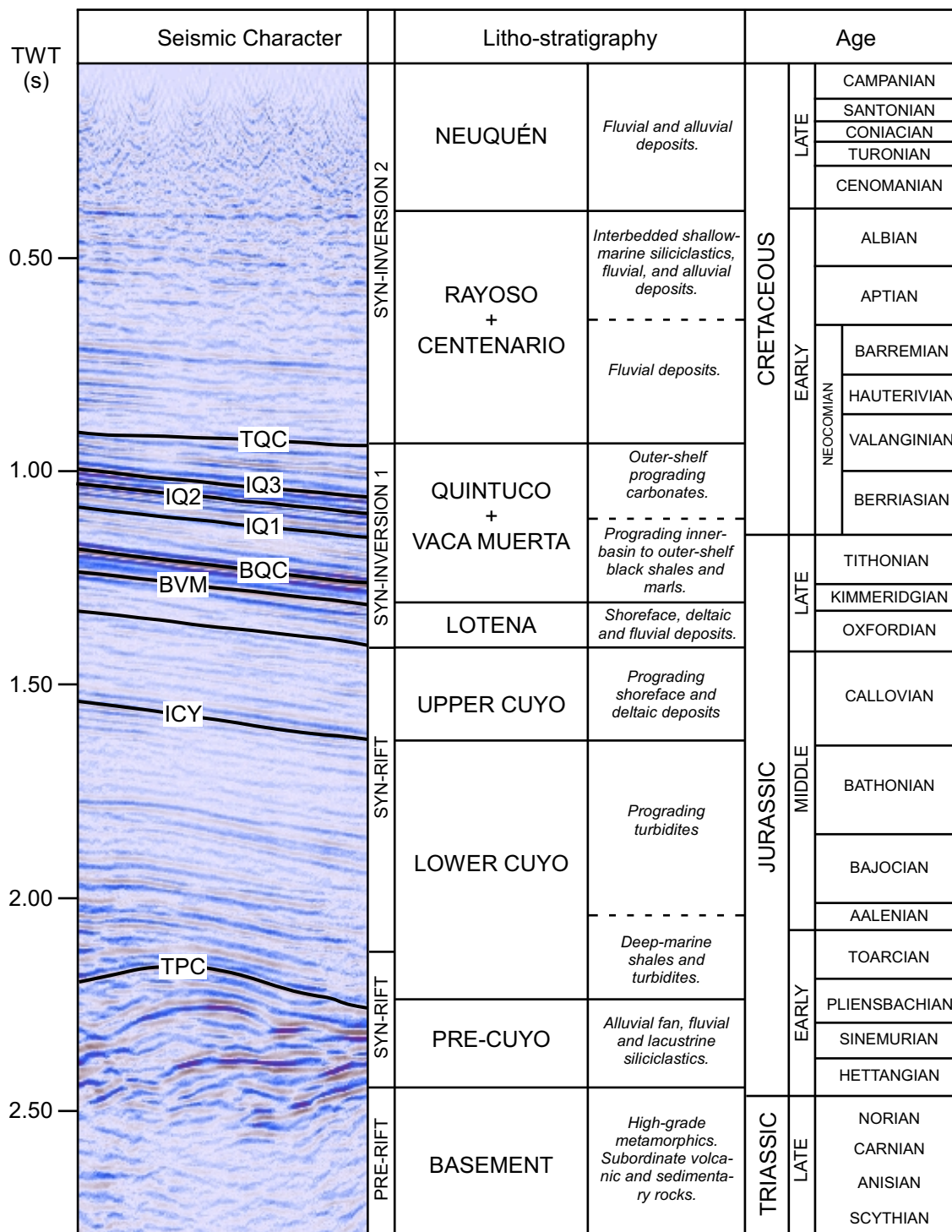
Figure 2.13. Seismic character and depositional facies for Mesozoic strata in the Northern Sub-basin area (around well B). Dates from Pando et al. (1984), Gulisano and Gutiérrez Pleimling (1994), Vergani et al. (1995), Zavala and Freije (2002), Cruz et al. (2002), and Freije et al. (2002).

continental siliciclastic strata that were deposited in isolated depocenters (Gulisano and Legarreta, 1987; Legarreta et al., 1993; Vergani et al., 1995).

Lowermost post-rift strata correspond to the Cuyo Group (deep marine shales and interbedded turbiditic sandstone of the upper Los Molles Formation), which are overlain by southeast-to-northwest prograding shoreface and deltaic deposits of the Lajas Formation (Figure 2.8).

The stratigraphic record of pulsed basin inversion exists throughout most of the post-rift section, and is seismically expressed by multiple angular unconformities across the crest of inversion highs and thin stratal packages that onlap against both limbs of inversion anticlines. Syn-inversion strata were divided into two units: syn-inversion 1 (strong) and syn-inversion 2 (mild). The lower part of syn-inversion 1 strata consists of fluvial to deltaic deposits of the Lotena Formation (discontinuous, subparallel, and low amplitude reflections), which are overlain by basinal shale and NW-prograding carbonate facies of the Lower Mendoza Group (high-amplitude, continuous, and parallel reflections). More significant inversion, however, is recorded within this unit by the upper part of the Quintuco Formation (Lower Mendoza Group) along the limbs of the Sierra Barrosa and Aguada Toledo structures. Onlap of high amplitude, continuous upper Quintuco reflections, together with thickness changes across the anticlines' crests, record inversion and uplift of the SBS and ATS during Berriasian and Valanginian time. Syn-inversion 1 strata are truncated by the Intra-Valanginian unconformity. Syn-inversion 2 strata, which comprises the upper Mendoza, Rayoso, and Neuquén Groups, are only mildly affected by inversion-related folding and uplift and stratal patterns show

that the intensity of inversion deformation waned up-section (Figure 2.15). Syn-inversion 2 strata contain another significant angular unconformity (Intra-Senonian), which reflects renewed folding and uplift during Cenomanian time. Sesmic facies consist of relatively discontinuous and low-amplitude reflections that are poorly imaged due to the low signal-to-noise ratio, which is characteristic of continental facies like the Neuquén Group (0-400 ms TWT).

Eight horizons were mapped across the entire merged 3D-surveyed area. These horizons correspond to either marine flooding surfaces or unconformities and were chosen because of their tectono-stratigraphic significance and their lateral continuity as markers for kinematic analysis. These horizons are, in ascending stratigraphic order: Top Pre-Cuyo (TPC), Intra-Cuyo (ICY), Base Vaca Muerta (BVM), Base Quintuco (BQC), Intra-Quintuco 1 (IQ1), Intra-Quintuco 2 (IQ2), Intra-Quintuco 3 (IQ3), and Top Quintuco (TQC) (Figure 2.13).

Description and interpretation of structural features

General description of Sierra Barrosa and Aguada Toledo structures

The SBS is an elongated asymmetrical inversion anticline, about 22 km long and a maximum of 6 km wide (Figure 2.14). The sinuous fold axis plunges gently to the west and east-southeast and fold amplitude decreases upsection, which results from the combination of parallel-style folding with significant erosion at certain stratigraphic levels (i.e., folded unconformities). Two substructures or areas of highest overall uplift within the SBS are linked by a "neck" whose width increases at higher stratigraphic
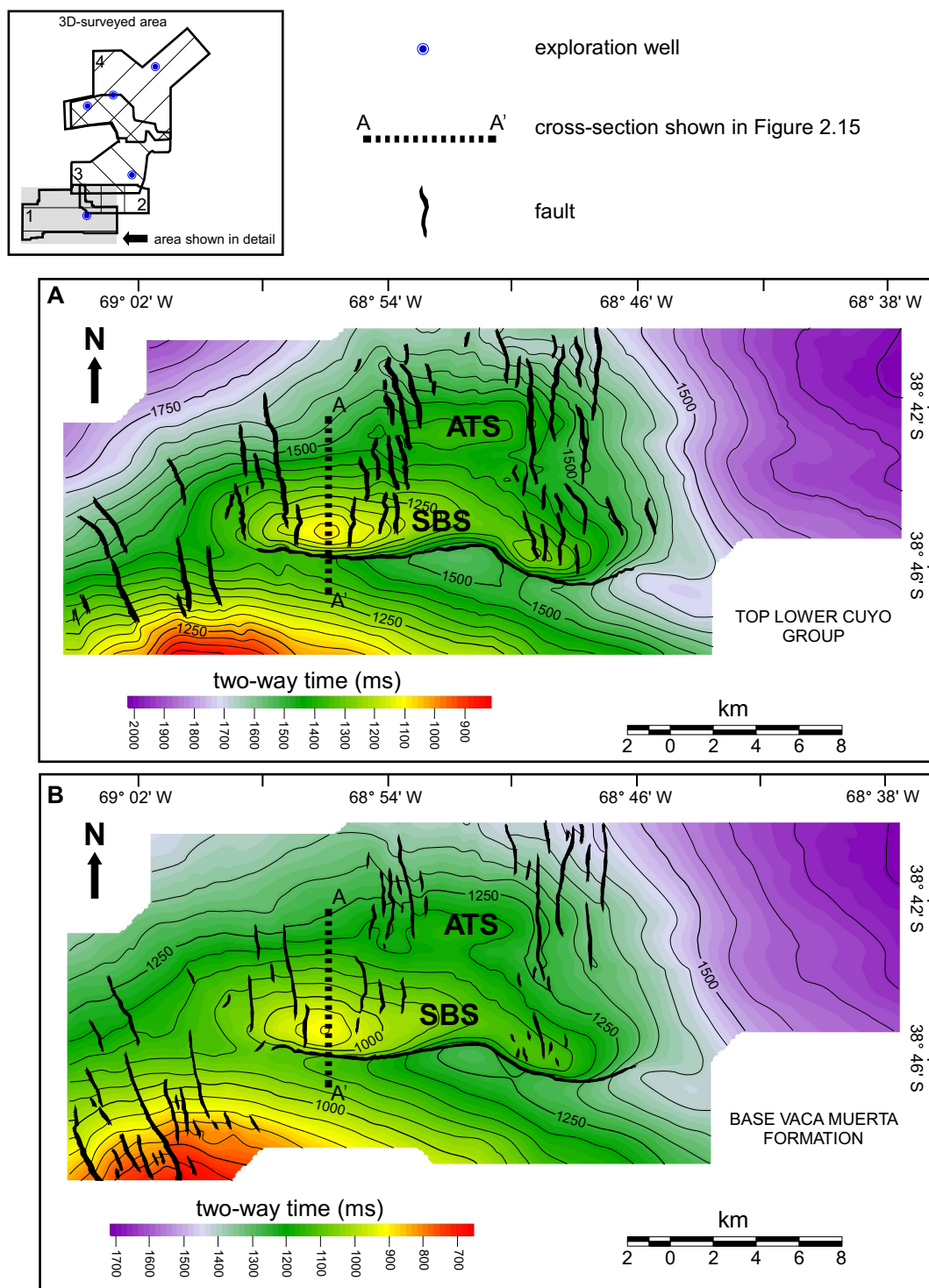
Figure 2.14. Time-structure maps of the Sierra Barrosa (SBS) and Aguada Toledo (ATS) inversion structures at the top of Lower Cuyo group (A) and base of Vaca Muerta Formation (B). Contour interval = 50 ms. Note how north-south oriented faults are fewer in number, have shorter lengths in plan view, and have less apparent heave at shallower Vaca Muerta level than at deeper Lower Cuyo level.

levels within the post-rift strata. The western substructure (Figures 2.14, 2.15) exhibits the largest amount of uplift, has a N- to NNE-dipping axial plane, and a southern limb cut by a southward-verging fault zone that changes from normal at depth to reverse at shallower levels. The southern limb of the SBS is defined by an E-W syncline, whereas the northern limb is locally affected by another inversion structure, the Aguada Toledo Structure (ATS) to the north.

A master reverse fault cuts the southern limb of the SBS and affects both basement and overlying strata. The master fault is mappable as a single surface on seismic sections with associated shortcut faults or antithetic normal faults in some parts of the structure. Clear offset of post-rift strata shows the reverse character of the master fault zone, but the high dip of reflectors in the vicinity of the fault zone and the poor reflectivity of early post-rift strata prevent the clear imaging of discrete structural elements, with the exception of some large antithetic normal faults (Figure 2.15). The master fault zone does not cut completely through the steeper southern limb of the SBS anticline, although flattening of the fault plane is observed in some parts of the structure. The average dip of the master fault is about 70° to the north in the faulted uppermost post-rift section, although the fault is listric at depth and flattens to 45° to 60°.

Another prominent inversion structure is located on the northern flank of the SBS. The Aguada Toledo Structure (ATS) is an elongated asymmetrical inversion anticline that extends in an E-W direction for about 10 km and has a maximum width of about 3 km (Figure 2.15). The fold axis, located ~5 km north of the SBS's axis, plunges gently to the east and west. The amplitude of the anticline decreases up-section, mostly
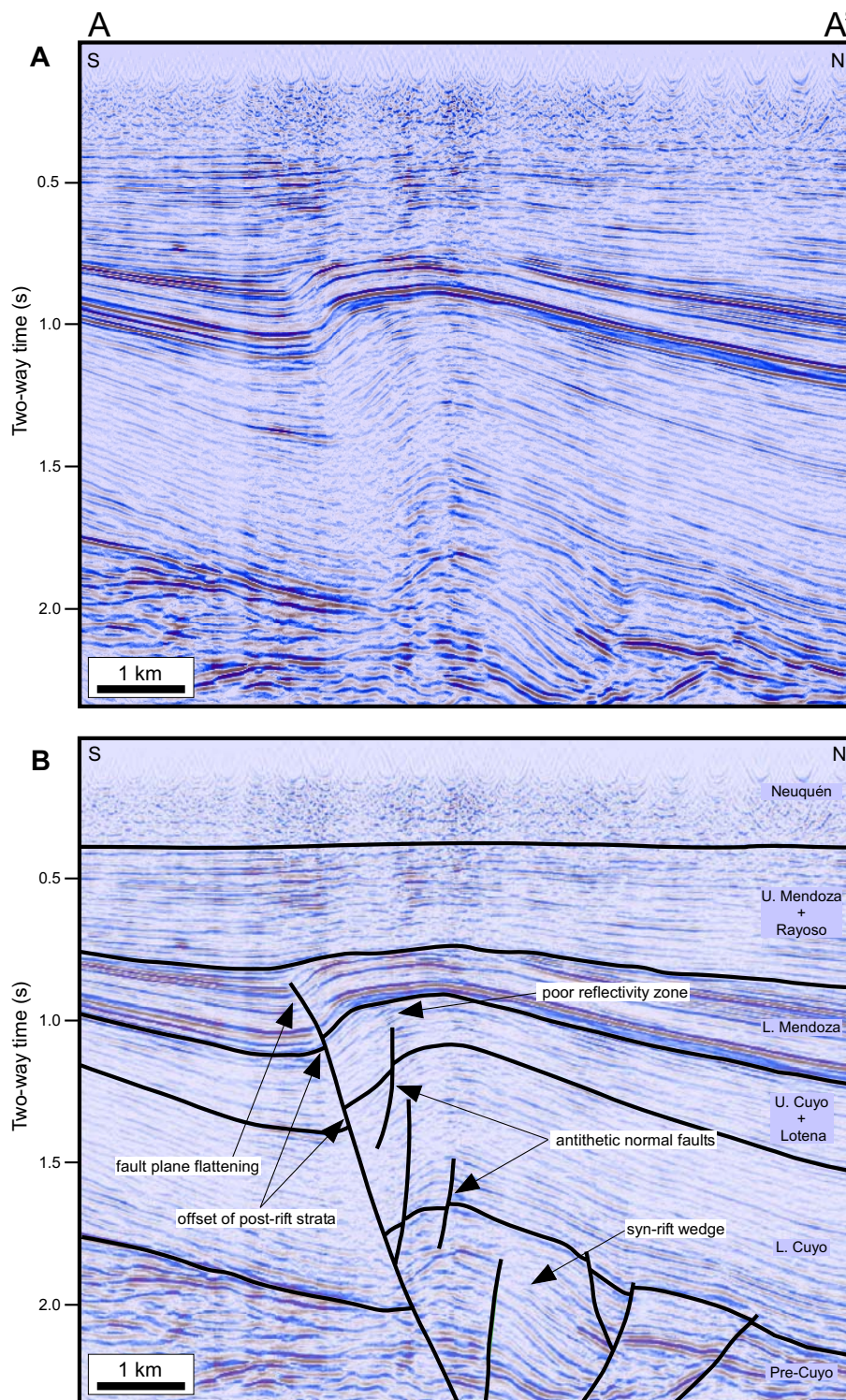
Figure 2.15. Uninterpreted (A) and interpreted (B) seismic section A-A' through the western portion of the SBS, depicting some structural elements (see text for description and Fig. 2.14. for line of section).

due to parallel-style folding (angular unconformities within the Cuyo and Mendoza groups are more subtle than for the SBS). A northward-dipping half-graben bounding fault was reactivated in a reverse sense during inversion and cuts up-section into the post-rift strata, resulting in an inversion-related fault-propagation fold. No displacement across this fault is observed at the Lower Mendoza Group level, although significant folding of these and shallower strata is apparent. The ATS's main bounding fault is listric, with northward dips ranging from 40° to 70°, and is imaged as a thin zone of discrete deformation that cuts through the uppermost Cuyo Group.

Fault framework for SBS and ATS

The structural framework that developed in conjunction with extension during rifting and later contraction during inversion can be divided into two main fault systems. The "deep" fault system affects mostly basement and syn-rift strata and has a general E-W orientation. It consists of reactivated and non-reactivated extensional faults that comprised the original rift fabric plus newly formed faults that accommodated the shortening associated with inversion (i.e., backthrusts and "shortcut" faults). Some of the syn-rift faults bound wedge-shaped syn-rift strata. The largest inverted half-grabens of the SBS are bounded by a composite extensional fault system comprised of three main segments and two accommodation zones (Figure 2.16). Listric half-graben bounding faults apparently join detachment levels at different depths. Bounding-fault segment 2 seems to be the deepest fault and is imaged as a clear reflection that flattens into a horizontal detachment at about 3.75 s TWT (Figure 2.17B). Segment 2 also bounds the largest and thickest syn-rift depocenter and corresponds to the portion of the SBS

structure with maximum structural inversion. Bounding-fault segments 1 and 3 flatten at shallower levels based on their dip angles at the syn- and post-rift levels, although detachment levels are interpreted to be between 3.00 and 3.25 s TWT (Figure 2.17A, C). Syn-rift wedges bounded by segments 1 and 3 have similar thickness, but uplift due to inversion is greater for the depocenter bounded by segment 3.
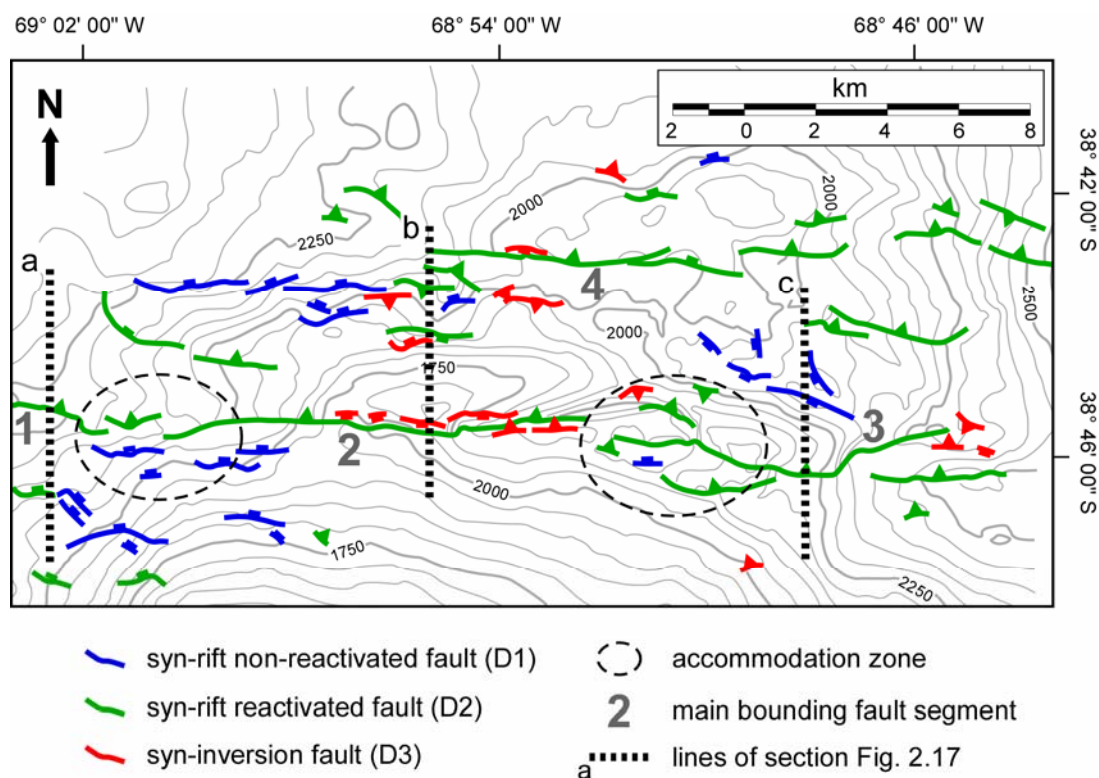
Figure 2.16. Time-structure map at the top of Pre-Cuyo (syn-rift). Contour interval = 50 ms.

Faults at the syn-rift level are classified into three types, based on their interpreted kinematic history: D1 (syn-rift faults not reactivated during inversion), D2 (syn-rift faults reactivated during inversion), and D3 (new syn-inversion faults). The
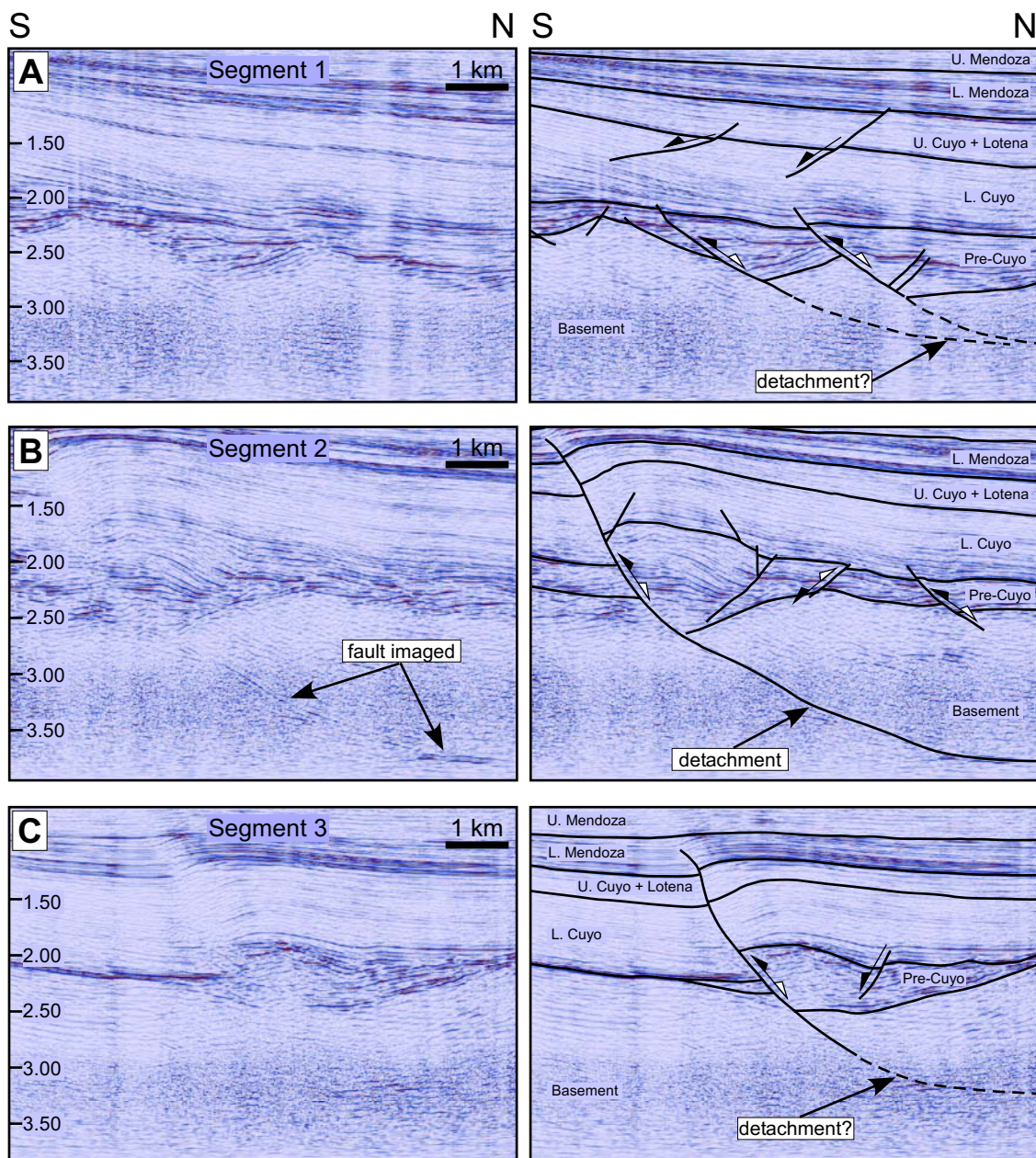
Figure 2.17. Uninterpreted and interpreted seismic sections through main fault segments 1, 2, and 3. Vertical scale is two-way time (seconds). See Figure 2.16 for location of seismic sections.

orientation of most faults of each type is very consistent (Figure 2.18), although the strikes of D1 faults show slight scatter and D3 faults deviate the least from the overall E-W orientation.

Fault dips for the "deep" system were measured on seismic profiles (time sections with minimum vertical exaggeration). Since most faults have a listric character, dips were consistently measured at the top of syn-rift strata. Equal-area plots for the three fault types (Figure 2.18) show that most syn-rift faults (i.e., D1 and D2 faults) dip toward the north, whereas D3 syn-inversion faults dip southward. Pole plots also show the larger scatter in fault attitude for D1 (syn-rift non-reactivated) faults.

Fault lengths were measured in map view at the top of syn-rift strata. Fault-length and fault-strike averages were determined for each fault type. These values then were plotted with fault-length and fault-strike standard deviations (Figure 2.19). Average strike for the three fault types differs slightly, with a difference of ~5° between D1 and D2 faults. Non-reactivated syn-rift faults (D1) are, on average, significantly shorter than their reactivated counterparts (D2 faults) although differences in length are smaller (i.e., lower standard deviation). Syn-inversion faults (D3) are the shortest and have the least scatter in length values. Syn-rift reactivated faults (D2) exhibit the greatest length variability, with a length range between 0.7 and 12.2 km. Smaller syn-rift synthetic and antithetic faults show the least amount of reactivation, whereas larger faults are strongly inverted.

Syn-inversion faults that cut the post-rift section show marked differences in geometry, attitude, and distribution with respect to faults that cut the syn-rift section.
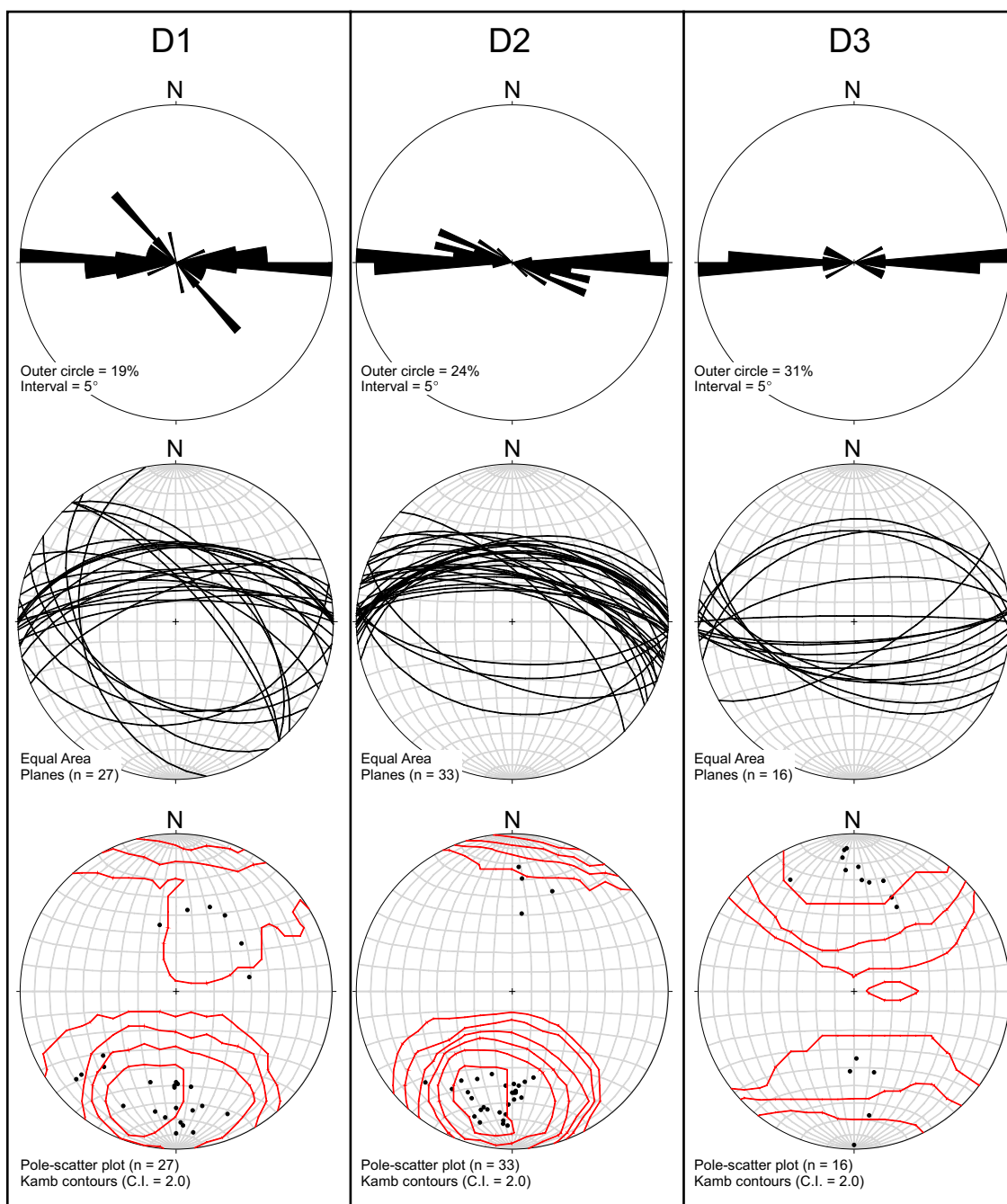
Figure 2.18. Rose diagrams, equal-area great circle and equal-area pole-scatter plots of faults at the syn-rift level. Fault types were defined based on fault kinematic history and time of development. D1: non-reactivated syn-rift faults; D2: reactivated syn-rift faults; D3: syn-inversion faults. Rose diagrams show orientation of fault traces in plan view. Note larger scatter in strike values for D1 faults. Equal area plots show orientation of fault planes. Most pre-existing faults (reactivated and non-reactivated) dip to the north. Most syn-inversion faults are antithetic (dip to the south).
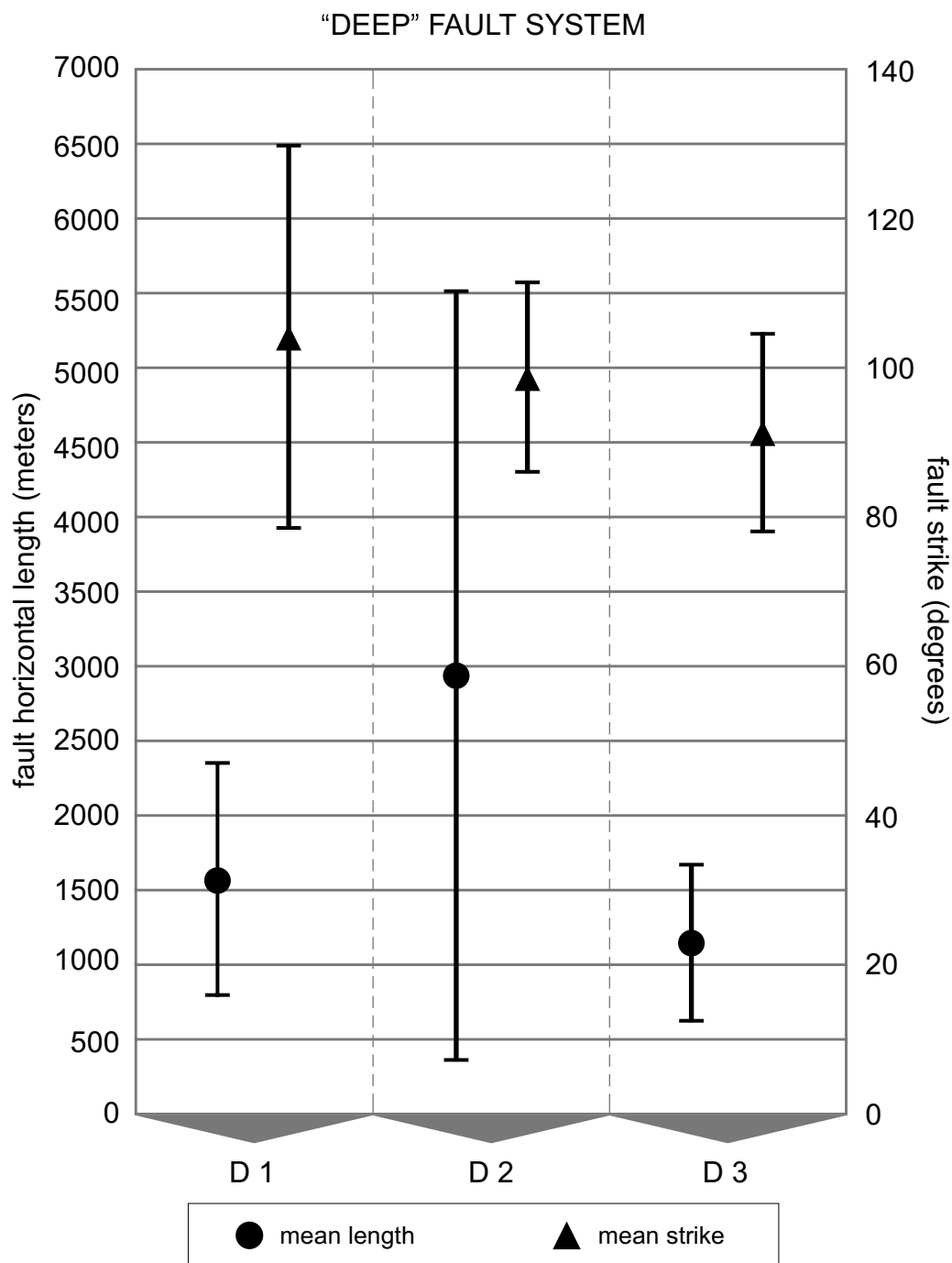
Figure 2.19: Summary plot of fault horizontal length and strike data (average and standard deviation) for the three fault types at the top of syn-rift strata. Note significant difference in average fault length between syn-rift non-reactivated (D1) and syn-rift reactivated faults (D2). Shorter syn-rift synthetic and antithetic faults show the least amount of reactivation, whereas longer faults are strongly inverted. Fault strikes for the three fault types differ by ~5°, although reactivated faults (D1 and D2) exhibit a more consistent strike. Domain D3 (syn-inversion) faults are the shortest and show the least variation in length values. Error bars correspond to one standard deviation.

Post-rift strata are cut by normal faults that are oriented N-S to NNW-SSE, dip predominantly to the west, and are mostly restricted to the SBS's hanging wall (Figure 2.20). These faults are grouped into three roughly N-S-trending domains that are recognizable at different stratigraphic levels on time-structure maps. The westernmost fault domain of the SBS's hanging wall (S1 faults; Figure 2.20) consists of NW-SE striking faults that extend ~10 km north of the master bounding fault. S1 faults exhibit a crude left-stepping *en échelon* pattern in map view that becomes less obvious southwestward, where S1 faults transition into a series of faults associated with another large inversion structure south of the SBS. On seismic sections perpendicular to the main bounding fault zone, S1 faults are imaged as upward-branching normal faults. Vertical displacement along the largest faults is greatest (~50 ms) at the top of Lower Cuyo horizon and diminishes upsection, with only minor local offset above the top of the Quintuco Formation. Vertical displacement on S1 faults diminishes downsection, becoming subseismic within basal Pre-Cuyo and basement levels (Figure 2.21).

The S2 fault domain in the center of the SBS inversion anticline consists of faults arranged in a right-stepping *en échelon* pattern. S2 faults extend ~12 km north of the SBS's master fault and flank the ATS on its western end. S2 faults are closely-spaced normal faults of roughly similar trace length at the top of lower Cuyo level. On vertical seismic sections, S2 faults are imaged as normal faults that splay upward from a relatively narrow but complex deformation zone at the syn-rift level (Figure 2.21). Both S1 and S2 fault domains converge slightly toward the south as they approach the master fault.
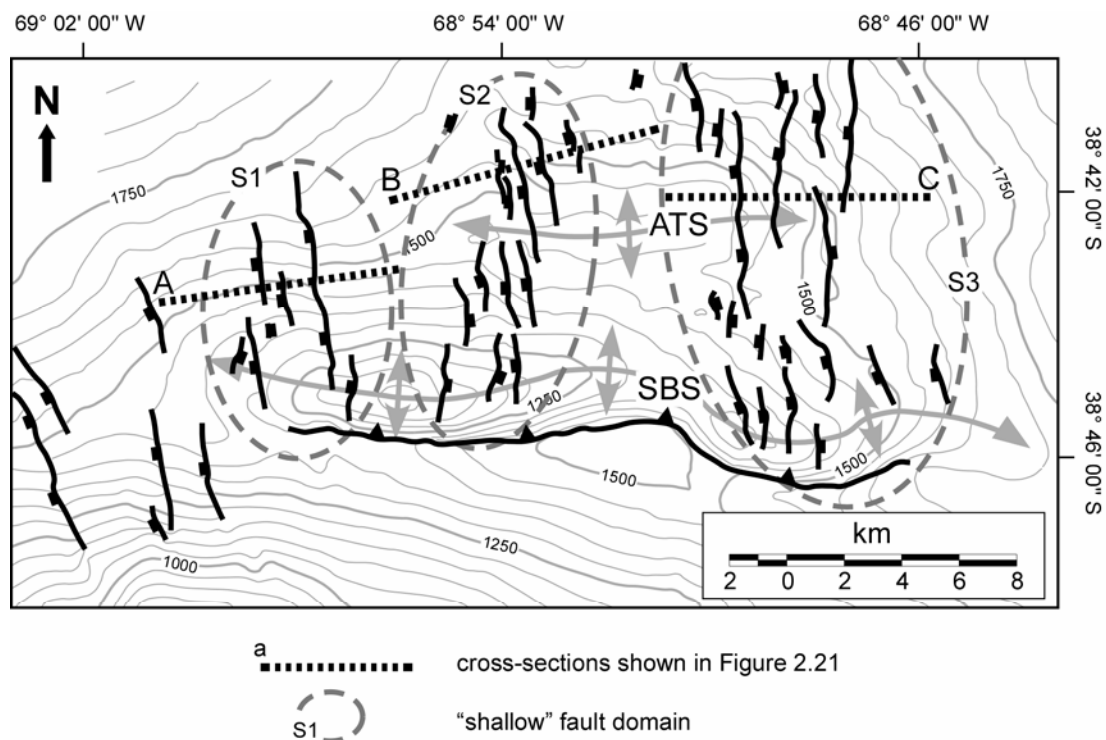
Figure 2.20. Time-structure map at the top of Lower Cuyo Group (Contour Interval = 50 ms), with "shallow" fault domains (encircled by dashed grey line) interpreted at this stratigraphic level. Fault domains S1, S2, and S3 group with approximately N-S orientation affecting the SBS's hangingwall and extend northward to cut the ATS.

The closely spaced faults of the S3 fault domain at the eastern end of the SBS extend for about 15 km north of the master fault to the eastern side of the ATS. S3 faults are arranged in a left-stepping *en échelon* pattern on both the eastern limb of the ATS and close to the SBS master fault, but the pattern is less obvious in the central part of the faulted area. On seismic sections, S3 normal faults converge downsection into a poorly-imaged deformation zone at the syn-rift level (Figure 2.21). Most S3 faults in the eastern SBS terminate upsection in lower parts of the Upper Cuyo Group. S3 faults flanking the eastern side of the ATS offset younger strata in the Lower Mendoza Group. The three

44
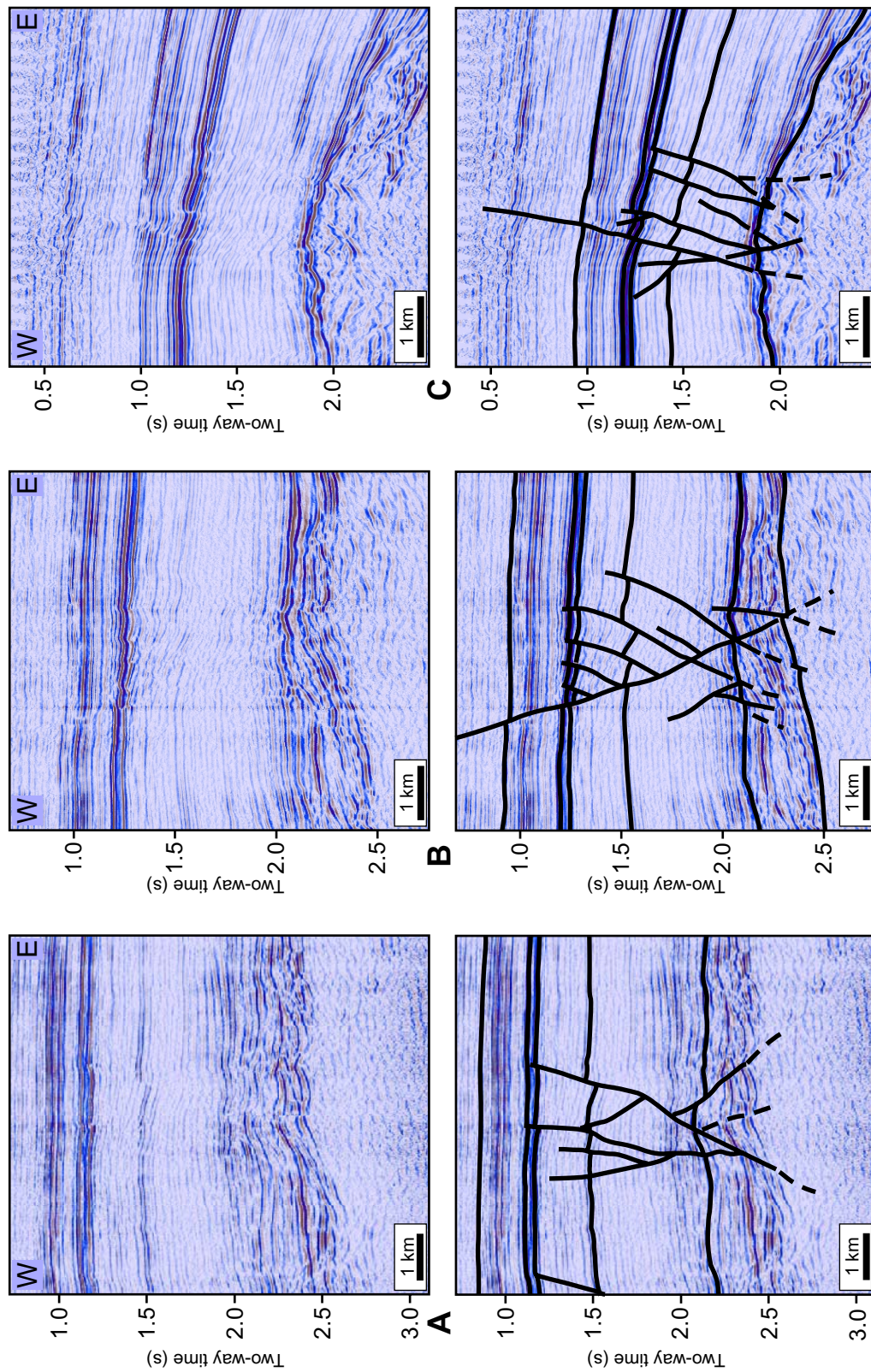
Figure 2.21. Uninterpreted (above) and interpreted (below) representative seismic profiles of "shallow" fault domains S1 (A), S2 (B), and S3 (C). See Figure 2.20 for location of profiles.

"shallow" fault domains are not restricted to regions of maximum uplift in either the

SBS or ATS.

Rose diagrams of fault traces in the three shallow fault domains (Figure 2.22)

show that S1 faults have the least variance, even though the number of samples is similar

for all cases (n = 25, 19, and 27 for S1, S2 and S3 domains, respectively). S2 faults show

significant variance, despite having the clearest *en échelon* fault arrangement. The

scatter reflects the gradual change from N-S trending faults close to the SBS master fault

to NNW-SSE trending faults on the eastern flank of the ATS. S3 faults have the greatest

variance in strike values, although 75% of the 27 fault strikes are between 152° and

180°.
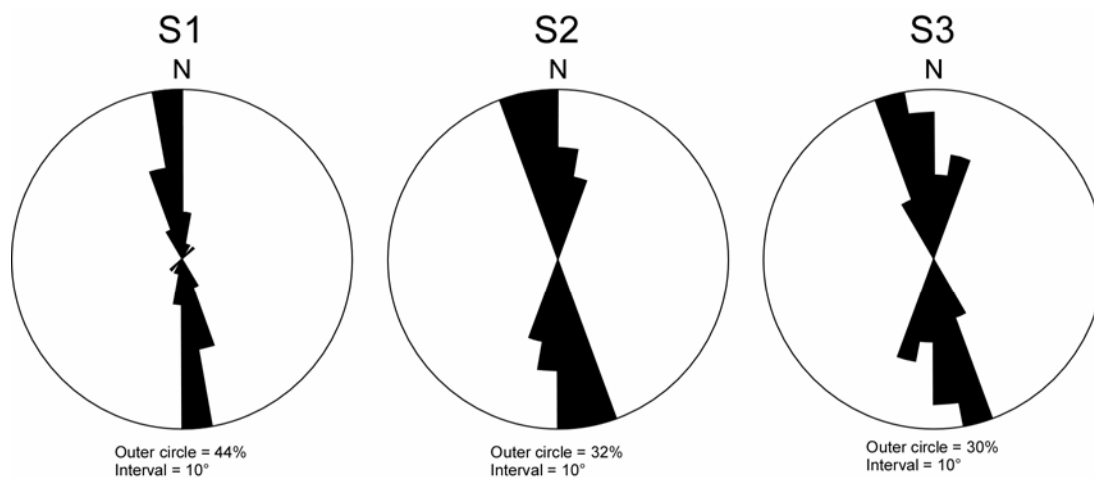
Figure 2.22. Rose diagrams displaying fault trace orientation for domains S1, S2, and S3 affecting mostly post-rift strata in the SBS's hangingwall.

Very subtle structural lineaments are also observed within the Upper Cuyo and

Lower Mendoza Group. These features are not obvious on time-structure maps and

vertical seismic profiles, but become prominent on time-dip maps (Figure 2.23). The
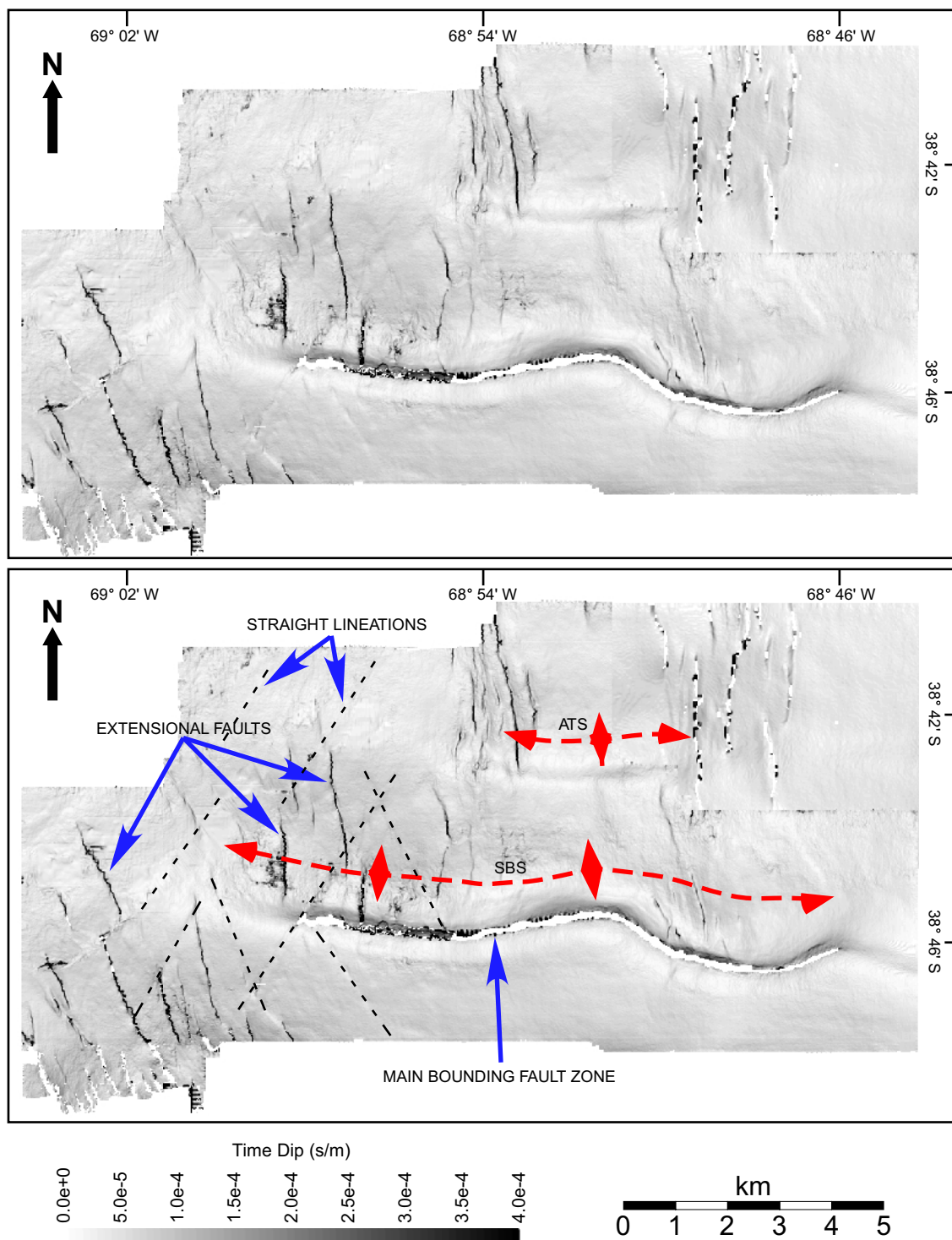
Figure 2.23. Unlabeled and annotated time-dip maps of the base of Vaca Muerta horizon. Darker shades indicate steeper dips. Main faults affecting the SBS's hangingwall are clearly visible. Subtle straight lineations are best imaged in the western part of the survey area and may correspond to conjugate sets of small-displacement faults.

lineaments are fairly straight and have two principal orientations: NW-SE and SW-NE. They are best imaged in the western part of the study area, whereas they are obscured by the dense normal faulting (S1, S2, S3 faults) that characterizes the SBS's hanging wall (Figure 2.23).

Along-axis variations in structural style

Along-axis variations in structural style are shown in seven 7 representative N-S oriented sections through the SBS and ATS (Figures 2.24, 2.25). Partitioning of contraction at the basement level changes gradually from more distributed (i.e., contraction accommodated by multiple shorter, small-displacement faults) in the structures' eastern and western ends (Figure 2.24A, F) to more localized along large-displacement faults in the areas of maximum uplift (Figure 2.24C, E).

Inverted half-graben fills show complex internal deformation, where style varies significantly along strike. These changes in style show that the syn-rift wedges did not behave as rigid blocks during inversion, with displacement occurring only along the main bounding fault. Additional faults were necessary to accommodate internal deformation during contraction upon inversion. One type of such structures is comprised by antithetic normal faults that do not involve basement (D3 fault type). They develop in the central and eastern portions of the structure and are associated with regions of maximum uplift. Antithetic reverse faults (back-thrusts) of the D2 and D3 fault types, though not the dominant mechanism, play a important role in accommodating contraction of the syn-rift wedges and are no necessarily restricted to areas of maximum uplift (Figure 2.24C-E). The central portion of the structure, around the eastern
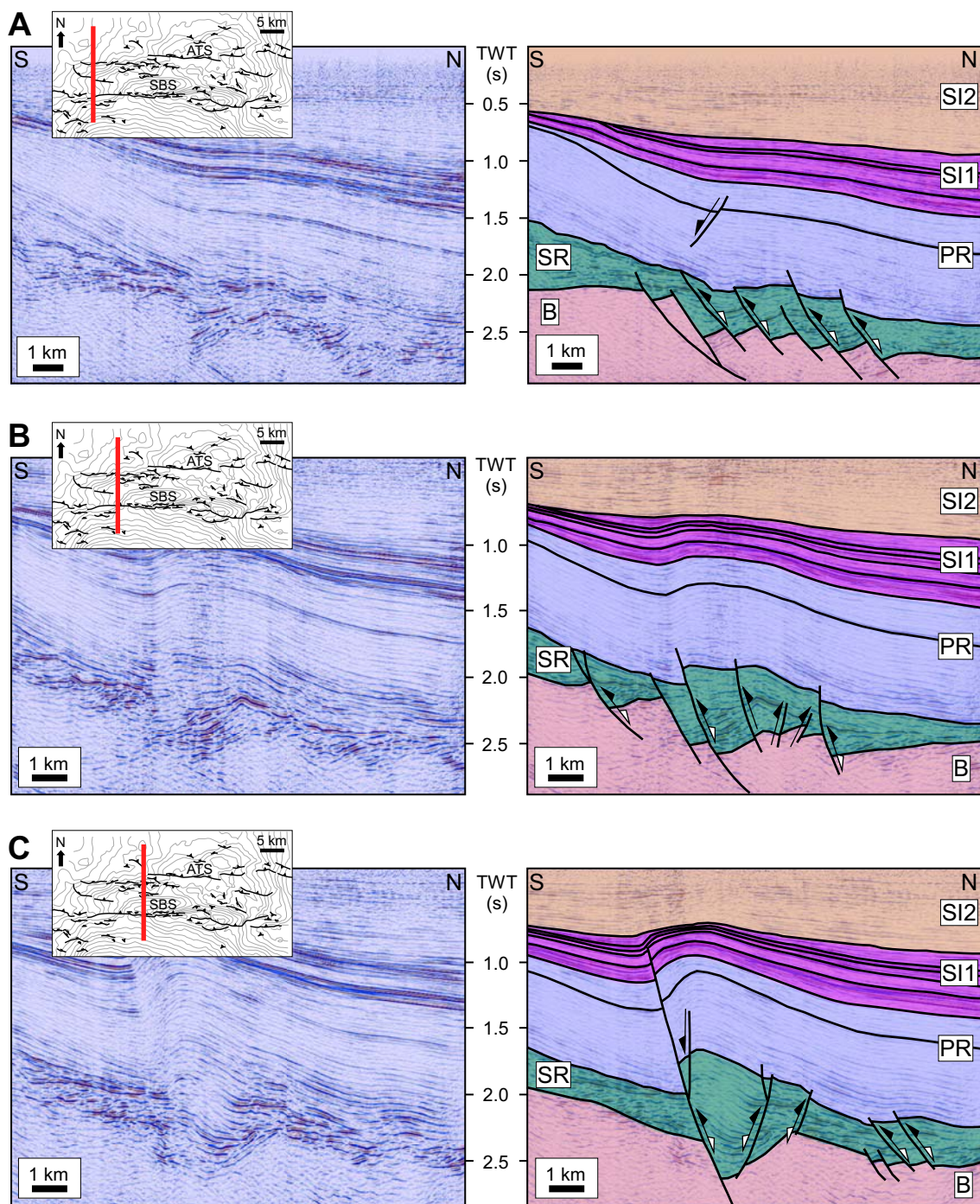
Figure 2.24. Uninterpreted (left) and interpreted (right) seismic profiles A, B, and C through the SBS. Insets show location of seismic sections and faults at the top of syn-rift level. B = Basement; SR = Syn-rift strata; PR = Post-rift strata; SI1 = Syn-inversion 1 strata; SI2 = Syn-inversion 2 strata.

Figure 2.24 - Continued. Uninterpreted (left) and interpreted (right) seismic profiles D, E, and F through the SBS. Insets show location of seismic sections and faults at the top of syn-rift level. B = Basement; SR = Syn-rift strata; PR = Post-rift strata; SI1 = Syn-inversion 1 strata; SI2 = Syn-inversion 2 strata.
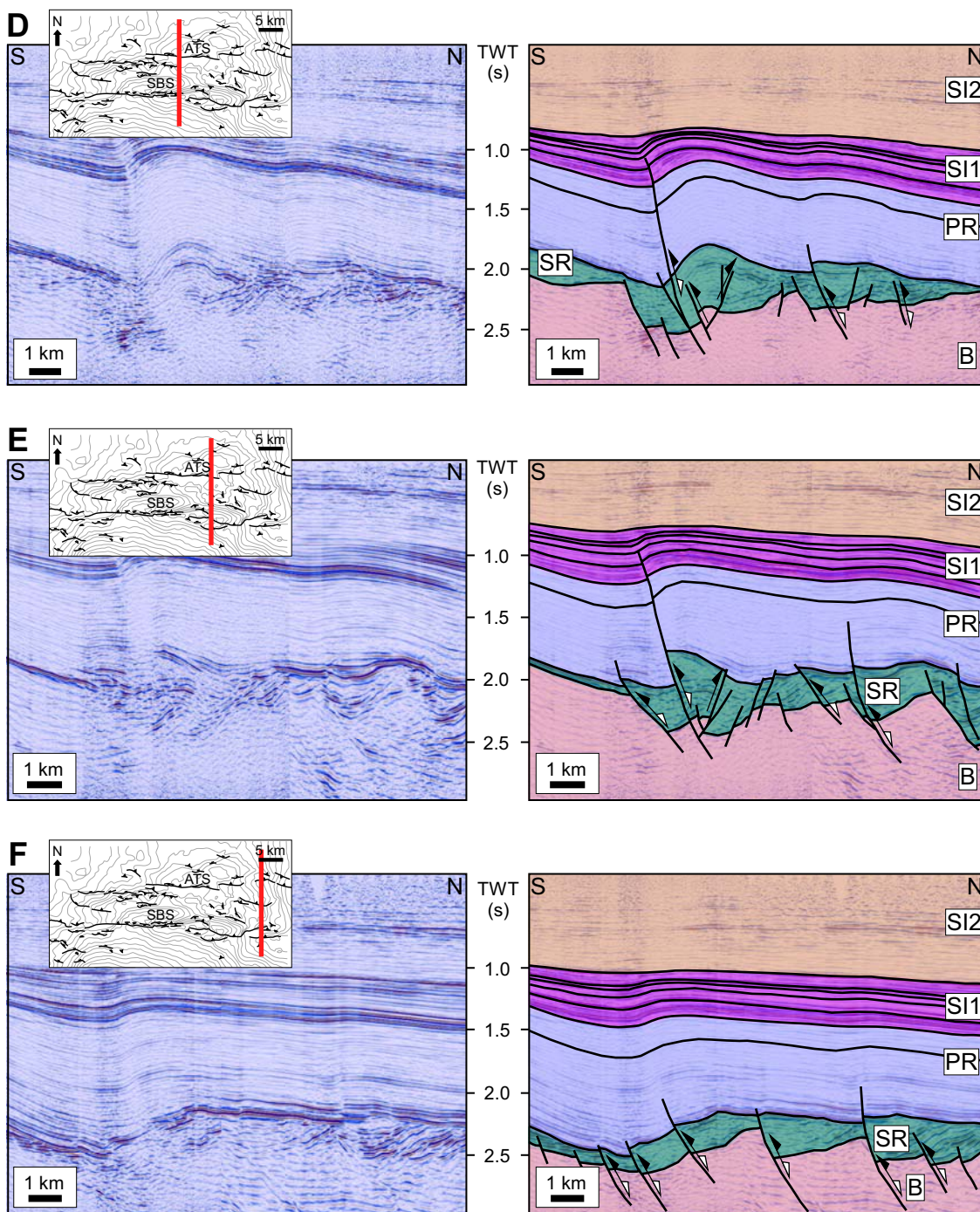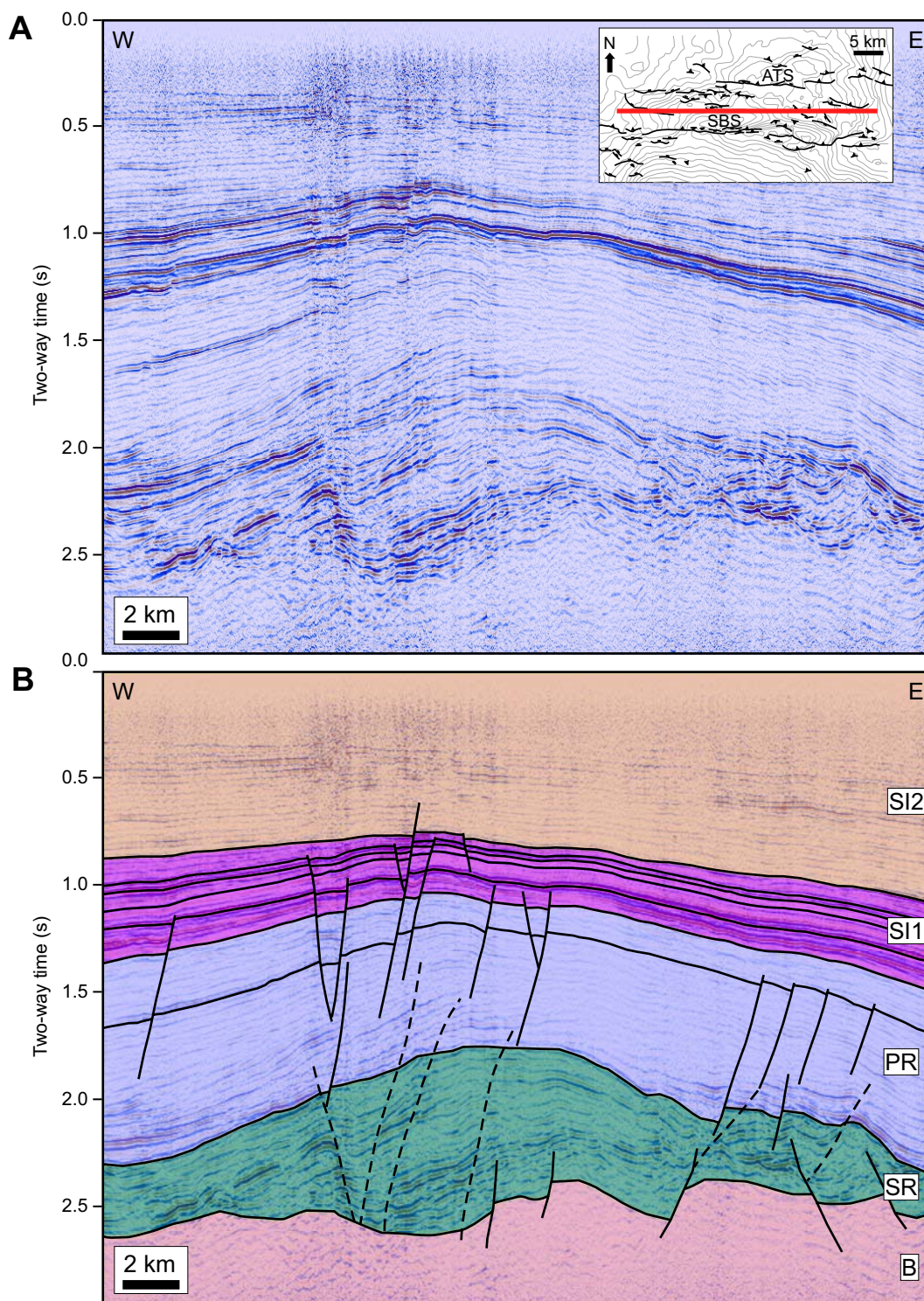
Figure 2.25. Uninterpreted (A) and interpreted (B) seismic profile G, which trends along the axis of the SBS. Inset shows location of seismic section and faults at the top of syn-rift level. Note greatest general uplift in central part of SBS. B = Basement; SR = Syn-rift strata; PR = Post-rift strata; SI1 = Syn-inversion 1 strata; SI2 = Syn-inversion 2 strata.

accommodation zone, exhibits more ductile deformation of the syn-rift wedge with minimum visible displacement along major faults, as suggested by the folding of the structure's core (Figure 2.24E).

Along-dip shortening of the post-rift section is partially accommodated by the development of a fault-propagation fold. The curvilinear trace of both the main bounding fault and adjacent fold are clearly visible on time-structure maps at different stratigraphic levels within the post-rift section (Figures 2.14, 2.20, 2.23). This contrasts with the rather more rectilinear but fragmented nature of the fault trace at the syn-rift level, which suggests the up-section linkage of different fault segments into a single fault plane of sinuous character.

Reverse displacement along the main bounding fault decreases upsection over the entire inversion structure, but varies significantly along strike. It is greatest in the two regions of highest uplift, and minimum in the center of the structure (over the eastern accommodation zone) and towards the structure's ends. A significant change in the proportion of bounding fault with net normal displacement and net reverse displacement (R_i) is observed along the SBS. In some segments of the structure, where the inversion index is greatest, the top of basement is interpreted to have reverse offset (e.g., Figure 2.24D, E), showing that the syn-rift wedge has been completely inverted and the basement contracted beyond the pre-rift state.

The kinematic history of structural elements and growth stratal patterns of the ATS are similar to those of the SBS. Along-strike variations in structural style, however,

are less dramatic in the ATS, with inversion-related shortening accommodated mostly by reverse displacement along the half-graben bounding fault (Figure 2.24D).

Evidence for fault interactions during extension and inversion

Careful analyses of syn-rift and syn-inversion fault systems and growth strata are necessary to evaluate the relative influence of preexisting faults on later inversion. In order to approximate the pre-inversion configuration of syn-rift half-grabens that form the core of the SBS, a traverse seismic section in mid-hanging wall position through the structure was flattened at the top of the syn-rift strata (Figure 2.26).

Two main depocenters, separated by an accommodation zone, are obvious on the flattened seismic section. The western depocenter is larger. Onlap of basal syn-rift strata against basement is apparent on the flattened sections, as well as divergent stratal patterns within the syn-rift fill. The top of the syn-rift wedge was downlapped by Lower Cuyo strata that apparently prograded from east to west across filled half-graben depocenters during early post-rift stages.

Lateral continuity of upper syn-rift strata across the eastern accommodation zone between the syn-rift half-graben depocenters indicates linkage of main bounding faults during extension. Some syn-rift deposition occurred before linkage, however, as indicated by onlap patterns within two distinct depocenters. This arrangement of syn-rift fault systems and accommodation zones contrasts with the single through-going curved fault zone that defines the southern boundary of the SBS inversion anticline (Figures 2.14, 2.16, 2.23). The sinuous character of this fault zone, as well as the geometry of the anticline's axial plane, however, are related to the location of the main basin-bounding
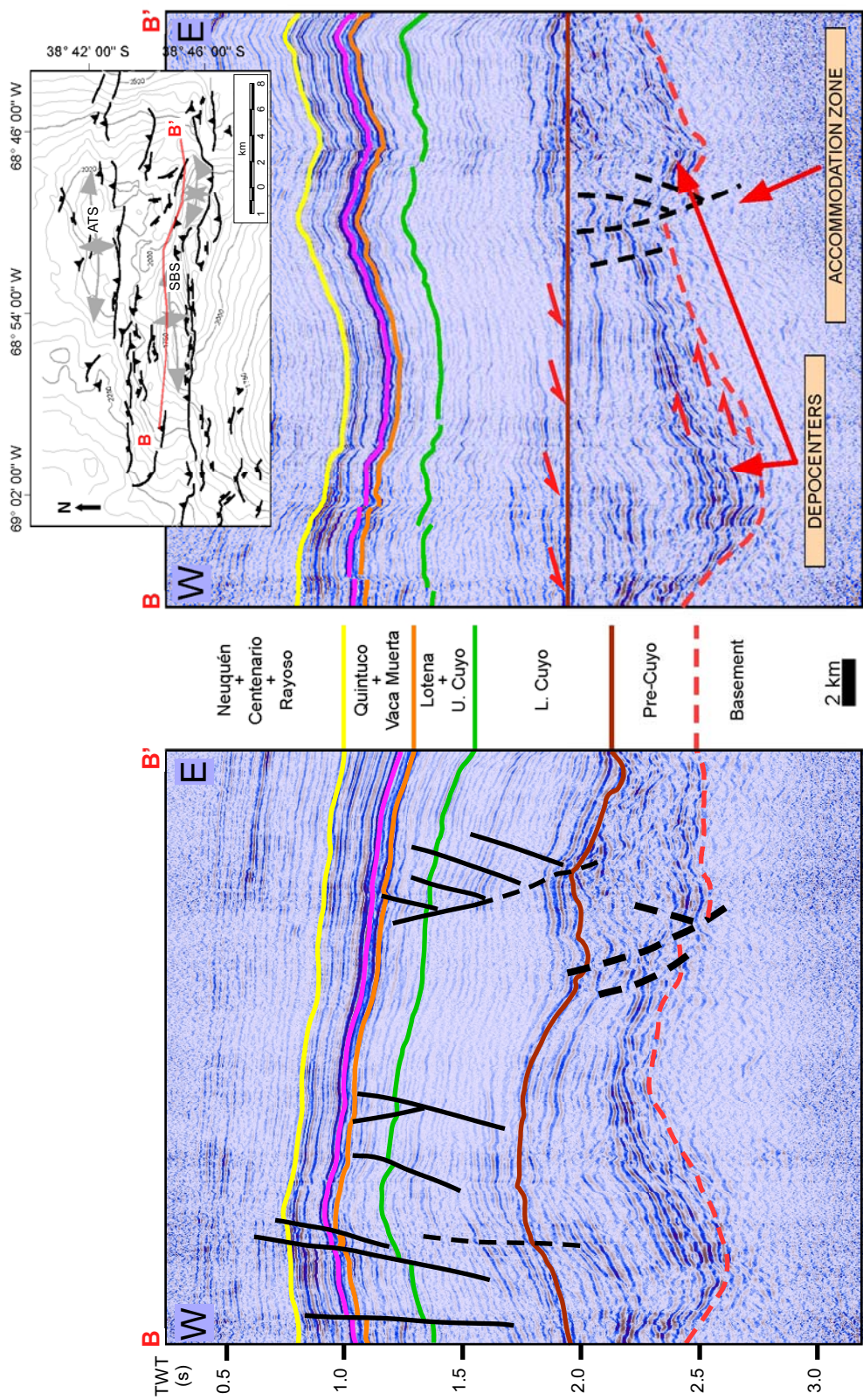
Figure 2.26. Unflattened (left) and flattened (right) seismic profiles through the SBS (mid-hanging wall position). Flattening removes structural perturbations below a reference horizon (top pf syn-rift in this case). Distortion is due to non-conservation of area or line length.

extensional fault segments and accommodation zones. In addition, the areas of greatest

inversion in each substructure of the SBS and ATS coincide with the thickest parts of the

syn-rift wedges, whereas less inversion occurred along the inferred syn-rift

accommodation zones.

Syn-inversion Growth strata

Multiple unconformities and complex stratal patterns within syn-inversion

growth strata of the SBS and ATS record the pulsed nature of inversion during Early

Jurassic to Late Cretaceous time (Figure 2.8). The best developed growth strata are

formed on the flanks of inversion anticlines within the Lower Mendoza Group (or

Quintuco Formation).

Depositional facies, stratal termination patterns, and time-thickness (or isochron)

maps of different intervals within the Quintuco Formation were investigated in order to

document the interactions between depositional systems and the growing inversion

highs. The Quintuco Formation was divided into four intervals that are bounded by five

seismic horizons (see "Seismic-stratigraphic relationships") and referred to here as, from

bottom to top, Quintuco I, II, III, and IV.

Quintuco I is underlain by the shale facies of the Vaca Muerta Fm. The base of

Quintuco I is seismic horizon BQC (Base Quintuco) and its top is IQ1 (Intra-Quintuco

1). Horizon BQC probably corresponds to a significant flooding event, which was

followed by SE to NW prograding outer-shelf shale and marl facies of the lowermost

Quintuco Fm. (Figure 2.27B, C). The Quintuco I interval thickens toward the north

(Figure 2.27A) and this suggests deepening of the basin in that direction. Quintuco I
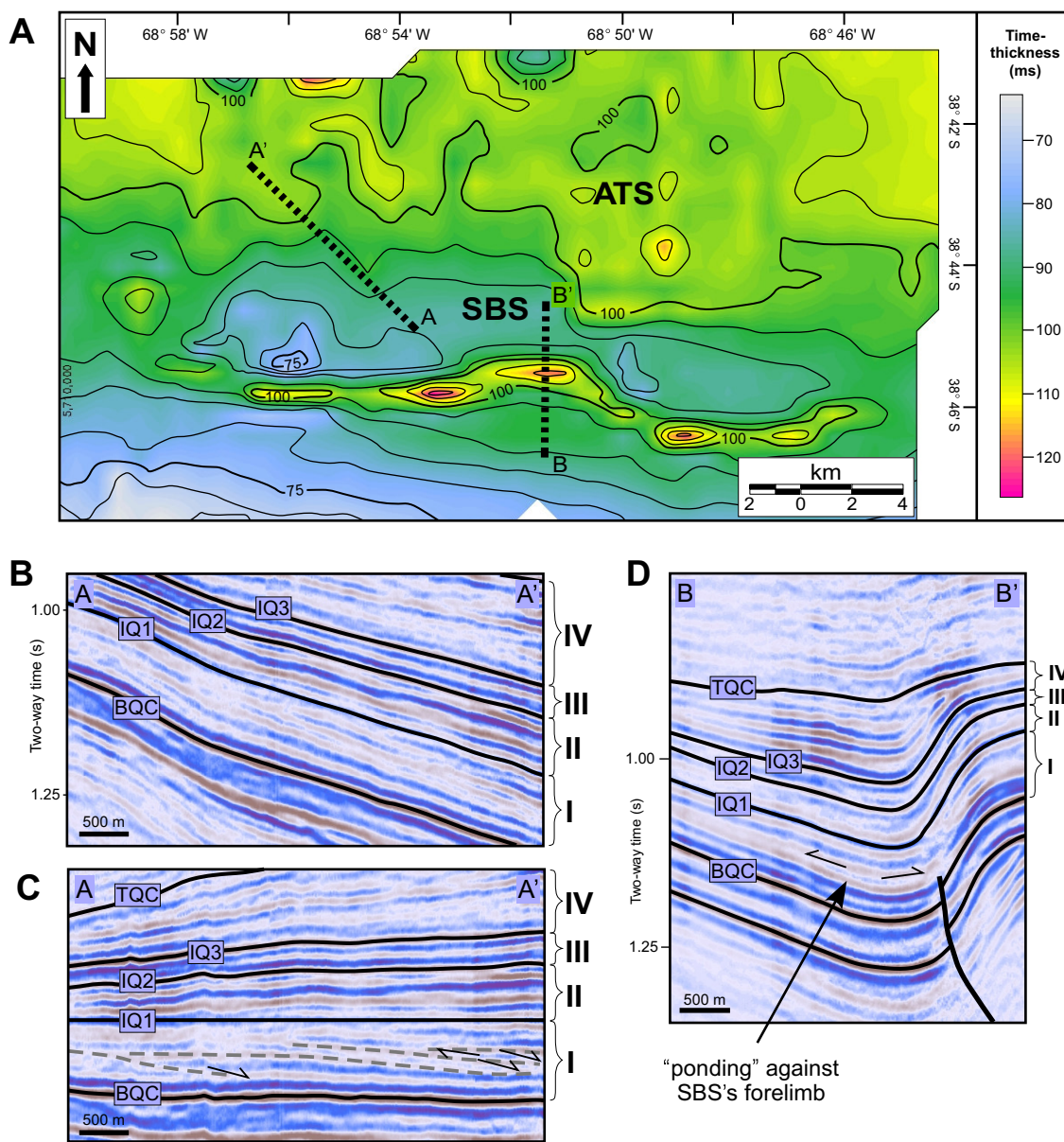
Figure 2.27. Lateral thickness variations, seismic facies and stratal termination patterns for Quintuco I growth strata. (A) Time-thickness map of Quintuco I over the SBS and ATS (Contour Interval = 5 ms). Thickness variations are evident over the SBS but do not affect the ATS. (B) Unflattened interpreted seismic profile representative of the facies character and stratal geometries of Quintuco I. (C) NW-prograding clinoforms imaged on an interpreted seismic profile flattened at the top of Quintuco I (IQ1 seismic horizon). d: Onlapping strata within Quintuco I in syncline that bounds the SBS to the south.

thins over the SBS's crest and thickens into the narrow syncline that bounds the structure to the south. No significant thickness variations in Quintuco I are associated with the ATS.

Bathymetry created by the growth of the SBS during late Tithonian to early Berriasian time may have caused some of the NW-prograding strata of Quintuco I to partially "pond" against the forelimb of the evolving structure (Figure 2.27D). The ATS, further north, does not seem to have been active during Quintuco I deposition, as there no thickness variations are observed.

Quintuco II onlaps the IQ1 horizon along the northern flank of the SBS; the Intra-Quintuco 2 horizon (IQ2) is the upper bounding surface of Quintuco II (Figure 2.28B, C). Quintuco II is characterized by strong parallel and continuous reflections that onlap the IQ1 horizon and are parallel to IQ2 except on the SBS's crest, where low-angle stratal terminations beneath IQ2 are apparent. Onlap within Quintuco II is also observed locally along the northern flank of the ATS (Figure 2.28D). These stratal relationships suggest the existence of antecedent bathymetry at the time of deposition and may also reflect minor syn-depositional growth of both anticlines during Berriasian(?) time. Most thickness variations within Quintuco II are restricted to the SBS, although incipient influence of the ATS is likely (Figure 2.28A).

The relatively thinner growth strata of Quintuco III are imaged as a group of reflections that onlap horizon IQ2 but are apparently conformable at the top of the unit, which is a high-amplitude positive reflection mapped as IQ3 (Intra-Quintuco 3 horizon). Seismic facies within Quintuco III consist of parallel to sub-parallel, high-amplitude, and
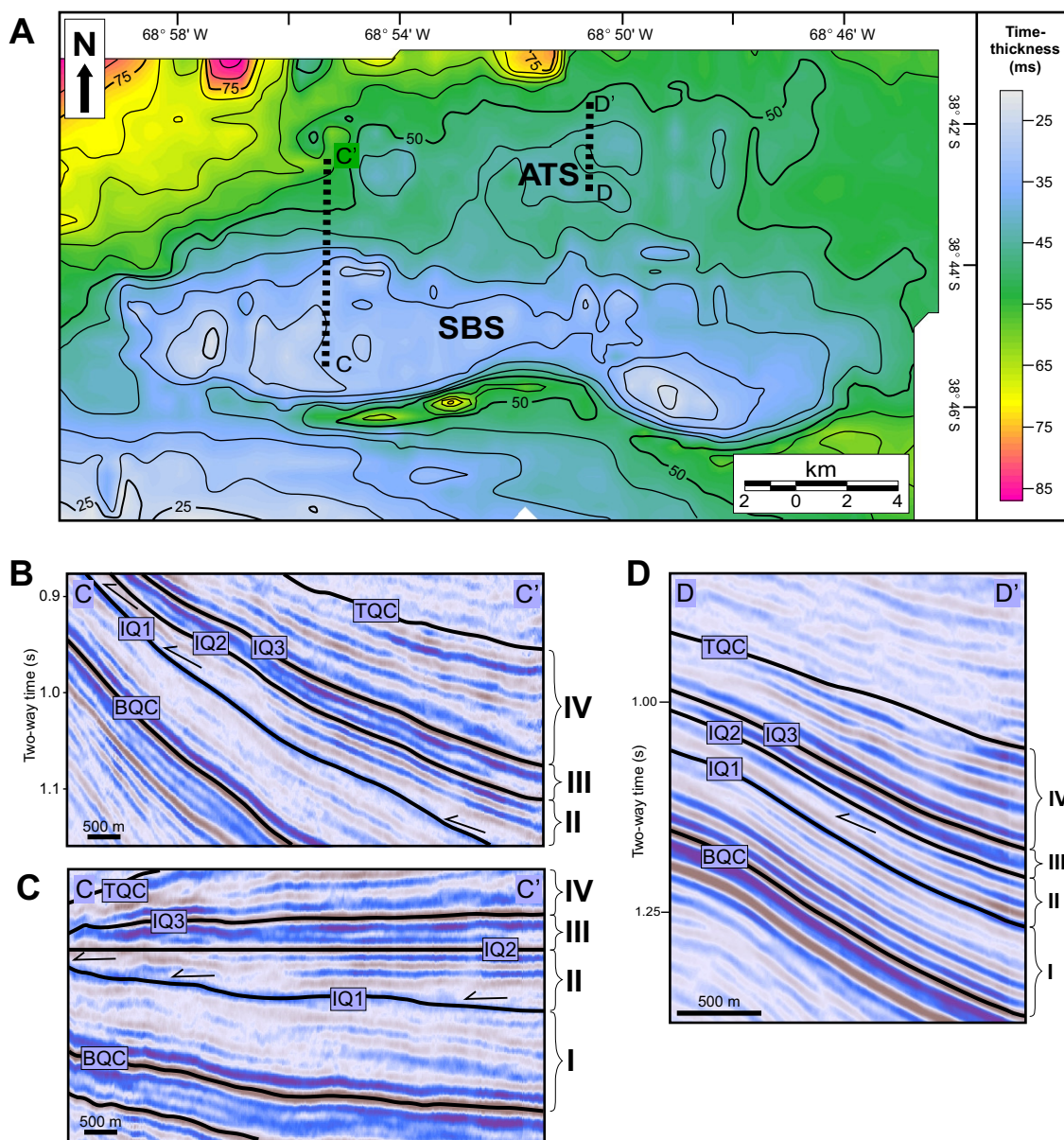
Figure 2.28. Lateral thickness variations, seismic facies and stratal termination patterns for Quintuco II growth strata. (A) Time-thickness map of Quintuco II over the SBS and ATS (Contour Interval = 5 ms). Thickness variations are noticed over both SBS and ATS. (B) Unflattened interpreted seismic profile representative of the facies character and stratal geometries of Quintuco II, characterized by onlap to seismic horizon IQ1. (C) Onlap stratal terminations imaged on an interpreted seismic profile flattened at the top of Quintuco II (i.e., along seismic horizon IQ2). (D) Onlapping strata within Quintuco II in back limb of ATS.

laterally continuous reflections at the base and top, which bound a group of dimmed but still laterally continuous parallel reflections (Figure 2.29B). Quintuco III varies in time-thickness from 8 ms along the crest of the inversion structures to about 16 ms along their flanks, with a locally thicker region (up to 47 ms) over the syncline that bounds the SBS to the south (Figure 2.29A). The minor thickness variations and parallel internal reflections within Quintuco III suggest this interval was deposited during a period of relative tectonic quiescence. The low-amplitude character of Quintuco III reflections may be indicative of muddy facies which could have draped any antecedent topography that existed at the time of deposition. Slightly thicker Quintuco III strata on the southern limb of the SBS suggest subtle bathymetric relief which may have caused "ponding" of some sediment.

Basal Quintuco IV reflections show low-angle onlap onto horizon IQ3. The top of Quintuco IV (horizon TQC) is a significant erosive unconformity (Intra-Valanginian) that separates the Upper and Lower Mendoza Groups (Figure 2.30B). Quintuco IV seismic facies are characterized by parallel to slightly divergent, high-amplitude reflections.

Time-thickness variations within Quintuco IV strata are greater than for any other interval of growth strata, reaching values over 100 ms between the SBS's crest and adjacent synclinal areas (Figure 2.30A). Quintuco IV is thickest in the syncline that bounds the structure to the south. Strata onlap both limbs of the syncline, especially along the central and eastern parts of the SBS (Figure 2.30C). Internal onlap and stratal truncation are also observed near the crests of the SBS and ATS Upper Quintuco strata
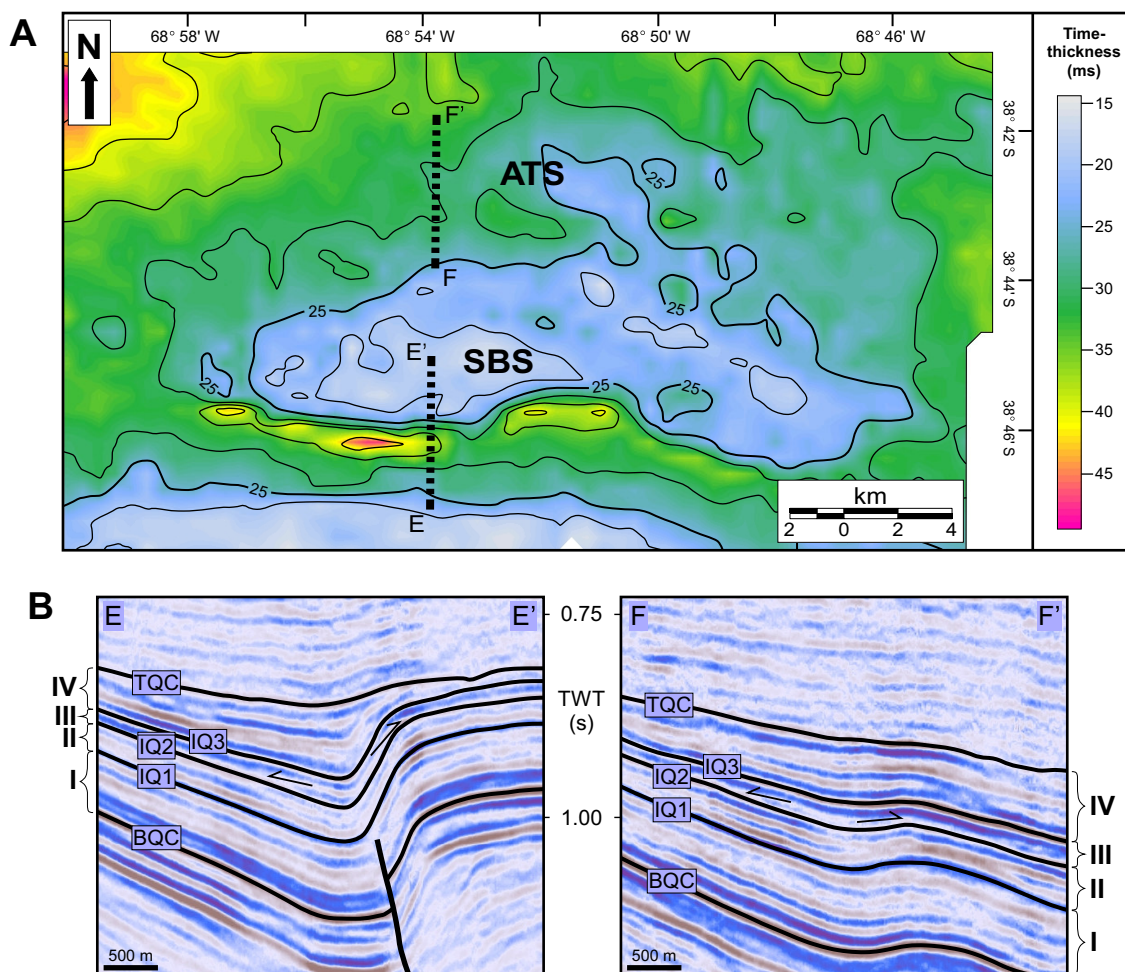
Figure 2.29. Lateral thickness variations, seismic facies and stratal termination patterns for Quintuco III growth strata. (A) Time-thickness map of Quintuco III over the SBS and ATS. Thickness variations are subtle over both SBS and ATS (note low range; Contour Interval = 5 ms). (B) Along-dip interpreted seismic profiles through the forelimbs of SBS (left) and ATS (right). Incipient internal onlap onto seismic horizon IQ2 restricted to structural lows.
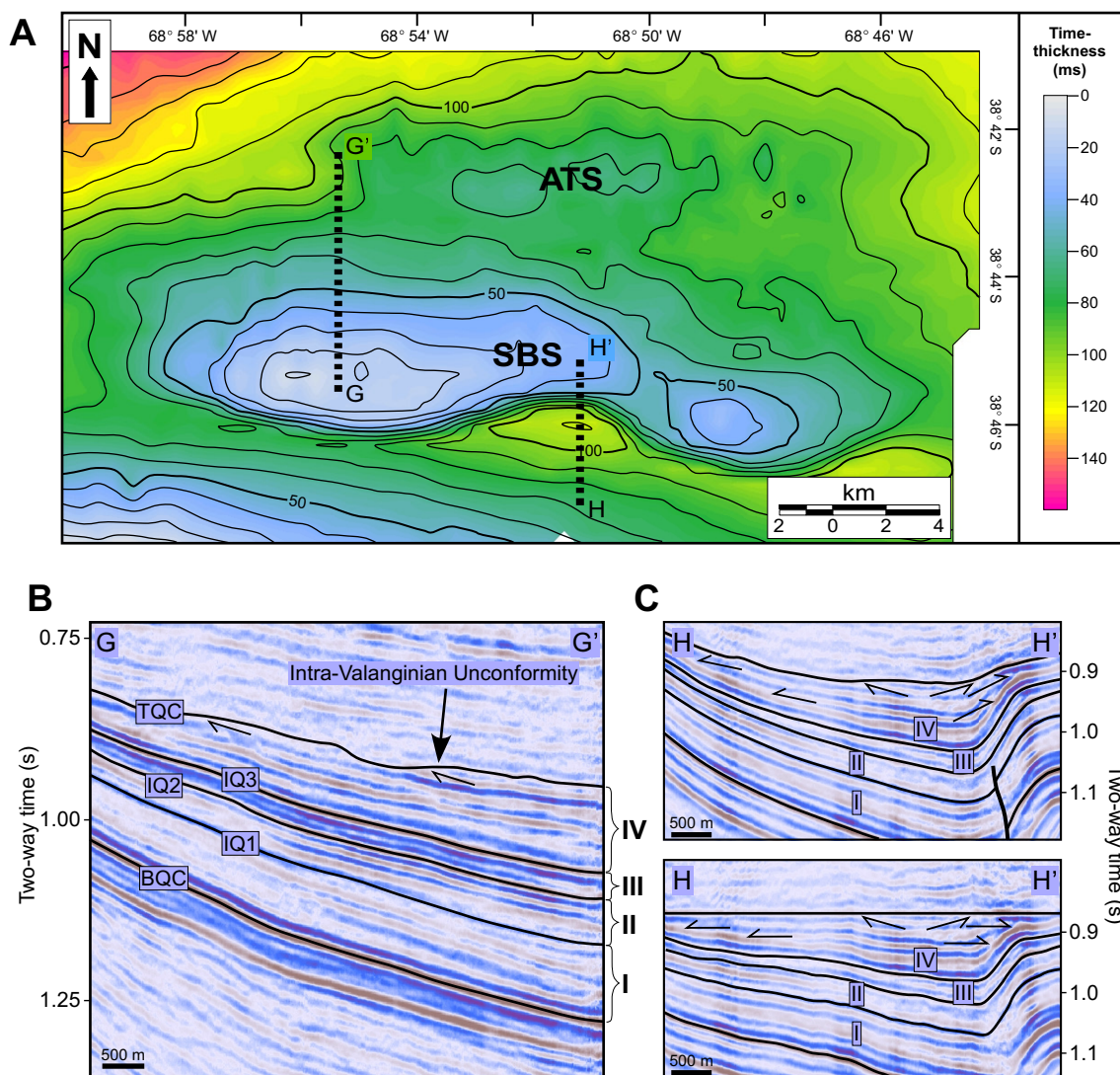
Figure 2.30. Lateral thickness variations, seismic facies and stratal termination patterns for Quintuco IV growth strata. (A) Time-thickness map of Quintuco IV over the SBS and ATS (Contour Interval = 10 ms). Thickness variations are significant over SBS and ATS (see time-thickness range). (B) Along-dip interpreted seismic profile through SBS's backlimb showing truncation at the Intra-Valanginian unconformity. (C) Time-thickness maxima and onlap against SBS's forelimb.

are highly eroded and truncated beneath the Intra-Valanginian unconformity, so Quintuco IV isochron map reflects the combined effects of Valanginian erosion and syn-tectonic deposition.

On along-strike sections, growth strata onlap the structures' eastern and western terminations and exhibit reflection patterns that are similar to those observed on across-strike sections (Figure 2.31B and C). The along-strike view shows the curved nature of the master bounding fault as it intersects the profile (Figure 2.31A). Laterally traceable onlapping reflections indicate synchronous uplift of both substructures and the development of accommodation space for sediments to "pond" in the frontal syncline between segments 2 and 3 of the SBS's main bounding fault (Figure 2.31D).

Section restoration and structure kinematics

The viability of the structural interpretation of the SBS was tested by balancing and restoring a cross-section through the structure to its pre-extensional stage. This analysis contributed to a better understanding of the geological evolution of the structure and allowed the estimation of amounts of extension and contraction along the structure from Late Triassic to Late Cretaceous time. Restoration also contributed to visualizing stratal geometries before and during the different Mesozoic inversion events. The western depocenter of the SBS was chosen for restoration because the amount of inversion is greatest there. In addition, the shape of the master fault at depth is best imaged in this region, which further constrains the restoration.
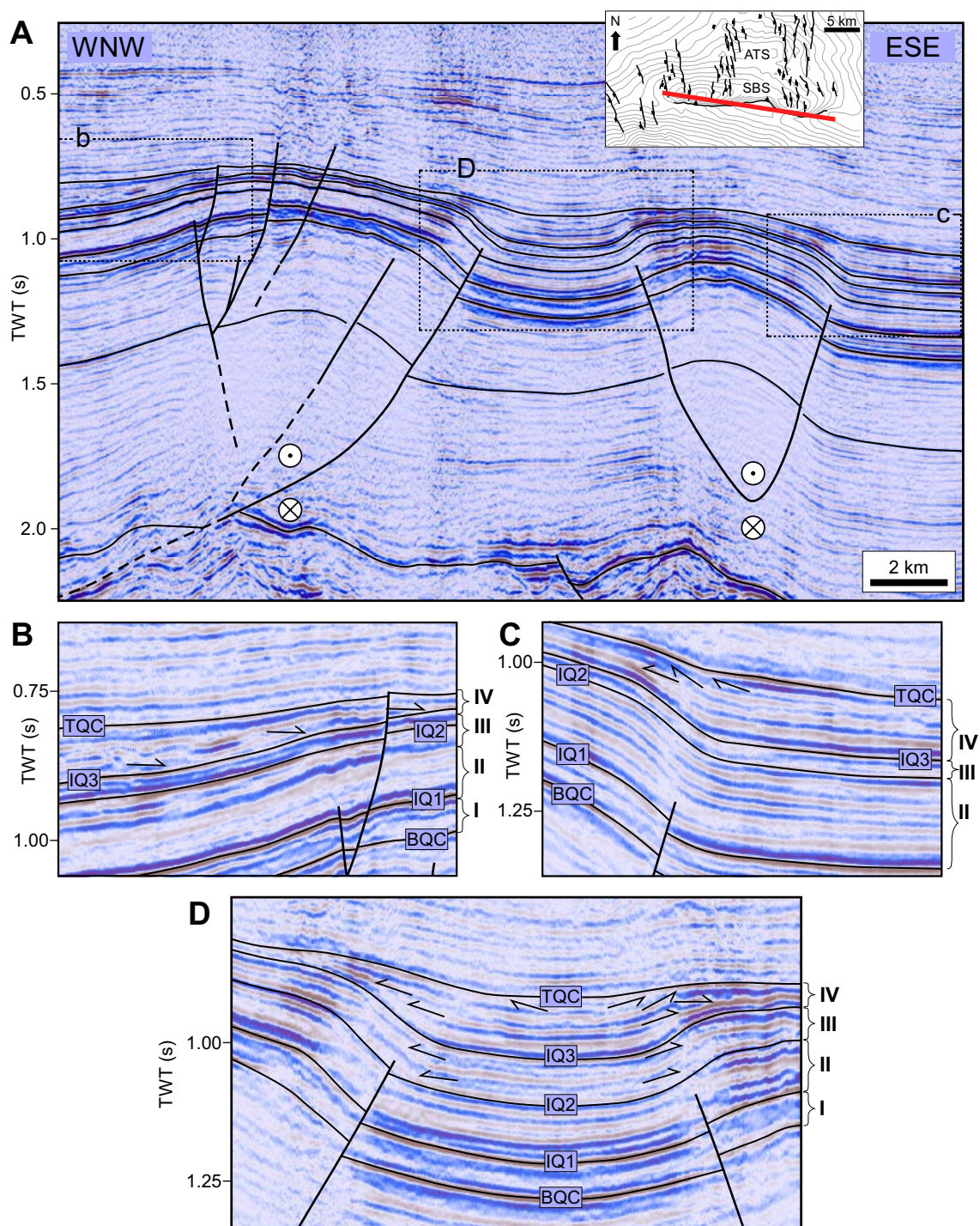
Figure 2.31: Along-strike growth-stratal geometries. (A) Near strike-parallel section intersecting the master fault's curved surface. Inset indicating profiles location shows fault traces at a stratigraphic level within the post-rift strata. (B) Detail of onlaps within Quintuco IV on SBS's western substructure. (C) Detail of onlaps and truncations within Quintuco IV on SBS's eastern substructure. (D) Detail of onlaps and lentiform stratal packages between SBS's substructures.

Tectonic transport directions

A balanced cross section should be ideally constructed in the direction of tectonic transport, which must be estimated based on kinematic indicators or structural features. For inverted rift basins, however, the transport direction is especially difficult to estimate because syn-rift extension and syn-inversion contraction may not be coaxial. Careful selection of transport direction(s) minimizes the departure from the plane-strain constraint for two-dimensional restorations. If the angle between the restored cross section and the direction of extension is <25°, then the error in the estimated amount of extension will be <10% with respect to an ideally-oriented section (Dula, 1991; Hill and Cooper, 1996). Applying the same concept to both contraction and extension directions, a cross section can be restored for transport directions up to 50° apart, if the cross section bisects the angle (Hill and Cooper, 1996).

Extension directions can be determined by analyzing the rotation or tilting of basement blocks (Scott et al., 1994). The true dip direction of pre-rift (or early-syn-rift) beds is assumed to be parallel to the extension direction regardless of fault orientation (cf. Scott et al., 1992; Scott et al., 1994; Cooper, 1995; Hill and Cooper, 1996).

The 3D seismic coverage of the study area allowed measurement of dip directions of early syn-rift beds over the western part of the SBS. Since only true dip directions were determined, no depth conversion of the seismic volume was necessary. Seventy six dip directions were determined in non-inverted parts of the western rift depocenter of the SBS and in some inverted areas after flattening along the top of syn-rift wedge (Figure 2.32A). The mean dip direction, with an azimuth of 199°, was used as
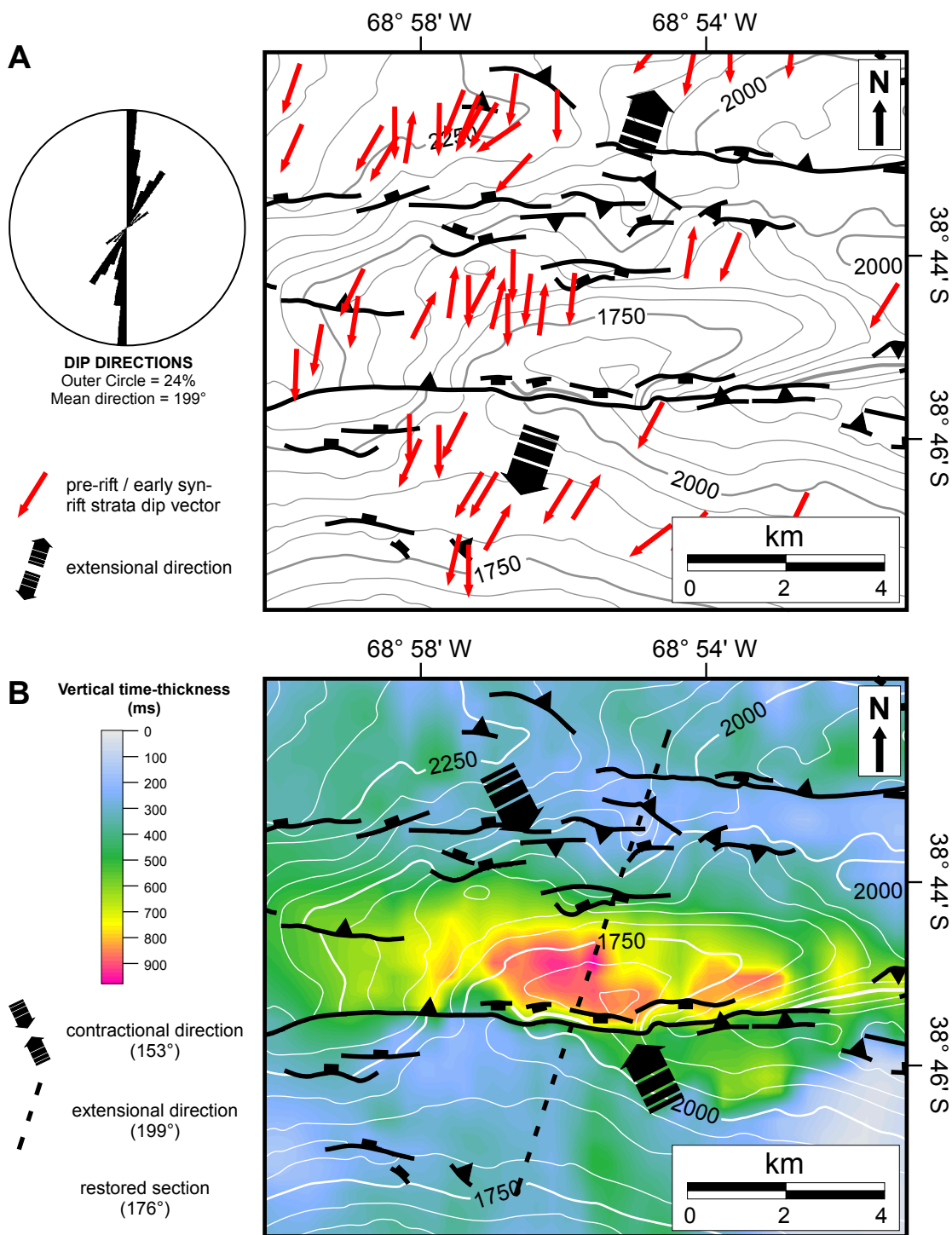
Figure 2.32. Estimated extension and contraction directions for the SBS's western depocenter. (A) Rose diagram and map distribution of measured dip directions for pre-rift and early syn-rift strata. (B) Syn-rift time-thickness map overlapped by time contours for the top of the syn-rift interval (Contour Interval = 50 ms). At this stratigraphic level, the crest of the anticline is offset to the SE with respect to the zone of syn-rift maximum thickness. This is interpreted as the result of NW-oriented compression and inversion.

the extensional transport direction. This represents a clockwise rotation of ~20° with respect to the extensional direction that would have been estimated by assuming transport was perpendicular to the E-W oriented longest fault traces.

Common criteria for determining the contractional transport direction are the shape and orientation of curved anticlinal crest formed by inversion (Woodward et al., 1989; Hill and Cooper, 1996). In the case of the inverted western depocenter of the SBS, the roughly east-west curved anticline indicates a N-S compressional transport direction. Closer examination of the inverted western depocenter, however, shows that the structure's crest at the top of the Pre-Cuyo syn-rift section is shifted ~1 km southwestward of the thickest Pre-Cuyo strata (Figure 2.32B). This offset may reflect NW-SE oblique contraction, which would cause the thicker portion of the syn-rift wedge to be obliquely displaced during inversion and to result in greater uplift within thinner parts of the syn-rift fill (Figure 2.33). The contractional transport direction can be then reasonably approximated by assuming its parallelism to a line connecting the syn-rift wedge's thickness and uplift maxima, which has an azimuth of ~153° for the inverted western depocenter (Figure 2.32B). The contractional features associated with the SBS's western substructure suggest a predominant dip-slip motion along the main bounding fault during inversion. The assumption then of NW-to-SE transport is reasonable and is in agreement with regional deformation patterns, which indicate the study area is within a larger zone of right-lateral transpressive deformation.

The estimated syn-rift and syn-inversion transport directions form an angle of 46°. A bisecting seismic section with an azimuth of 176° was selected for structural

restoration. Such orientation, within 25° from compression and extension directions,

should result in restorations with small error in the estimated amount of extension and

shortening.
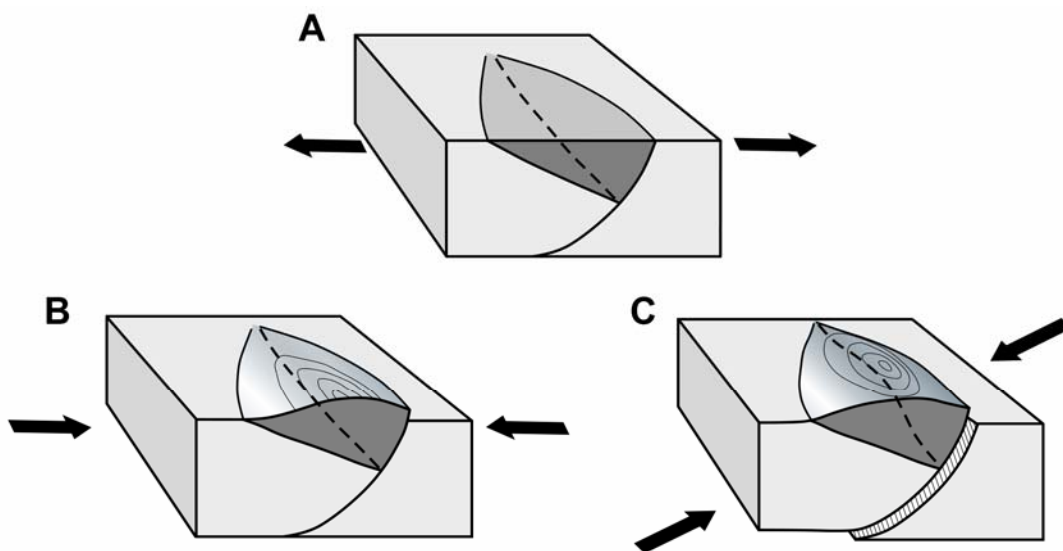
Figure 2.33. Compressional transport direction in an inverted half graben. Contour lines indicate topography at the top of syn-rift strata. (A) Development of a half graben bounded by a curved listric normal fault. (B) Inverted syn-rift wedge with maximum compressive stress parallel to the original extension direction. Thickest portion of the syn-rift wedge coincides with the region of greater uplift. (C) Inverted syn-rift wedge with maximum compressive stress forming an angle with the original extension direction. The region of greater uplift is offset with respect to the thickest portion od the syn-rift wedge.

Section restoration and structure kinematics

The seismic profile selected for structural restoration was converted to the depth

domain using a velocity model consisting of twelve layers. Average interval velocities

were assigned to each layer based on dominant lithology and sonic-log data from well B

(Figures 2.9, 2.12). The 1:1 depth-converted section (Figure 2.34) was digitized and
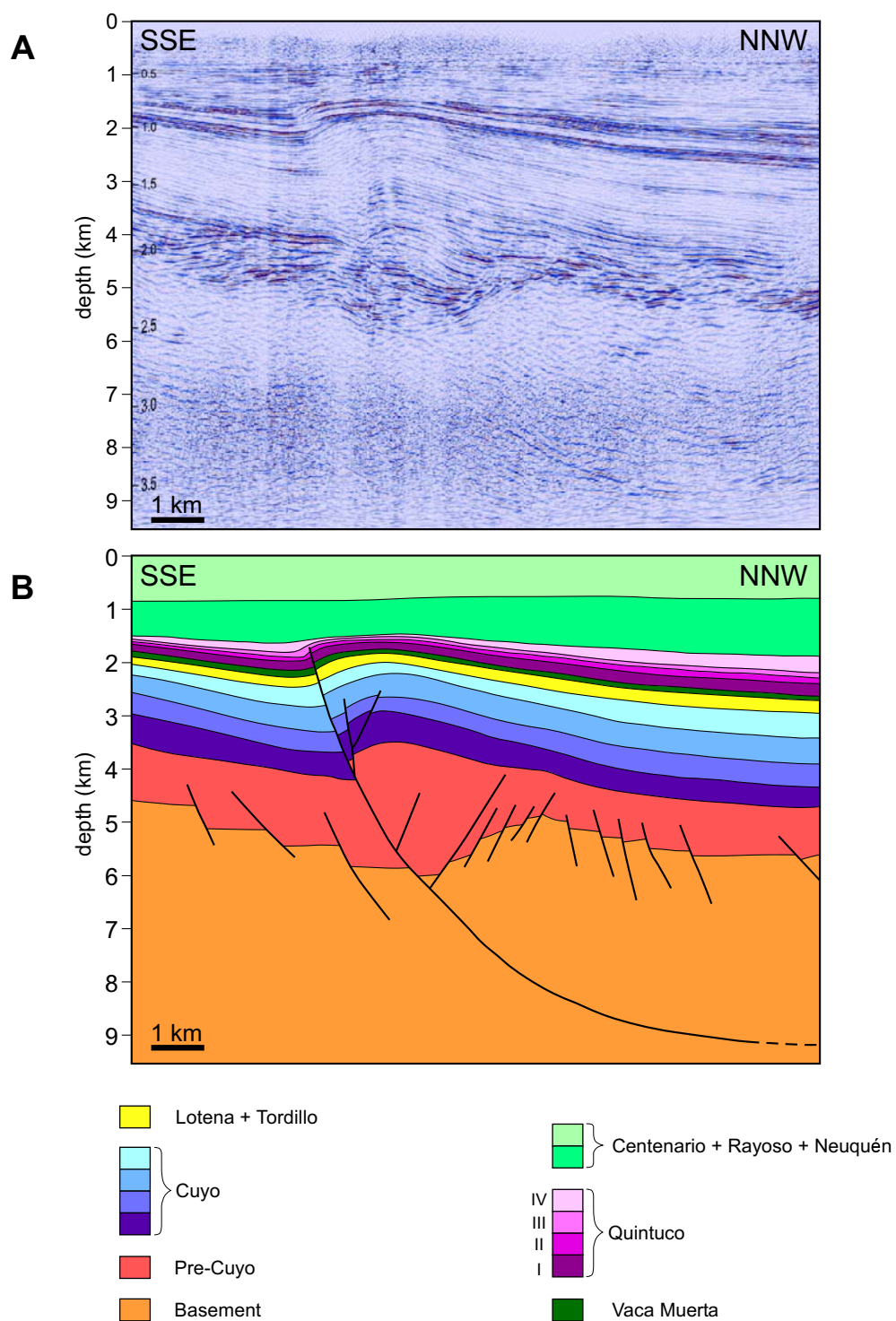
Figure 2.34. Vertical section through the SBS chosen for structural restoration. (A) Uninterpreted present-day depth-converted seismic section. (B) Color coding for main tectono-stratigraphic units sequentially decompacted and restored. Section is oriented N 4° W. See Figure 2.31 for location.

sequentially undeformed at different stratigraphic horizons to show the development of the hangingwall anticline and the progressive displacement along the master fault.

Restorations were done using a combination of algorithms within the 2DMove™ software package. The algorithms were selected based on the need to maintain fault geometry and area-balance constraints, rather than assuming the folding mechanism was critical to the restoration. The fact that some algorithms worked better than others at a particular restoration stage may indicate that different deformation mechanisms were dominant at different stages. For example, the master fault does not cut through the uppermost Lower Mendoza Group. The algorithm chosen to restore the section at the top of Quintuco Formation ("trishear"; Erslev, 1991; Hardy and Ford, 1997) had to account for the unfolding only of the shallower part of the section while both unfaulting and unfolding the underlying strata cut by the master fault. Displacement along the master fault increases with depth. Inclined shear (Gibbs, 1983; Withjack and Peterson, 1993) was the algorithm chosen to restore the top of Vaca Muerta because it considers the effects of fault geometry on hangingwall deformation. After decompacting strata down to Lotena Formation, fault displacement had been consumed. A flexural-slip algorithm (Davison, 1986) was therefore needed to unfold the Cuyo and Pre-Cuyo groups without further displacement along the master fault.

For successive restoration stages, part of the sedimentary column was stripped off and underlying units were decompacted and isostatically adjusted. The restoration and decompaction procedures caused slight northwestward tilting of layers in the footwall for the Callovian and Bathonian restoration stages. The results of nine stages of

restoration and backstripping are shown in Figures 2.34 and 2.35 and discussed below in a forward fashion to characterize the kinematic evolution of the structure from Late Triassic to Recent time.

Restoration to the Late Triassic pre-extension stage (Figure 2.35H) was performed by removing fault displacement with an inclined-shear restoration algorithm. In order to facilitate footwall restoration, faults were hypothetically extended to merge the main detachment. Hangingwall faults, both synthetic and antithetic, were assumed to be the result of hangingwall deformation above a listric detachment and were therefore hypothetically linked with it. This fault arrangement at depth is a tool for section restoration purposes only, and does not intend to illustrate the real fault geometry. The restored section exhibits a total extension of ~14% (1.7 km) with significant topography at the top of Pre-Cuyo. This antecedent relief is seismically expressed by a series of onlaps against the seismic horizon at the top of syn-rift.

The restoration at the top of the Middle Cuyo Group (Figure 2.35G) shows that no significant inversion of the SBS occurred during Early Jurassic time (Pliensbachian to early Aalenian). This is expressed by the constant thickness and dip of Lower to Middle Cuyo strata and lack of offset across the master fault. General deepening of the basin to the NNW is observed. During this time, the Northern Sub-basin was filled with prograding turbidites that were sourced mostly from the south and southwest.

The Intra-Callovian unconformity on top of upper Cuyo strata on the SBS is documented in other parts of the basin and is seismically expressed in the SBS as major truncation surface with erosive thinning of the uppermost Cuyo interval over the

A

SSE — NNW

VALANGINIAN
~135 Ma

Thickness reconstruction of Quintuco Formation.
Increased displacement along main fault at the top of syn-rift strata.
Restored shortening is ~ 0.1 km

1 km   extension ≅ 0.1 km →

B

SSE — NNW

BERIASIAN
~140 Ma

Restoration at the top of Quintuco Formation. Depositional thickness variations were estimated from growth stratal geometries within the Quintuco Fm.
Increased displacement along main fault at the top of syn-rift strata.
Restored shortening is ~ 0.2 km

1 km   shortening ≅ 0.2 km →

C

SSE — NNW

TITHONIAN
~147 Ma

Restoration at the top of Vaca Muerta Formation. Notice uniform thickness of the top unit (no reconstruction preformed). Lotena Formation thins over the structure's crest due to Kimmeridgian erosion.
Increased displacement along main fault at the top of syn-rift strata.
Restored shortening is ~ 0.5 km

1 km   shortening ≅ 0.5 km →

D

SSE — NNW

OXFORDIAN-EARLY KIMMERIDGIAN
~160 Ma

Restoration at the top of reconstructed Lotena Formation. Notice erosive thinning of upper Cuyo strata (lightest blue) along the Intra-Callovian unconformity.
Incipient displacement along main fault at the top of syn-rift strata.
Restored shortening is ~ 0.7 km

1 km   shortening ≅ 0.7 km →

Figure 2.35. Restoration sequence of a depth-converted balanced cross section through the western substructure of the SBS. Length of the present-day depth-converted seismic section is 12,977 km. The total amount of shortening during inversion is ~1 km (8 %). Total pre-inversion extension is ~1.7 km (~14%).

E — **CALLOVIAN** ~162 Ma

Thickness reconstruction for Upper Cuyo strata, before development of the Intra-Callovian unconformity.
Incipient displacement along main fault at the top of syn-rift strata.
Restored shortening is ~ 0.7 km

F — **BATHONIAN** ~167 Ma

Restoration at the top of Upper Cuyo. Mild folding of syn-rift wedge. No fault displacement at the top of syn-rift.
Restored shortening is ~ 0.8 km

G — **PLIENSBACHIAN-AALENIAN** ~190 Ma

Restoration at the top of Middle Cuyo (early post-rift strata). Uniform thickness of Lower Cuyo suggests no significant inversion.
Total restored shortening is ~ 1 km (~8 %).

H — **LATE TRIASSIC** (Hettangian?) ~210 Ma

Significant basement-top paleotopography. Total early Mesozoic extension is ~ 1.7 km (~14 %).

Figure 2.35 - Continued.

structure's crest (Figure 2.34). The restoration at the top of the Cuyo level therefore required reconstruction of the missing section eroded from the crest of the SBS. The amount of section added was based on the thickness of the Cuyo Group in non-inverted areas and on the trend of reflections truncated by the Intra-Callovian Unconformity (Figure 2.35E). The restoration was accomplished by unfolding the entire cross-section flattening along the top of the reconstructed Upper Cuyo Group (Figure 2.35F). This restoration stage shows incipient folding of Pre-Cuyo and Lower Cuyo strata, suggesting the initiation of inversion during Bathonian to early Callovian time. No displacement along the master fault is observed at the top of syn-rift strata, although the amount of extensional displacement at the top of Basement had been reduced.

After the Callovian inversion event, the basin was filled with shoreface and deltaic facies of the late Callovian to early Kimmeridgian Lotena Formation. Further inversion during late Kimmeridgian time caused significant erosion of the Lotena Formation, expressed by the Intra-Malm unconformity. Thickness reconstruction of Lotena strata was needed before performing the restoration at the top of this unit (Figure 2.35D). Increased shortening during this inversion stage was accommodated by folding at the top of syn-rift and early post-rift levels. Displacement along the master fault at the top of the syn-rift wedge still was not significant, although it is readily visible at the top of basement level, where the amount of original extensional displacement was further reduced.

The Intra-Malm unconformity is overlain by Vaca Muerta shale facies, of Tithonian age. Restoration at the top of this unit (Figure 2.35C) shows the initial

displacement along the master fault at the top of syn-rift strata, in addition to folding of the entire section. Offset along the master fault increases downsection. The thickness of the Vaca Muerta Formation was not reconstructed, as it is fairly constant throughout the SBS. This unit was deposited during the most important flooding event in the basin, and its uniform thickness may suggest a period of tectonic quiescence during Tithonian time.

The Quintuco Formation comprises most of the syn-inversion strata in the SBS. Restoration at the top of this unit required reconstruction of original Quintuco thicknesses to account for the strata eroded along the Intra-Valanginian unconformity. The missing Quintuco section was estimated based on the unit's thickness in nearby areas. In addition, stratal onlap onto the SBS's limbs indicating syn-tectonic deposition and thinning over the structure's crest further constrained the thickness reconstruction process. Iterative forward modeling using the "trishear" algorithm in 2DMove allowed the estimation of a pre-erosional Quintuco Profile (Figure 2.35A). The Quintuco Fm. was then restored to estimate the amount of shortening and structural configuration prior to the Valanginian inversion (Figure 2.35B). Previous to the Quintuco bed reconstruction, backstripping of the Neuquén Group and restoration at the top of Rayoso Group (not shown) was done using an inclined shear algorithm, which accounted for the small displacement along the main detachment observed in Figure 2.35A.

DISCUSSION

The 3D seismic data and interpretation tools in GeoFrame were used to document the structural and stratigraphic relationships associated with tectonic inversion

in the Central Neuquén Basin. The complex structures and stratigraphic patterns associated with development of the SBS and ATS suggest that multiple deformation processes (e.g., fault linkage during extension and contraction, expansion of post-rift fill in the hangingwall during inversion, oblique inversion, and growth stratal development) played important roles in determining the final configuration of these inversion structures.

Faulting associated with inversion

Differential uplift and detachment depth

There is significant along-strike variation in the amount of uplift in the substructures that comprise the SBS. This may be related to differences in detachment depths for the different half-graben bounding fault segments. Coincidence of the deepest detachment level along segment 2 (Figure 2.17B) with the region of maximum uplift is consistent with observations from analog models (Buchanan, 1991; Bulnes and McClay, 1999). For deeper detachment levels, the same amount of shortening will cause a larger volume of material to be uplifted above the pre-inversion "regional". For syn-rift wedges with similar volume, those with deeper detachments will be more strongly inverted (Figure 2.36). In the SBS, the apparent volume of syn-rift depocenters bounded by fault segments 1 and 3 are similar, but uplift is greater for the depocenter bounded by the deeper segment 3. Greatest uplift along segment 2 may be the combined result of a slightly bigger syn-rift wedge and the deepest detachment level (Figure 2.17). Different

detachment levels can, therefore, occur within a single inversion structure, which may be controlled by the original segmentation of older extensional faults.
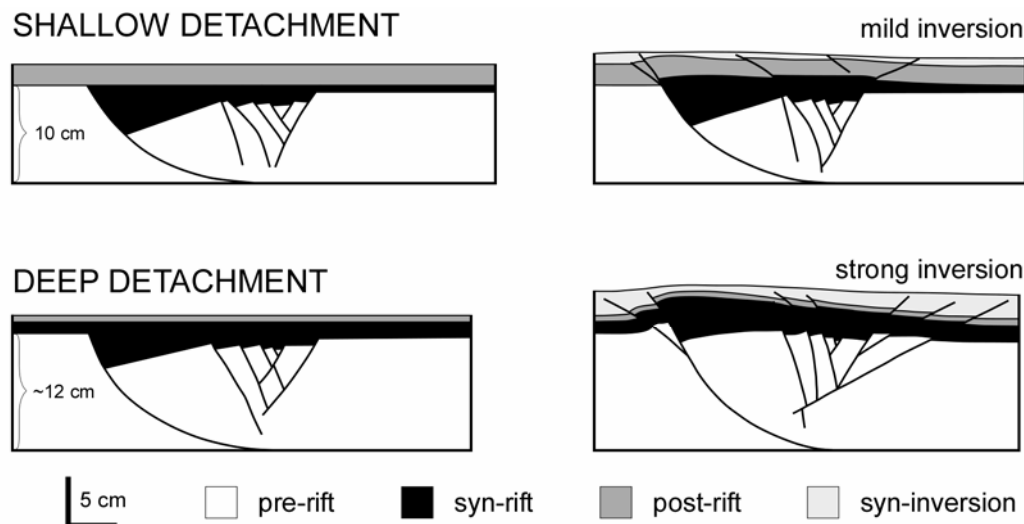
Figure 2.36. Analog-model results of inversion with different detachment depths. For the same amount of shortening, greater uplift is observed in the section with deeper detachment level. After Bulnes and McClay (1999).

Trends in fault reactivation

The two principal inversion structures identified in the study area, SBS and ATS, present a fault framework that combines non-reactivated structures with syn-inversion reactivated and newly-formed faults. The "deep" fault system is characterized by a significant difference in fault-trace lengths, dips, and, to a lesser degree, orientation between non-reactivated (D1) and reactivated (D2) syn-rift extensional faults (Figure 2.16).

The occurrence of a few fault segments that are significantly larger than the rest is a consequence of some faults propagating and linking at the expense of others during extension (Kim and Sanderson, 2005). The data show that the larger syn-rift master fault segments were preferentially reactivated and accommodated much of the contractional strain during inversion, with only minimum reverse displacement along smaller faults. Mean fault-trace lengths of ~3 and 1.5 km for D1 faults and D2 faults, respectively (Figure 2.19), suggests a threshold length value between 1.5 and 3 km above which faults were reverse-reactivated during inversion, whereas faults smaller than the threshold may or may not have reactivated (Figures 2.18, 2.19). A similar trend has been observed, at a smaller scale (100s of meters), in outcrop studies where larger faults, assumed to have lower frictional strength due to the formation of a thicker fault gauge, are more likely to undergo reverse reactivation (Marone, 1995; Kelly et al., 1999). Newly-formed syn-inversion faults (D3 fault type) are consistently short throughout the SBS and ATS (average length ~1.2 km; Figures 2.16, 2.19). This trend suggests that reactivated preexisting faults controlled most of the shortening, whereas syn-inversion faults developed mostly to accommodate syn-rift wedges internal deformation.

Orientation variations among different types of preexisting faults (D1 and D2) are not interpreted to influence fault reactivation significantly. The wider range of strike and dip values for syn-rift non-reactivated faults (D1), however, may contribute in part to their behavior, due to greater departure from optimum orientations (Figure 2.18).

Coalescent syn-rift wedges on flattened seismic profiles through both SBS's main depocenters indicate fault linkage during extension (Figure 2.26). The development

of accommodation zones between bounding-fault segments produced a zone of distributed deformation during the extensional phase. During the contractional phase, however, fault systems in accommodation zones evolved into a through-going reverse fault at post-rift and syn-inversion stratigraphic levels (Figure 2.37). The correspondence between master fault bends, structure's crests, and extensional accommodation zones evidences the fundamental control of syn-rift fault architecture on inversion geometry. In this way, the displacement-transfer zones that developed during extension remained active during the inversion phase (Keller and McClay, 1995), resulting in regions of lesser uplift.

Inversion and hangingwall deformation

The "shallow" fault system that affects the SBS and ATS probably reflects (1) uplift and expansion of post-rift strata in the hangingwall during inversion and (2) hangingwall deformation to accommodate the curved shape of the master fault. Restriction of the shallow fault domains to the SBS's hangingwall reflects their syn-inversion origin.

The expansion of the post-rift section during inversion can be inferred from the formation of extensional faults within an overall contractional setting. Some of the extensional faults exhibit downward-decreasing displacement and terminate within shale-rich levels in the Lower Cuyo Group, where contraction might have been taken up by ductile or more widely distributed deformation. No extensional faults formed over the structure's accommodation zones, which in turn experienced the least amount of uplift during inversion (Figure 2.20). Higher extensional fault density occurs along the
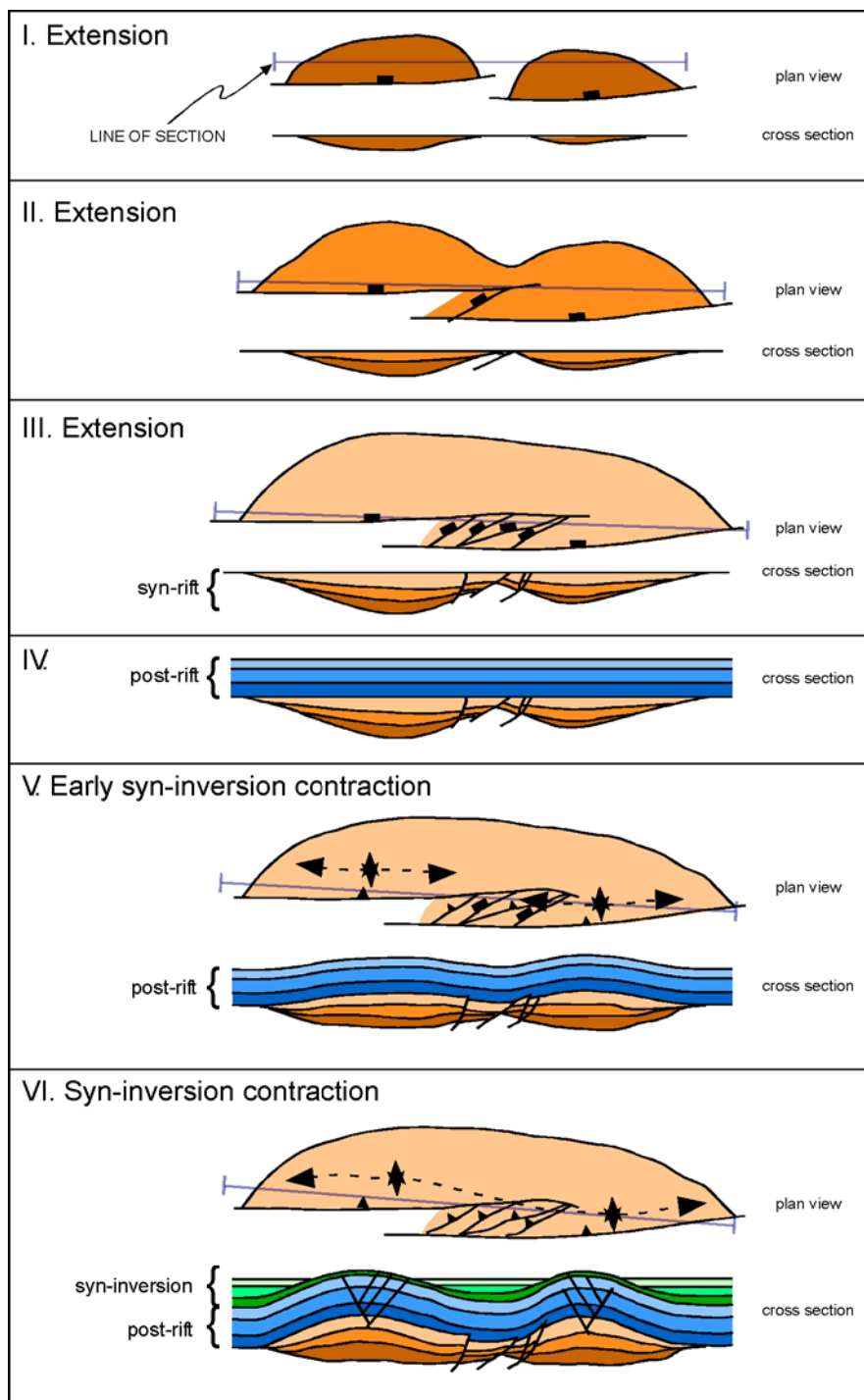
Figure 2.37. Conceptual models for syn-rift, post-rift, and syn-inversion fault linkage pattern for the SBS's main depocenters, bounded by fault segments 2 and 3. Based in part on Schlische and Anders (1996).

inverted depocenters. Syn-inversion faults, however, are not restricted to the regions of maximum uplift, which would be expected if only E-W tensile stress upon inversion would have developed. This is particularly obvious in the SBS's western substructure and in the ATS, where extensional faults flank the structures rather than cutting through the regions of maximum elevation. Surface curvature analysis, which was not conducted in this study, could provide additional insights into the factors affecting syn-inversion fault distribution.

The attitude of syn-inversion "shallow" extensional faults, showing *en échelon* arrangement within each domain in map view (Figure 2.20) and negative-flower-structure geometries in cross section (Figure 2.21) suggest that a deep-rooted mechanism also influenced strain partitioning. Flower structures are interpreted to result from incipient strike-slip motion between discrete blocks within the SBS's hangingwall as it is obliquely thrusted over a highly corrugated footwall. The relative motion of blocks allows the hangingwall to accommodate to the shape of the footwall. This mechanism acts in conjunction with the post-rift section expansion during inversion (Figure 2.38). Superimposed inversion and incipient strike-slip deformation, along with mild translation of the hangingwall parallel to the master fault, produces significant structural overprinting. This is more pronounced near the SBS's and ATS's axes, where deformation is more intense and contributes to the scatter observed in fault orientation within each domain (Figure 2.22). Subtle rectilinear features observed in time-dip maps (Figure 2.20) are interpreted as conjugate faults whose kinematics may be related to strike-slip displacement and could be accommodating internal block deformation.
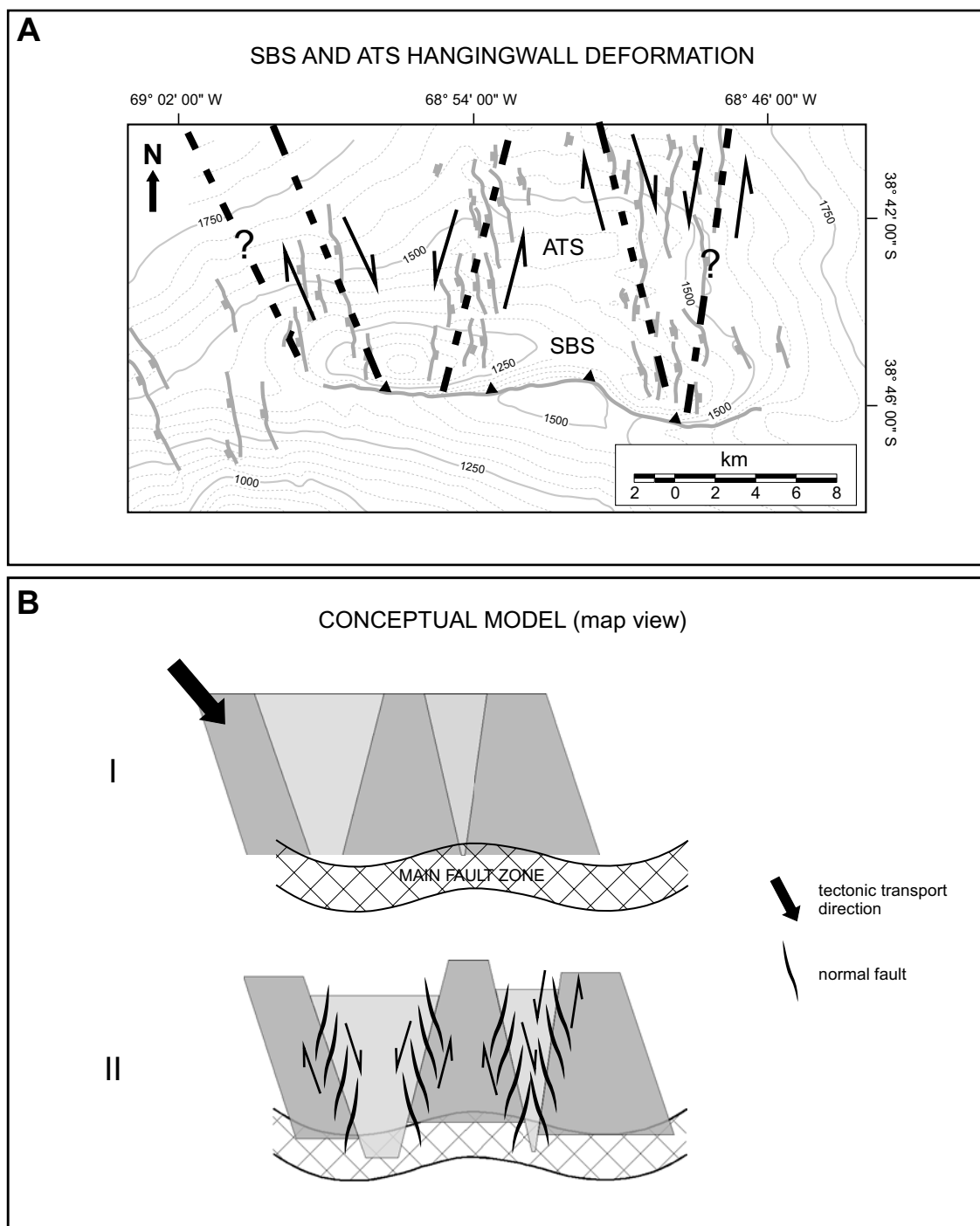
Figure 2.38. Hangingwall deformation of the SBS during inversion. (A) Annotated time-structure map at the top of Lower Cuyo Group indicating interpreted extensional faulting in SBS's and ATS's hangingwalls. (B) Conceptual model for block relative motion to accommodate to curved footwall. Displacement parallel to the main fault and between blocks are exaggerated for clarity.

Substantial hangingwall internal deformation should be expected in highly "three-dimensional" inversion structures, where strong overprinting may occur between faulting purely associated with inversion and structural features that result from hangingwall along-strike translation and expansion. In addition, observations from this study suggest the need to incorporate more complex deformation scenarios into scaled-model experiments, like oblique inversion of curved (in plan view) faults and hangingwall block deformation mechanisms.

Stratigraphic record of inversion

Several unconformities within the post-rift strata along the SBS and ATS are erosive surfaces that record significant breaks in the stratigraphic record over the structures' crests. These unconformities record tectonic activity with no associated syn-kinematic strata. Other growth strata deposited during late Tithonian to early Valanginian time record the structural evolution of inversion features and provide elements to investigate deformation mechanisms and sediment dispersal patterns.

Several models have been proposed to describe the kinematics of fault-related folds and the resulting growth stratal development. They can be divided into two main groups: kink-band migration (Suppe and Medwedeff, 1990; Suppe et al., 1992) and limb-rotation models (Hardy and Poblet, 1994; Poblet et al., 1997). These two geometric approaches produce different stratal termination patterns on cross sections that are oriented perpendicular to the axes of the inversion structures. The growth strata associated with the SBS and ATS displays wedge-shaped packages of divergent reflections on along-dip profiles of both fold limbs, indicating progressive limb rotation

during fold development (cf. Shaw et al., 2004). Absence of kink bands and growth triangles (Suppe et al., 1992) suggests that the kinematics of SBS and ATS cannot be described by kink-band migration.

Growth of the SBS and ATS may have affected sediment dispersal from late Tithonian to Valanginian time. Marine conditions predominated during deposition of the Quintuco Formation and the mild syn-depositional bathymetric relief that can be inferred from growth stratal geometries suggests that the rate of uplift of the anticlines' crests slightly exceeded the rate of syn-tectonic sedimentation. This resulted in more accommodation space along the anticlines' limbs and in the front synclines, where sediments preferentially accumulated.

Lowest intervals of Vaca Muerta and Quintuco basinal shale and possibly distal carbonate turbidite facies in the central Neuquén Basin have been linked to coeval proximal clinoforms prograding from east and southeast of the SBS and ATS (Zilli et al., 1979; Mitchum and Uliana, 1985; Hurley et al., 1995). Therefore, the orientation of the SBS and ATS with respect to the sediment source during the deposition of the Vaca Muerta and Lower Quintuco Formations may have caused significant sediment ponding against steeply dipping forelimbs of inversion anticlines. The backlimbs may dip in the direction of regional sediment transport, in a sort of "shadow zone" behind the growing anticline (Shaw et al., 2004). Periods of relatively more intense tectonic activity may have resulted in sediments filling in front synclines. In contrast, periods of tectonic quiescence would result in the anticlines' crests being draped by background muds and filling of the backlimb accommodation space. According to this model, ponding

sediments will be coarser-grained, as sandy units would fill the lows first and pinch out onto fold limbs (Figure 2.39; Shaw et al., 2004). Fine-grained sediments deposited between pulses of tectonic activity may then drape the sands. More detailed stratigraphic analysis within the post-rift section is needed in order to evaluate this sediment dispersal model for different intervals, especially reservoir formations.
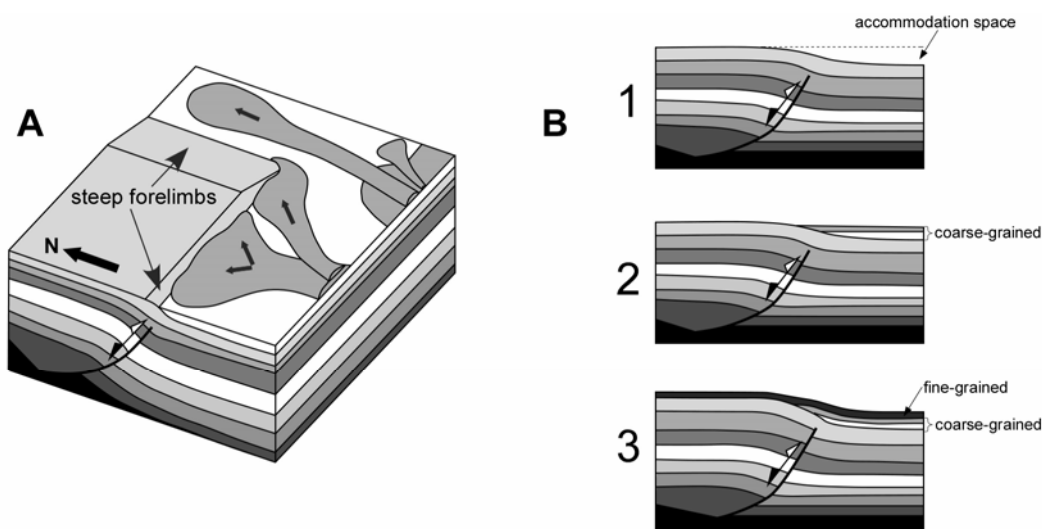
Figure 2.39. Conceptual model for an active fold tectonic control on sediment dispersal and accumulation. (A) Block diagram of a growing inversion structure showing the control of bathymetric perturbations on sediment ponding against the forelimb. (B) Deposit of a coarse-grained sedimentary body filling available accumulation during structure's growth. A later quiescent period results in background mud draping the sandy wedge (modified from Shaw et al., 2004).

Kinematic evolution

The workflow employed for structural restoration in this study may result in significant error accumulation through its various stages, namely: (1) well data-to-seismic correlations, (2) seismic mapping, (3) estimation of tectonic transport directions, (4) depth conversion, (5) decompaction and isostatic adjustment, and (6) selection of

restoration algorithms. After completion of all these steps, the sequential restoration also involves additional interpretive challenges like estimation of the original thickness of eroded strata, paleobathymetry, and restoration parameters. The limitations and caveats of this process are especially important when studying inversion structures, since the existence of reactivated structures adds significant complexity to the problem of restoration. In spite of the considerations described above, some clear trends emerged from the analysis.

The earliest manifestation of inversion in the SBS occurred by Bathonian (~167 Ma) time and is expressed by mild warping of the post-rift section above the half-graben but with no visible stratal offset across the master fault except for small displacement at the top of basement. The lack of offset within the syn- and post-rift fill cannot be interpreted, however, as lack of movement along the master fault during this time. Deeper segments of the listric master fault may have been reactivated during earliest stages of inversion because fault dips are lower and the fault was easier to reactivate there. At the same time, steep dips at shallower stratigraphic levels may cause the fault to lock up during reactivation so that the structure accommodates shortening by dilation and internal deformation of the hangingwall (Sibson, 1995). Similar patterns are observed in analog studies, where significant shortening is accommodated by fault-parallel movement of particles deep in the section, whereas there may be no shallow manifestation of inversion (Eisenstadt and Withjack, 1995; McClay, 1995). Thus, about 20% of the overall shortening along the SBS occurred by ~167 Ma with incipient fault displacement at the top of syn-rift strata (Figure 2.40). Continued shortening with

incipient offset of syn-rift strata is observed until early Tithonian time (~147 Ma), when

fault offset within post-rift strata began. Most syn-inversion faults of the D3 type may

have developed during this stage of inversion, as most shortening had to be

accommodated by internal syn-rift wedge deformation.
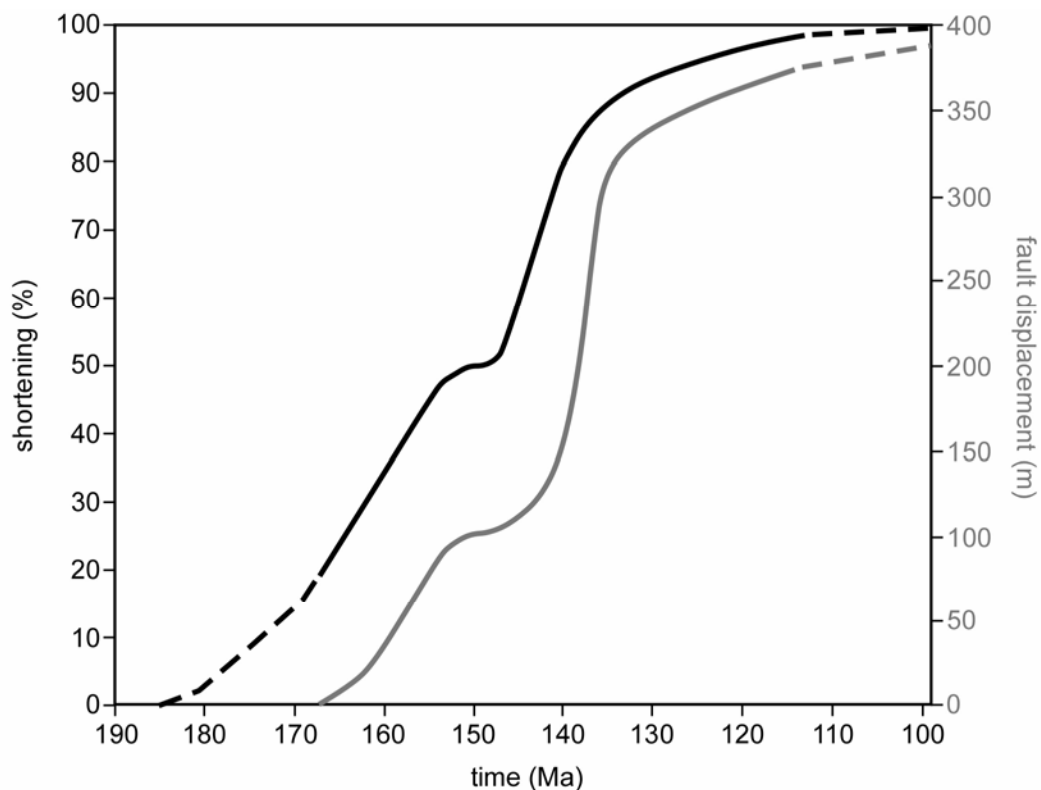
Figure 2.40. Variation of overall shortening and displacement along the main detachment through time during inversion of the SBS. Mild folding of the post-rift section above the half-graben but with no visible stratal offset across the master fault occurred during Bathonian (~167 Ma). About 20% of the overall shortening along the SBS occurred by ~167 Ma with incipient fault displacement at the top of syn-rift strata. Continued shortening with incipient offset of syn-rift strata is observed until early Tithonian time (~147 Ma), when fault offset within post-rift strata began. From Tithonian time on, displacement along the steepest part of the fault produced most of the stratigraphic offset observed in present-day sections. This coincides with a sharp increase in displacement along the master fault at the top of syn-rift. The last stage of inversion is characterized by reduced displacement along the main detachment at the top of syn-rift strata, probably due to increased resistance to displacement along the fault because of increased overburden.

From Tithonian time on, displacement along the steepest part of the fault produced most of the stratigraphic offset observed in present-day sections. This coincides with a sharp increase in displacement along the master fault at the top of syn-rift (Figure 2.40). During this stage of inversion, most fault reactivation probably occurred (D2 fault type), as internal syn-rift wedge deformation was "consumed". Upsection propagation of the master fault may have also occurred at this time.

The master fault tip did not propagate upsection beyond the Berriasian-Valanginian Quintuco Formation, even though folding continued and the anticline kept growing until Cenomanian time. This last stage of inversion is also characterized by reduced displacement along the main detachment at the top of syn-rift strata, probably due to increased resistance to displacement along the fault because of increased overburden (Figure 2.40).

The amounts of extension and inversion-related shortening of the SBS are an order of magnitude smaller than typically suggested by analog studies of inversion structures. The small amounts of shortening estimated by structural restoration may explain the lack of pervasive backthrusting or shortcut faulting in the SBS. Backthrusts and shortcut faults are common in scaled models for inversion, but typically develop where shortening values are the same as or greater than the amount of extension (Eisenstadt and Withjack, 1995; McClay, 1995; Yamada and McClay, 2004). Where backthrusts form at relatively low amounts of shortening (Buchanan and McClay, 1991), they commonly nucleate at the tip of preexisting hangingwall collapse grabens that

formed during prior extension. The SBS and ATS do not have collapse grabens and their syn-rift wedge structure may be, therefore, less likely to nucleate faults as backthrusts.

Although structural and stratigraphic relationships within the SBS and ATS are more complex and varied than predicted by analog model studies, the natural examples are similar to scaled-model results. The highly-complex faulting of the SBS and ATS documented in this three-dimensional study, even for mild extension and contraction amounts, evidences the high sensitivity of natural structures and arises concerns about scaling considerations in analog models.

The definition of geometrical constraints like "null line" (Williams et al., 1989; Turner and Williams, 2004) or inversion ratios (Williams et al., 1989; Song, 1997) are based on two-dimensional descriptions and seem insufficient to characterize amounts of inversion. Along-strike variations in those parameters within a single inversion structure, such as the SBS, cast serious doubts about their usefulness as measures of inversion intensity. The increasing availability of 3D seismic data and computer applications for 3D structural modeling may facilitate the use of volumetric parameters to characterize inversion. In the case of an inverted half-graben, for example, the ratio of volumes of syn-rift fill above and below a regional datum could provide more reliable estimates of the intensity of inversion, regardless of along-strike variations.

CONCLUSIONS

This study documented the structural style and stratigraphic relationships of inversion structures in the central Neuquén Basin. Interpretations were based on detailed

structural and stratigraphic mapping of a 3D seismic dataset, fault orientation analysis, and structural restorations. Observations were compared with findings from analog-model studies in order to test the validity of assumptions used during the analyses, evaluate scaling relationships, and consider new ideas to parameterize and measure inversion.

Conclusions from this study include:

1) The Northern Sub-basin of the Neuquén Basin includes a series of inversion structures that consist of older Triassic half-grabens that underwent pulsed inversion between Early Jurassic and Late Cretaceous time. Two of these inversion structures, the Sierra Barrosa (SBS) and Aguada Toledo (ATS) anticlines, are some of the most prominent subsurface features in the Northern Sub-basin.

2) The SBS inversion structure has two main fault systems. A deep fault system that affected basement and syn-rift strata was selectively reactivated during inversion. Larger faults that formed during extension were preferentially reverse-reactivated during inversion, whereas smaller faults were typically not reactivated during inversion.

3) A complex set of syn-inversion normal faults formed at high angle to the master fault of the SBS during inversion. These faults affected both post-rift and syn-inversion strata in the SBS. The map patterns, location, and kinematic history of these faults indicate that the hangingwall of the SBS expanded upon uplift and internally deformed as it accommodated to the shape of the curved footwall

during oblique inversion. Similar structures are not reported in analog-model studies.

4) Within the post-rift and younger section, a single through-going but curved fault defines the southern boundary of the SBS inversion structure. This single fault changes into a series of fault segments, separated by accommodation zones, at depth. Fault systems in former accommodation zones that formed during extension became linked into a through-going reverse fault during inversion.

5) Growth strata were deposited between late Tithonian and early Valanginian time on the flanks and crests of the SBS and ATS. The growth strata suggest a folding mechanism controlled by limb rotation with no significant kin-band migration.

6) Folding and internal deformation were probably the dominant mechanisms that accommodated contraction during the SBS's early and late stages of development. Initial fault "lock-up" at shallower stratigraphic and structural levels was due to the steep dips of the master fault at these levels, which is not conducive to reactivation. As internal syn-rift wedge deformation was "consumed", the half-graben bounding fault became reverse-reactivated and propagated upsection. By Berriasian to early Valanginian time, the weight of the overburden inhibited additional fault displacement and folding became the main mechanism that accommodated shortening until late Cretaceous time.

7) Along-strike variations in structural style are significant within the SBS and ATS. Structural features and intensity of inversion (position of null point and

inversion ratio R_i) vary significantly within these inversion structures. This variability emphasizes the need for volumetric descriptors of inversion.

8) The SBS shows significant structural complexity associated with relatively small amounts of extension and inversion, which suggests the need to incorporate more complex deformation scenarios into scaled-model experiments, like oblique inversion of curved (in plan view) faults and hangingwall block deformation mechanisms.

CHAPTER III

STYLES AND PATTERNS OF PROPAGATION OF MESOZOIC TECTONIC

INVERSION IN THE CENTRAL NEUQUÉN BASIN, ARGENTINA

INTRODUCTION

Intraforeland deformation is commonly associated with the reactivation of preexisting structures (Harding, 1985; Ziegler, 1989; Dorobek et al., 1991; Coward, 1994; Dellapé and Hegedus, 1995; Homovc et al., 1995; Lowell, 1995; Manceda and Figueroa, 1995; Morley, 1995; Peroni et al., 1995; Thomas and Coward, 1995; Uliana et al., 1995; Welsink et al., 1995; Yang and Dorobek, 1995; Beauchamp et al., 1996; Ramos and Aleman, 2000; Turner and Williams, 2004). Intraforeland contraction and uplift typically involves older extensional basins, where many of the fault systems associated with the basin's early rift history are reactivated. In addition, pre-existing heterogeneities in foreland regions (e.g., basement lithology contrasts, suture zones, etc.) may concentrate stress and strain, and play a key role in subsequent deformation by nucleating inversion structures that may form >1000 km from orogenic fronts (Kluth and Coney, 1981; Badley et al., 1989; Butler, 1989; Peroni et al., 1995; Ziegler et al., 1995; Marshak et al., 2000; Bailey et al., 2002; Vanbrabant et al., 2002).

Basin inversion can be defined as the compressional or transpressional deformation of a former extensional basin (Turner and Williams, 2004). Inversion can have significant effects on the structural and stratigraphic evolution of an area and must be carefully evaluated when dealing with regional restoration of structural cross sections, shortening estimations, assumptions about the nature of structures at depth, subsidence

patterns, and analysis of syn-inversion sedimentation (Coward, 1994; McClay, 1995). In addition to the geometric characteristics that may make inversion structures suitable as structural traps for petroleum accumulations, inversion tectonics can have important effects on other aspects of petroleum systems. For example, inversion causes uplift of a basin, with consequent effects on burial history and oil generation and maturation, porosity evolution, fracture development, migration pathways, and alteration of fault sealing properties (Coward, 1994).

Structural and stratigraphic relationships associated with inversion structures have been described elsewhere for both natural examples (Gillcrist et al., 1987; Cartwright, 1989; Roure et al., 1992; Hill and Cooper, 1996; Song, 1997; Bulnes and McClay, 1998; Betts, 2001; Bailey et al., 2002; Bjorklund and Burke, 2002) and analog models (Buchanan and McClay, 1991; Mitra and Islam, 1994; Eisenstadt and Withjack, 1995; Keller and McClay, 1995; McClay, 1995; Brun and Nalpas, 1996; Dubois et al., 2002; Yamada and McClay, 2004).

Reactivation of syn-rift extensional faults depends on several factors, although orientation of these faults relative to the stress field responsible for inversion is probably the most critical (Sibson, 1985; Letouzey, 1990; Coward, 1994). A fault can be reactivated even when its orientation with respect to the stress field is not "favorable" in terms of Andersonian fault theory and Coulomb failure criteria. The likelihood for reactivation of a severely misoriented fault increases dramatically with increasing pore fluid pressure, which can result in a very low compressive, or even tensile, effective σ_3 (Sibson, 1990, 1995; Sibson and Xie, 1998).

Large-scale studies of basin inversion have examined the interaction between in-plane stress, lithosphere rheology, and basin fill. Typically, basin inversion is associated with horizontal compressive stress that is generated along a convergent plate margin and transmitted into the plate interior where inversion occurs (Lowell, 1995). Vertical stresses in the lithosphere (e.g., stresses caused by mantle plumes, post-glacial isostasy, or basaltic underplating) might also induce or overprint basin inversion caused by in-plane compressive stress (Platt and England, 1993; Brodie and White, 1995; Nadin et al., 1995; Ware and Turner, 2002). Widespread basin inversion commonly develops within plate interiors where the lithosphere is weaker than adjacent areas (van Wees and Beekman, 2000), although this remains controversial (Turner and Williams, 2004).

Spatial and temporal patterns of inversion structures across foreland regions are also affected by variations in the intra-plate compressive stress field which, in turn, are commonly controlled by forces acting along convergent plate boundaries. Thus, the location and kinematic history of inversion structures can provide insight into plate-scale tectonic events and relative influence of processes acting along plate margins. For example, Late Cretaceous to Cenozoic inversion structures in Western and Central Europe have been attributed to in-plane stresses associated with the Alpine orogeny. Basement blocks were uplifted and Mesozoic grabens inverted >1500 km north of the Alpine deformation front (Gillcrist et al., 1987; Badley et al., 1989; Cartwright, 1989; Chapman, 1989; Ziegler, 1989; Coward, 1994; Deeks and Thomas, 1995; Hooper et al., 1995; Thomas and Coward, 1995; Ziegler et al., 1995; Brun and Nalpas, 1996). Inversion structures across Western Europe are mostly NW trending and are associated

with movement along pre-existing normal faults that formed during Paleozoic and Mesozoic extensional events. In general, the intensity of inversion shifted westward through time and decreased with distance from the Alpine front (Ziegler, 1989; Ziegler et al., 1995). The timing and location of the main inversion phases, however, may be due to fault orientation and contrasts in the amount of prior extension (Ziegler, 1989).

The Ancestral Rockies and related foreland uplifts have been interpreted as an intra-plate response to convergent-margin development along the western, southern, and possibly eastern margins of North America during Carboniferous to Permian time (Kluth and Coney, 1981; Kluth, 1986; Yang and Dorobek, 1995; Ye et al., 1996; Kluth et al., 1998; Marshak et al., 2003). Most workers agree that intraplate stress transmitted through the foreland region during late Paleozoic time caused reactivation of preexisting structures, which are mostly related to Precambrian extensional basins (Marshak et al., 2000).

The Andes are a dramatic manifestation of Late Cretaceous to Recent subduction of the Nazca plate beneath South America. Across the Andean foreland, stratigraphic and structural evidence, earthquake focal mechanisms, and in situ stress measurements show overall E-W oriented compression over a region extending ~ 1,000 km east of the Andes (Assumpção, 1992). Geologic evidence from the Brazilian craton suggests that Cenozoic deformation due to Andean tectonics is actually continent-wide (Assumpção, 1998; Lima, 2000; Cobbold and Meisling, 2001; Lima, 2003).

Late Cretaceous to Recent basin inversion has been described for various parts of the Andean foreland. Examples include the Golfo San Jorge Basin (Homovc et al., 1995;

Peroni et al., 1995; Uliana et al., 1995; Rodriguez and Littke, 2001), Santa Barbara

System (Kley and Monaldi, 2002), Noroeste Basin (Kress, 1995; Uliana et al., 1995;

Cristallini et al., 1997; Kley and Monaldi, 2002), Cuyo Basin (Dellapé, 1993; Dellapé

and Hegedus, 1995), Sierras Pampeanas (Schmidt et al., 1995), Beazley Basin (Yrigoyen

et al., 1989), Chacopampeana Region (Chebli et al., 1999), and Neuquén Basin

(Manceda and Figueroa, 1995; Uliana et al., 1995; Vergani et al., 1995). Most of these

basins were inverted during the main phases of the Andean Orogeny (Paleocene –

Recent time) and were associated with transmission of in-plane stress across the foreland

region. Few studies, however, have focused on Mesozoic inversion across the Argentine

foreland and its relationship to coeval plate-scale tectonics.

The Neuquén Basin of west-central Argentina is structurally complex due to

protracted tectonic activity from Late Triassic to Recent time. Prominent structural

features in the Neuquén Basin predate the main phases of the Andean orogeny and

played an important role in controlling basin configuration and the development of

petroleum systems within the basin. The most conspicuous of these structures is the

Huincul Arch, a 200-km long right-lateral shear zone that was most active during

Jurassic to Cretaceous time. The origin of this intra-foreland transpressional feature is

controversial, although it has been attributed to inboard continuation of transform fault

zones related to breakup of Gondwana and opening of the South Atlantic Ocean (Uliana

et al., 1989; Light et al., 1993; Uliana et al., 1995; Vergani et al., 1995). A series of

transpressive uplifts associated with a convex-to-the-north restraining bend along the

Huincul Arch divide the Neuquén Basin into two main sub-basins, known as the

Southern and Northern Sub-basins (de Ferrariis, 1947). Compressive stress induced by the restraining bend produced shortening in a roughly north-south direction and the tectonic inversion of Late Triassic half-grabens in the Northern Sub-basin. These inversion structures had a significant influence on basin configuration, facies distribution, and sediment dispersal patterns from early Jurassic to Late Cretaceous time.

No previous studies have examined relationships between Mesozoic inversion structures in the central Northern Sub-basin and regional deformation associated with the tectonic evolution of the Huincul Arch. The objective of this chapter is to investigate the style and kinematics of Mesozoic tectonic inversion across the central Neuquén Basin in order to provide insight into plate-scale deformation mechanisms and patterns of inversion propagation across a segment of the Argentine foreland.

An extensive 2D and 3D seismic and borehole dataset covering the south-eastern portion of the Northern Sub-basin was interpreted and integrated with published literature on the Mesozoic tectono-stratigraphic evolution of southwestern Gondwana. Based on structural and stratigraphic evidence, this study proposes a model for the propagation of Mesozoic tectonic inversion across the central Neuquén Basin. The progressive, lateral migration of inversion across the Neuquén Basin shows that for a preexisting fault fabric with homogeneous structure orientation, progressive lock-up of inversion structures results in shortening being transmitted farther inboard, inverting other previously-inactive structures. Implications for the deformation of the Argentine foreland region and the Mesozoic tectonic evolution of southern South America are discussed.

GEOLOGIC SETTING AND HISTORY OF THE NEUQUÉN BASIN

Evolution of the Neuquén Basin

The Neuquén Basin of NW Patagonia, west-central Argentina, is a triangular-shaped basin in map view that extends from 33° to 41° S and from 67° to about 72°W across the Andean foreland of Argentina and neighboring Chile (Figure 3.1). It is surrounded by the North Patagonian Massif, the Sierra Pintada Massif, and the Andean Cordillera, and covers an area of approximately 160,000 km^2 (Digregorio and Uliana, 1980; Uliana and Legarreta, 1993; Vergani et al., 1995).

Two major tectonic phases characterize the basin's evolution: a Late Triassic – Early Cretaceous extensional backarc stage that was followed by a Late Cretaceous – Recent retroarc foreland-basin stage. The inception of Late Triassic rifting in the basin has been linked to the gravitational collapse of the Permian to Early Triassic orogenic belt that bordered the southwestern margin of Gondwana (Dewey, 1988; Legarreta and Uliana, 1991; Uliana and Legarreta, 1993; Vergani et al., 1995; Franzese and Spalletti, 2001; Franzese et al., 2003). Extensional faulting produced a series of roughly subparallel, crudely en echelon, NW-trending troughs across parts of Argentina (Uliana et al., 1989). Principal Triassic fault trends are oriented NW-SE in the northeastern half of the basin and N-S in the western part (Figure 3.2A). In the southern part of the basin, NE-SW and ENE-WSW faults developed during backarc extension (Ramos, 1978; Vergani et al., 1995).

During Hettangian (earliest Jurassic) time, a change to a more regional, but still fault-partitioned subsidence pattern allowed the onset of the first marine incursion from
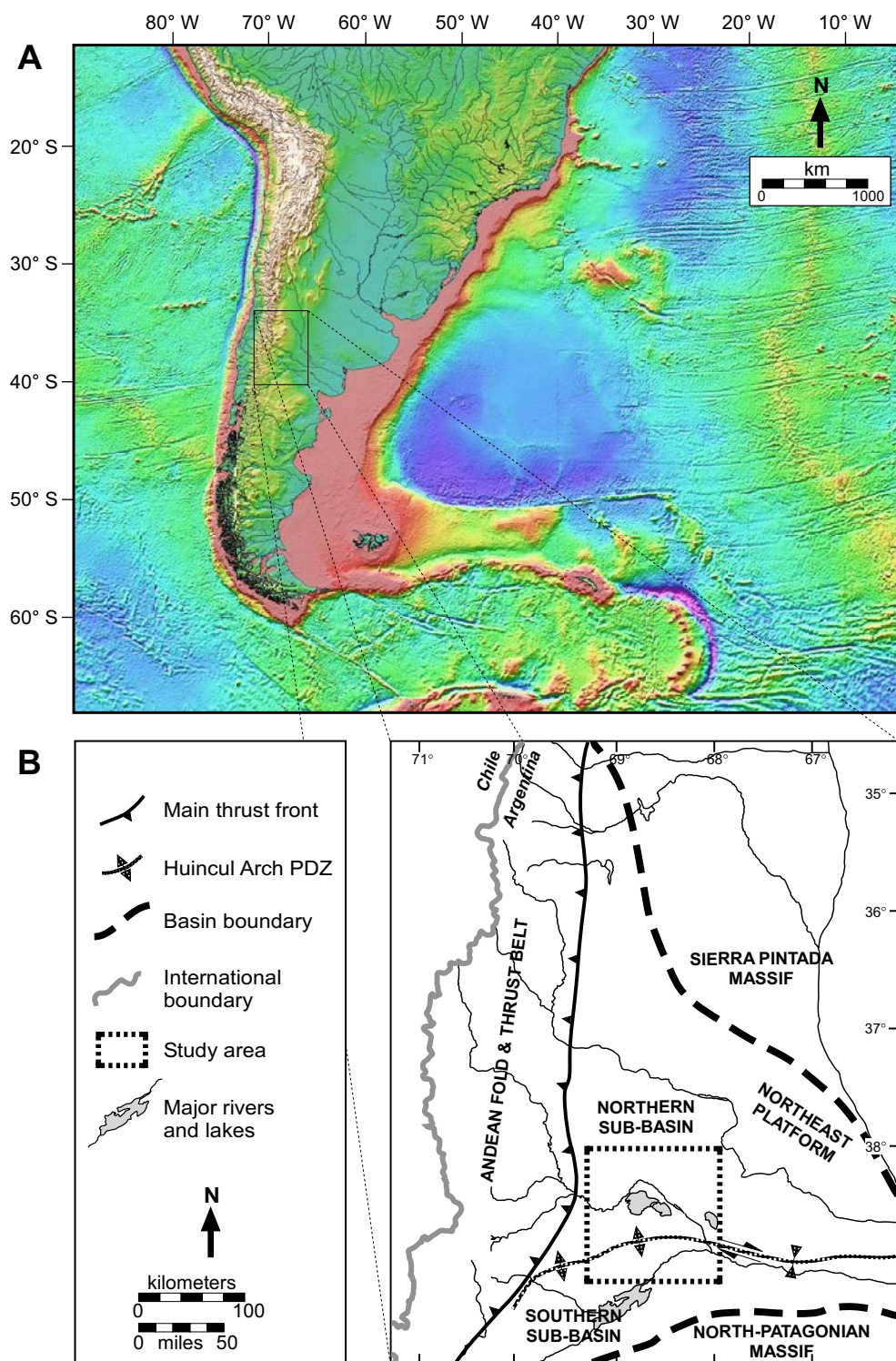
Figure 3.1. Location of the Neuquén Basin in southern South America. (A) Topography and ocean floor bathymetry from Smith and Sandwell (1997). (B) Generalized tectonic map of the Neuquén Basin showing main provinces and tectonic elements.

the Pacific (Uliana et al., 1989; Urien and Zambrano, 1994; Vergani et al., 1995;

Franzese et al., 2003), which flooded most of the basin (Figure 3.2B). Angular

unconformities separate Upper Triassic continental sediments and marine Jurassic rocks

and are related to continued extension-related block rotation during Early Jurassic time

(Uliana et al., 1989). A gradual change to thermal subsidence began at about Late

Toarcian time and allowed post-rift strata to cover the entire basin (Figure 3.2C;

Digregorio, 1978; Urien and Zambrano, 1994; Vergani et al., 1995). During late

Callovian time, general uplift and erosion occurred across the basin, but was particularly

dramatic along the Huincul Arch. Transpressive uplift along the arch was a precursor to

more intense late Oxfordian – early Kimmeridgian tectonic deformation. Inversion of

syn- and post-rift deposits along the axis of the Huincul Arch resulted in erosion of more

than 2 km of basement through Middle Jurassic strata (Ploszkiewicz et al., 1984;

Legarreta and Uliana, 1996).

During late Callovian – early Oxfordian time, connection with the Pacific Ocean

was reestablished, which began another, although more areally limited, second-order

transgressive-regressive stratigraphic cycle. The increase in basin-wide accommodation

has been attributed to relaxation of compressional stresses by some workers (Vergani et

al., 1995), whereas others invoke global eustasy and the onset of sea-floor spreading in

the Central Atlantic as causes for the relative sea-level rise (Legarreta and Uliana, 1996).

An intense period of tectonic inversion occurred during late Oxfordian-early

Kimmeridgian time (Vergani et al., 1995) and caused the basin to become a restricted

shallow-marine setting (Legarreta, 2002). During this tectonic event, known as the
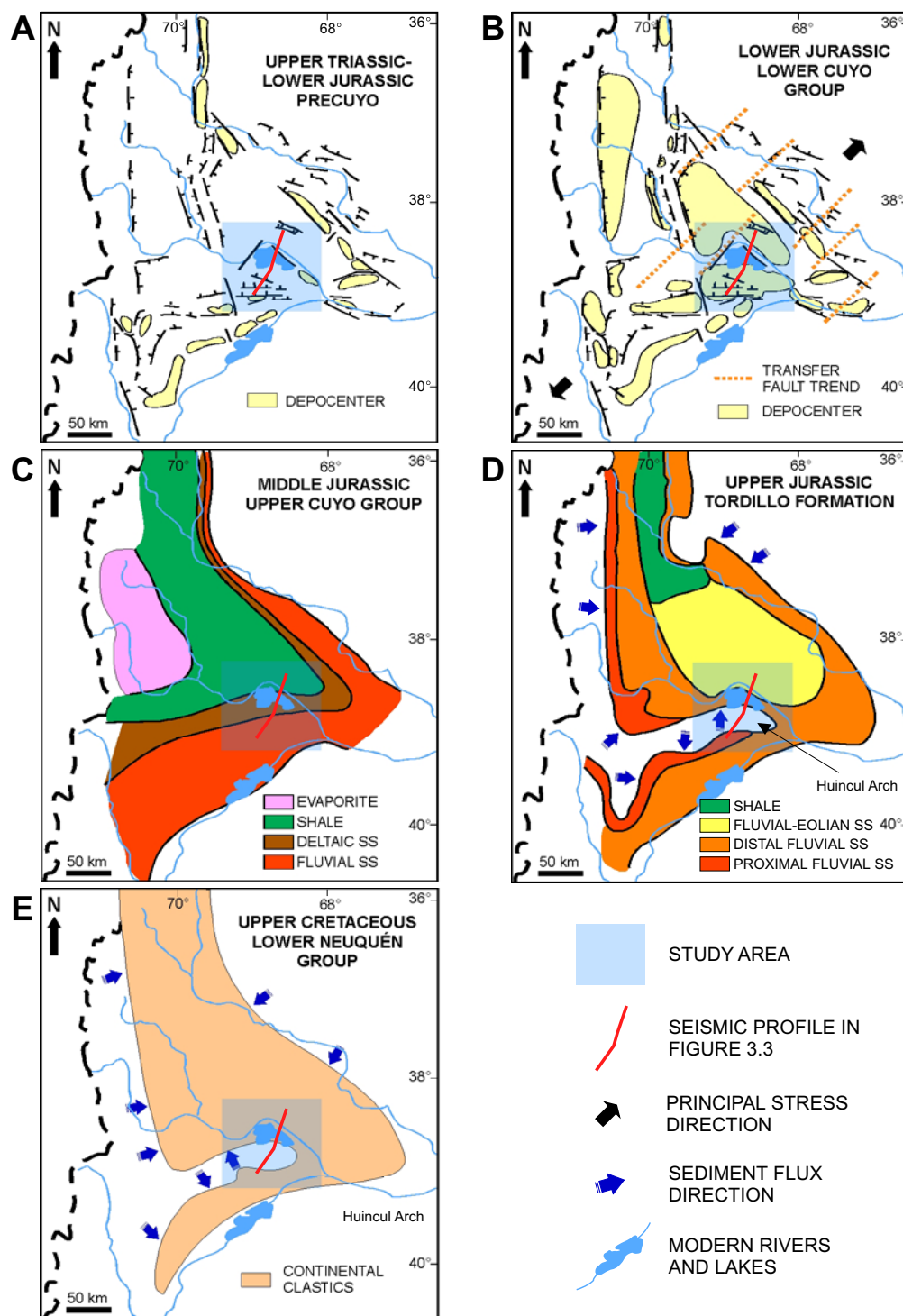
Figure 3.2. Main stages of the Mesozoic structural and paleogeographic evolution of the Neuquén Basin (from Vergani et al., 1995). (A) General syn-rift fault trends; (B) Late syn-rift - early post-rift depocenter expansion; (C) Post-rift depositional facies patterns (Upper Cuyo Group); (D) Araucanian inversion event along Hincul Arch and depositional facies patterns across Neuquén Basin; (E) Mirano inversion event and depositional facies.

"Araucanian" or "Inter-Malm" orogeny (Digregorio and Uliana, 1980), older extensional structures were selectively reactivated, especially in the western and southern parts of the basin and in particular the Huincul Arch (Figure 3.2D). Upper Jurassic strata were deeply eroded in those areas (Vergani et al., 1995). NW-SE trending transfer faults divide the Huincul Arch into three main segments, with the intensity of the inversion decreasing from west to east. Pyroclastic deposits of Late Jurassic age record the presence of an active volcanic arc west of the basin (Legarreta and Uliana, 1996).

Oceanic communication was again fully restored during Tithonian time. Increased subsidence (attributed to relaxation of in-plane stress by Vergani et al., 1995) resulted in the development of a new transgressive-regressive cycle (Legarreta and Uliana, 1996). Another period of tectonic inversion during Valanginian time caused further reactivation of extensional faults along the Huincul Arch and in the western part of the basin. This pulse of inversion is recorded by an erosional unconformity of early Neocomian age (Valanginian unconformity) that extends across the arch. The inverted areas contributed sediment to the Southern Sub-basin (Vergani et al., 1995). Renewed marine transgression started during late Valanginian time and ended with general shallowing of the basin during late Albian time.

The "Mirano" orogeny (also referred to as "Intra-Senonian" movements) describes renewed inversion during Cenomanian time and is recorded by erosion of Upper Cretaceous strata in the western part of the basin (Figure 3.2E; Uliana et al., 1975). This episode of deformation apparently closed the basin to oceanic circulation from the Pacific Ocean (Digregorio et al., 1984). At the same time, the Andean arc

became the dominant sediment source area for the Neuquén Basin (Legarreta and

Gulisano, 1989; Uliana and Legarreta, 1993). These significant changes are also

associated with the beginning of foreland basin development in the Argentine backarc

region. Incipient backarc thrusting to the west and emplacement of Cretaceous batholiths

may have produced regional uplift on the Andean side of the basin (Barrio, 1990; Uliana

and Legarreta, 1993). A progressively increasing proportion of volcaniclastic rocks

accumulated in eastward-migrating depocenters and record the eastward migration of the

volcanic arc (Digregorio et al., 1984; Ramos and Aleman, 2000). A marine incursion

from the eastern side of the basin during Maastrichtian to Paleocene time led to

deposition of shallow-marine siliciclastic, limestone and evaporite facies (Legarreta and

Gulisano, 1989; Barrio, 1990).

Early Eocene to Recent subsidence patterns in the Neuquén Basin are largely due

to backarc thrusting. The main bounding faults of half-graben depocenters, as well as

secondary faults within these basins, were reactivated to varying degrees during this

phase (Manceda and Figueroa, 1995). Thin Eocene strata extend across most of the

basin, which suggests only limited flexural subsidence (Uliana and Legarreta, 1993).

Overprinting by subsequent tectonic events associated with the Cenozoic Andean

orogeny determined the present structural configuration of the Neuquén Basin, which

consists of: (1) a western or "internal" fold-and-thrust belt, (2) a transition zone or

"external" fold-and-thrust belt to the east, and (3) an eastern region, known as the

Neuquén Embayment, comprised of the Neuquén Sub-basin, Huincul Arch shear zone,

and northeastern platform (Figure 3.1; Bracaccini, 1970; Ramos, 1978; Urien and

Zambrano, 1994; Vergani et al., 1995). Deformation intensity generally decreases from west to east with increasing distance from the Andean orogen.

Stratigraphy of the Central Neuquén Basin

Pre-Mesozoic basement rocks beneath the Neuquén Basin consist of a complex of Paleozoic metamorphic and igneous rocks, with minor Carboniferous strata. A 7 km-thick Mesozoic-Cenozoic sedimentary succession overlies these basement rocks (Figure 2.8).

Early syn-rift strata in the Neuquén Basin are known as the "pre-Cuyo" cycle and consist mostly of siliciclastic facies that were deposited in alluvial fan, fluvial, and lacustrine environments (Legarreta and Gulisano, 1989; Urien and Zambrano, 1994). Overlying the syn-rift interval is a post-rift succession of marine and fluvial sedimentary rocks known as the "Cuyo Group", which was deposited during a transgressive-regressive cycle that lasted from Hettangian to Callovian time (Digregorio, 1972; Digregorio and Uliana, 1980; Gulisano and Pando, 1981; Hinterwimmer and Jáuregui, 1985; Legarreta and Gulisano, 1989; Urien and Zambrano, 1994).

The 1,500 m-thick Cuyo cycle is a progradational, basinward-thickening sequence, which consists of basal marine shales (Los Molles Formation) that grade laterally and upward into alluvial and deltaic deposits (Lajas Formation) (Digregorio and Uliana, 1980; Urien and Zambrano, 1994; Vergani et al., 1995; Legarreta, 2002). The early Callovian sea-level rise caused significant transgression across western Argentina as recorded by the upper part of the Lotena Formation, which consists of marginal marine siliciclastic facies that grade basinward into marine carbonate (Barda Negra

Formation) and evaporite (Auquilco Formation) facies (Legarreta and Gulisano, 1989; Urien and Zambrano, 1994; Vergani et al., 1995; Legarreta, 2002).

Local tectonic uplift that occurred during the Araucanian inversion caused fluvial deposits (Lower Tordillo Formation) to be intermixed with volcanics in depositional lows. Siliciclastic sediments were sourced from the south, northeast, and west. Western units are thicker due to the contribution of pyroclastic sediment from the Andean volcanic arc (Vergani et al., 1995).

Communication with the Pacific Ocean was reestablished during Thithonian time, with a major flooding surface between continental facies of the Tordillo Formation and the overlying and northwestward-prograding basinal to inner-shelf facies of the Tithonian-Berriasian Lower Mendoza Group (Verzi et al., 2002). The Lower Mendoza Group is a 1 km-thick unit that consists of the Vaca Muerta black shales (main petroleum source rock in the basin), and overlying, northwestward progradational carbonate ramp facies of the Quintuco Formation.

Selective uplift due to inversion along the Huincul Arch during Valanginian time provided another sediment source to the basin, resulting in deposition of the Upper Mendoza Group. Continental facies (fluvial and alluvial sandstone and conglomerate facies of the Mulichinco Formation) along the eastern and southeastern basin margin grade northwestward into shoreface to outer shelf facies in the basin center (Vergani et al., 1995). Relative sea-level rise during late Valanginian time caused deposition of black shale facies (Agrio Formation) in the inner basin, which interfinger with prograding fluvial siliciclastic facies (Centenario Formation) in eastern parts of the

Northern Sub-basin. This depositional cycle ends with regional shallowing of the Neuquén Basin and with deposition of continental red beds of the Rayoso Group during Albian time. Reactivation of source areas along the Huincul Arch during the Mirano orogeny caused subtle erosion of Rayoso strata and accumulation of continental deposits with significant pyroclastic material, known as the Neuquén Group during early Cenomanian – late Campanian time (Legarreta and Gulisano, 1989; Vergani et al., 1995). Continental and marine sediments of the Maastrichtian - Paleocene Malargüe Group comprise the last significant deposits in the Neuquén Basin.

The Huincul Arch and the Northern Sub-basin

The Northern Sub-basin of the Neuquén Basin is bounded to the south by the Huincul Arch (Cruz et al., 2002). Late Triassic rift depocenters within the Northern Sub-basin were tectonically inverted when subjected to N-S to NW-SE compression induced by a convex-to-the-north restraining bend along the Huincul Arch's principal displacement zone (Figure 3.3A). Consequently, Pre-Cuyo to lowest Cuyo syn-rift sedimentary wedges within the Northern Sub-basin were uplifted with decreasing intensity from south to north (Figure 3.3B). Nearby areas characterized by *en échelon* extensional faults and negative flower structures (e.g., Ramón Castro Extensional Zone; Figure 3.3A) are attributed to local bends along the main principal displacement zone (PDZ) that defines the axis of the Huincul Arch (Ploszkiewicz et al., 1984; Pángaro and Bruveris, 1999). The PDZ extends eastward but shows a dominantly transtensional character near the southeastern basin boundary (Orchuela and Ploszkiewicz, 1984).
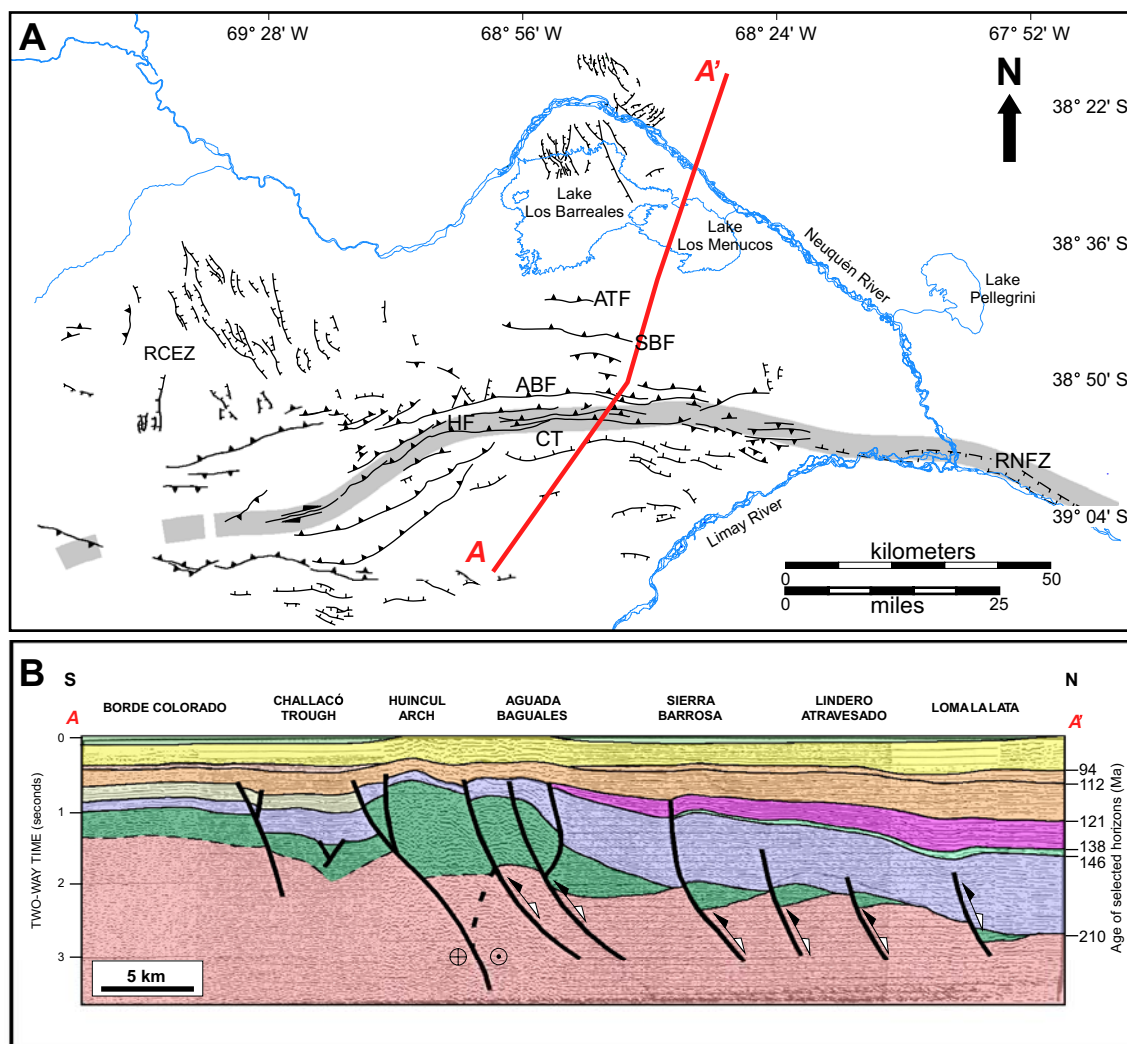
Figure 3.3. Main structural elements of the central Neuquén Basin. (A) Main faults associated with the Huincul Arch following Mesozoic transpressional tectonics. The Huincul Arch is the approximately 10-km wide deformation zone indicated by the shaded line. RCEZ: Ramón Castro Extension Zone, HF: Huincul Fault, ABF: Aguada Baguales Fault, CT: Challacó Trough. ATF: Aguada Toledo Fault, SBF: Sierra Barrosa Fault, RNFZ: Río Negro Fault Zone. Based on Maretto and Lara (2002), Orchuela et al. (1981), Pángaro and Bruveris (1999), Ploszkiewicz et al. (1984), and Vergani et al. (1995). (B) Composite seismic section across the southern Neuquén Basin showing location and style of early Mesozoic faults and associated inversion structures. Modified from Uliana et al. (1995). Line of section shown in A.

DATA AND METHODS

A 2D and 3D seismic and borehole dataset covering part of the central Neuquén Basin (Northern Sub-basin) was released to Texas A&M University by Repsol-YPF. The seismic data consist of four 3D surveys covering a total area of ~1500 km^2 and ~4000 line-km of 2D surveys covering an area of ~10,000 km^2 (Figure 3.4). The borehole dataset consists of digital well logs from ten exploratory wells and thirty development wells located mostly in the central and northeastern portions of the Northern Sub-basin. Most "deep" exploratory wells penetrate Middle and Lower Jurassic strata, whereas the "shallow" development wells penetrate the Lower Cretaceous to Upper Jurassic section. Repsol-YPF also provided access to proprietary reports on the stratigraphy of the Northern Sub-basin. An extensive literature survey on the tectonics and stratigraphy of southern South America was conducted, with emphasis on Mesozoic inversion, plate-scale features, and related tectonic events. Information from these published sources was integrated with interpretations from this study in order to provide a regional-scale tectono-stratigraphic framework for Mesozoic inversion events across the Argentine foreland.

All digital data were loaded onto UNIX workstations from 8-mm tapes. Subsurface characterization software (GeoFrame™ by Schlumberger™) was used for structural and stratigraphic mapping. Coherency volumes were generated using the Variance Cube™ module within GeoFrame™ to improve structural mapping. Time-structure and time-thickness maps were constructed using the gridding algorithms available in BaseMap Plus™. Well data was time-converted using Synthetics™.
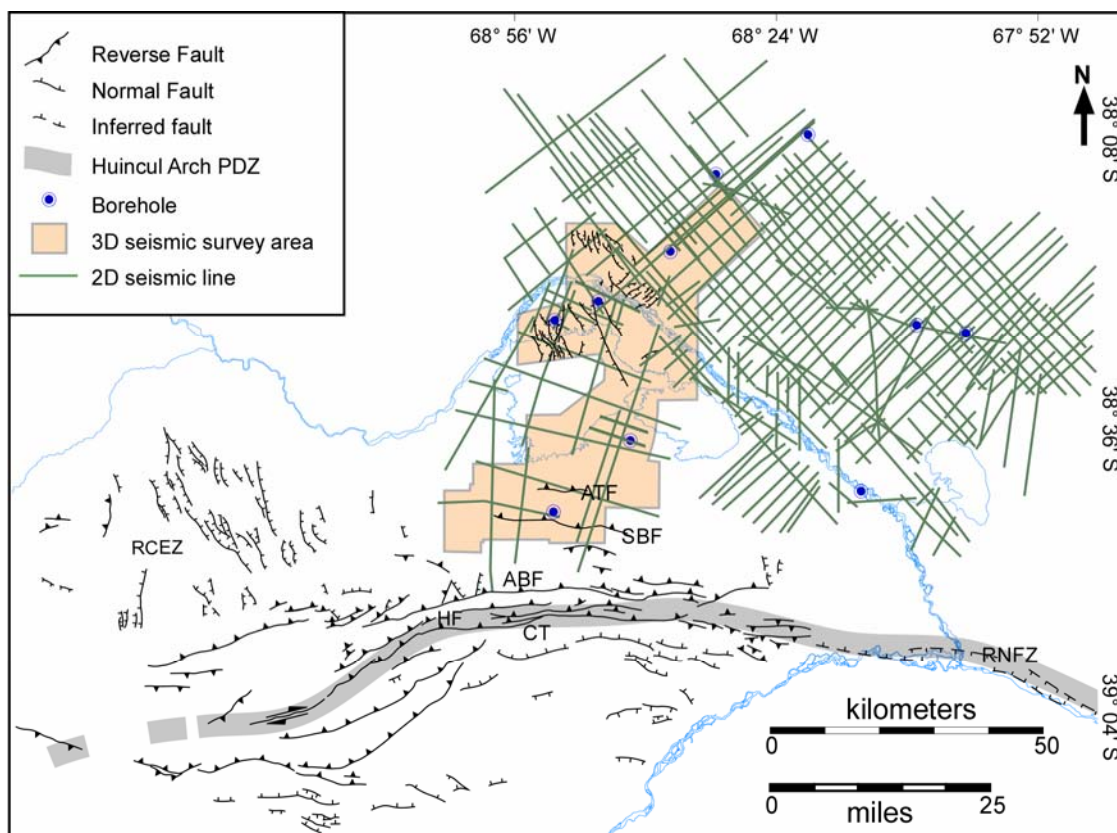
Figure 3.4. Location of the borehole and seismic dataset used in this study. RCEZ: Ramón Castro Extension Zone, HF: Huincul Fault, ABF: Aguada Baguales Fault, CT: Challacó Trough. ATF: Aguada Toledo Fault, SBF: Sierra Barrosa Fault, RNFZ: Río Negro Fault Zone. Based on Maretto and Lara (2002), Orchuela et al. (1981), Pángaro and Bruveris (1999), Ploszkiewicz et al. (1984), and Vergani et al. (1995).

RESULTS

Well-seismic correlation

Synthetic seismograms were constructed for all exploratory wells from available checkshot surveys and sonic logs (Figure 3.5). Formation tops picked on log curves were seismically correlated across the entire dataset.
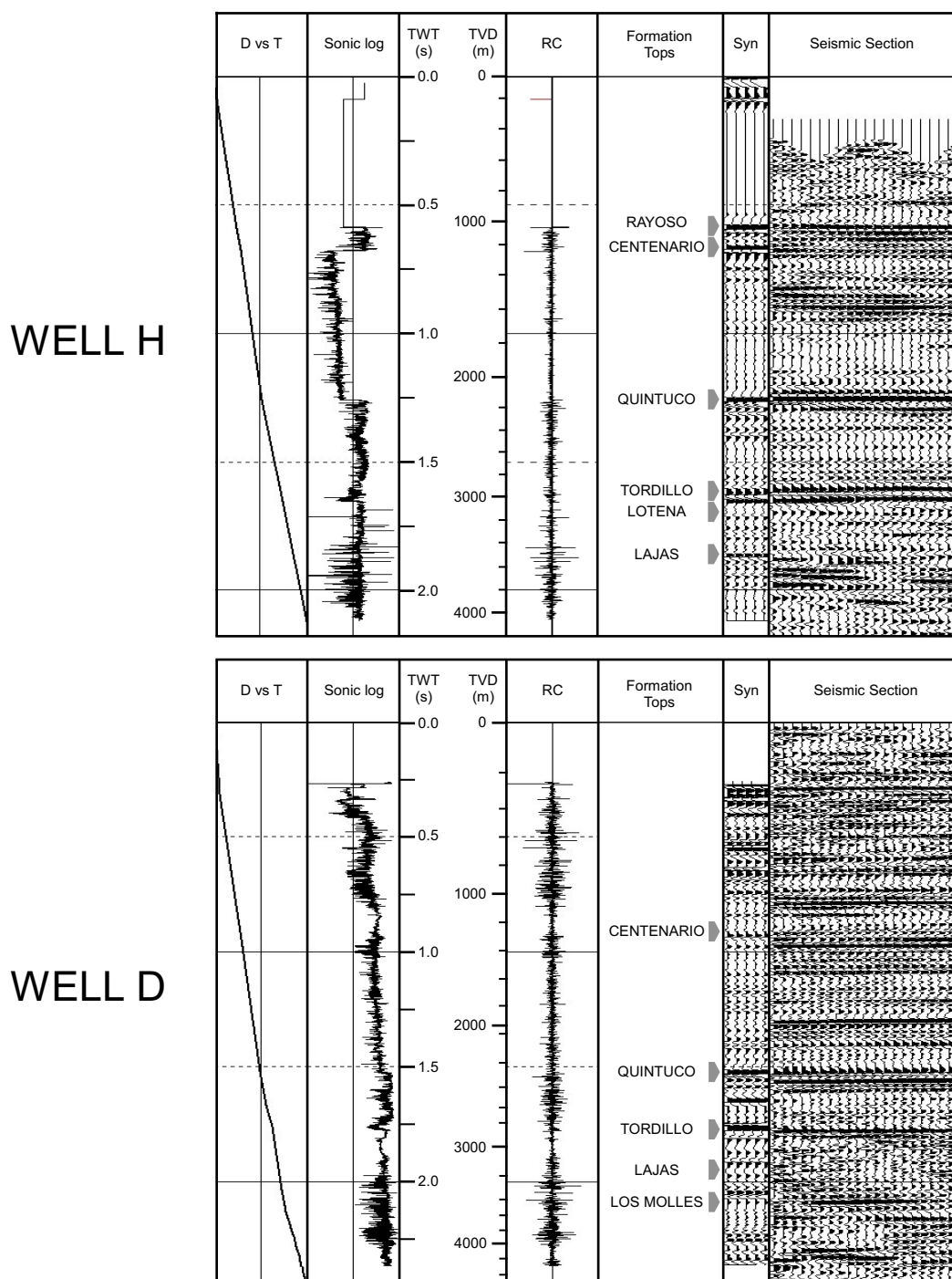
Figure 3.5. Synthetic seismogram generation panels for wells H and D and representative seismic section from well locations. See Figure 3.4 for well locations. D vs T = Depth vs time curve; TVD = True Vertical Depth; TWT = Two-way time; RC= Reflection Coefficients; Syn = Synthetic Seismogram.

Six stratigraphic horizons were picked in well logs and posted on seismic data, including top basement, top Pre-Cuyo (syn-rift), base of Lotena, base of Vaca Muerta, top of Quintuco, and base of Neuquén Group. Formation tops identified in exploratory wells further constrained stratigraphic mapping across the study area.

Seismic interpretation

Inversion structures

Basement structural level within the Neuquén Basin shallows toward the Huincul Arch and all Mesozoic sedimentary units show general thinning in that direction. Tectonic inversion along the Huincul Arch caused uplift of the southern part of the Northern Sub-basin (Figure 3.6A), which is an excellent setting to study the timing and stratigraphic response to regional patterns of inversion. Farther away from the Huincul Arch, the stratigraphic record is more complete, unconformities are less amalgamated, and seismic data of better quality, which allow identification of more detailed structural and stratigraphic relationships.

Five main inversion structures associated with reverse-reactivated E-W normal faults were identified. From south to north, these are the Aguada Baguales, Sierra Barrosa, Aguada Toledo, El Cordon, and Sauzal Bonito structures (Figure 3.6B). Stratal relationships and ages of key horizons were used to estimate timing of deformation events and to identify patterns of strain distribution and inversion propagation. All inversion structures have a similar fault configuration at the basement level, consisting of inverted half-grabens with faulting and folding of the overlying stratigraphic section.
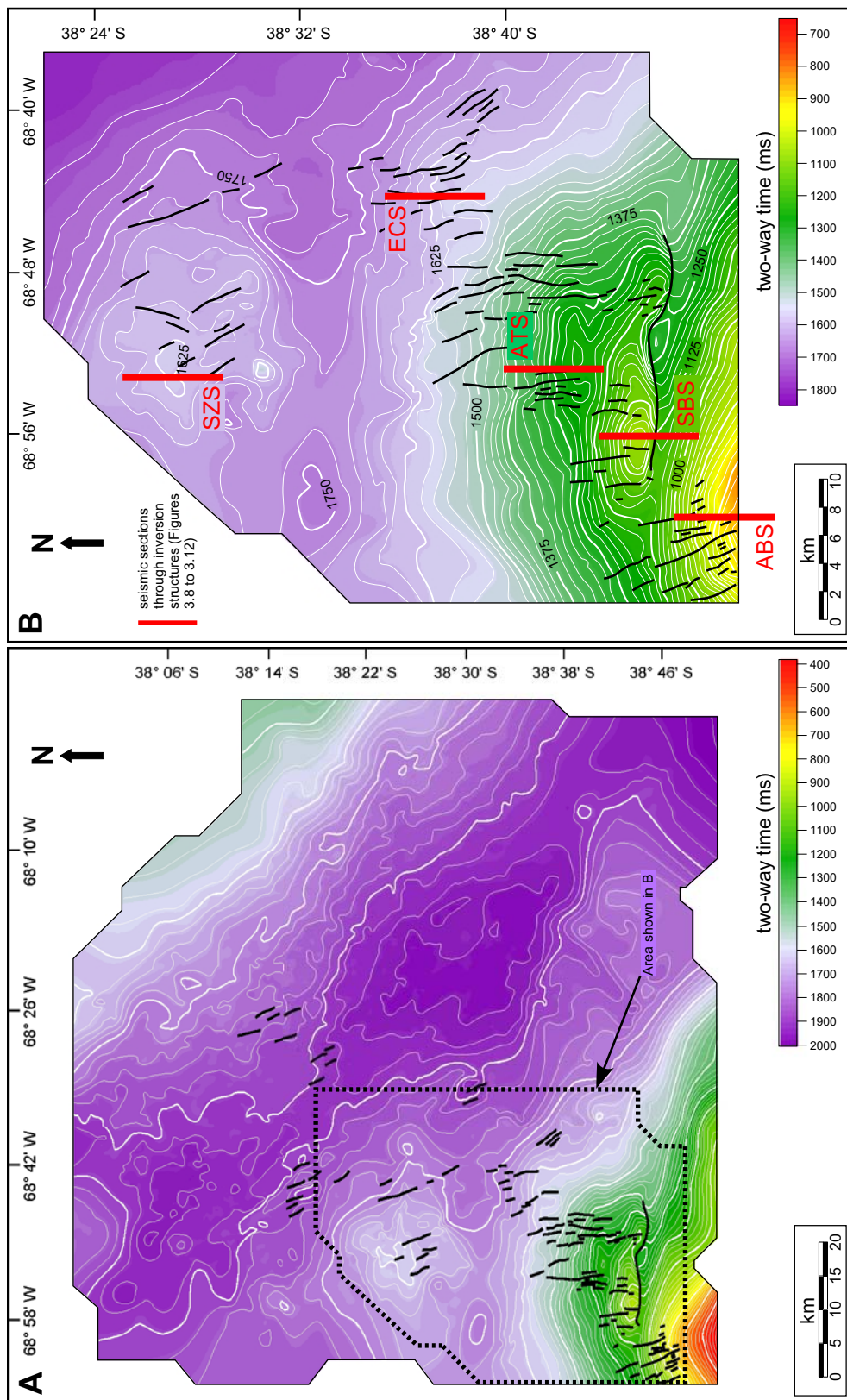
Figure 3.6. Basin configuration for the Northern Sub-basin, north of the Huincul Arch. (A) Time-structure map at the base of Vaca Muerta Formation showing the general northward-deepening of the basin away from Huincul Arch. (B) Detail of the area closest to the Huincul Arch, where inversion structures identified in this study are located. Contour Interval = 25 ms. ABS: Aguada Baguales Structure; ATS: Aguada Toledo Structure; ECS: El Cordón Structure; SBS: Sierra Barrosa Structure; SZS: Sauzal Bonito Structure.

Aguada Baguales Structure

The "Aguada Baguales" Structure (Ploszkiewicz et al., 1984; Legarreta et al., 1999; Gómez Omil et al., 2002) is an E-W elongated anticline, ~40 km long and 9 km wide that is interpreted as an inverted half graben. The back limb of this inversion anticline is partially imaged in the 3D seismic dataset examined during this study (Figure 3.6B). A regional 2D seismic line cuts through the crest of this structure (Figure 3.7) and was used to document stratigraphic and structural relationships between this structure and the Sierra Barrosa structure to the north.

The Aguada Baguales Structure is the largest and structurally highest inversion anticline in the study area. It is characterized by intense backthrusting, where antithetic faults accommodate part of the shortening as the master bounding fault locked up during inversion. Given the Aguada Baguales Structure's proximity to Huincul Arch's principal displacement zone, there may have been significant oblique slip along the main bounding fault of this structure.

Lack of well control along the structure's forelimb precludes accurate estimation of displacement along the master fault or detailed investigation of syn-inversion growth-stratal patterns. Amalgamated unconformities, however, reflect missing strata of the Cuyo, Lotena and Mendoza groups along the structure's crest, where Late Cretaceous Neuquén Group deposits overlie Cuyo strata. In addition, younger strata successively onlap the top of Vaca Muerta horizon and within the lower Quintuco Formation on the structure's backlimb (Figure 3.7), which indicates syn-inversion deposition from Tithonian to Berriasian time. Overlying the Mendoza Group, the Intra-Senonian unconformity

Figure 3.7. Uninterpreted (A) and interpreted (B) seismic sections through Aguada Baguales inversion structure. Sections are oriented perpendicular to the main bounding fault of this inversion structure. Significant stratal pinch-outs and unconformity amalgamation at the structure's limbs reflect recurrent tectonic activity from Middle Jurassic to Late Cretaceous time. See Figure 3.6B for location.

is slightly folded over the structure's crest, reflecting mild tectonic activity during Late Cretaceous time.

Sierra Barrosa Structure

The Sierra Barrosa Structure (Bettini, 1984; Ploszkiewicz et al., 1984; Uliana et al., 1995; Gómez Omil et al., 2002; Hechem and Veiga, 2002; Schiuma et al., 2002) is an E-W trending, ~22 km long and 6 km wide anticline with a slightly curved crest and two distinct areas of maximum overall uplift (Figure 3.6B). A reverse-reactivated fault defines the southern flank of the anticline. The Sierra Barrosa Structure is characterized by a strongly-folded and uplifted syn-rift wedge with minor backthrusting affecting the lowest part of the syn-rift section (Figure 3.8). The structure's hangingwall has a dense array of syn-inversion extensional faults that are roughly perpendicular to the master bounding fault (Figure 3.6B).

No amalgamated unconformities are observed, although thinning of different stratigraphic units is visible over the structure's crest. Internal onlap and reflection divergence within the Upper Quintuco Formation suggest syn-inversion deposition on both limbs of the structure during Berriasian and early Valanginian time. Lower Quintuco strata, however, have more uniform thickness and an internal arrangement of parallel and subparallel reflections (Figure 3.8C).

The Intra-Valanginian unconformity is well imaged, although the lowest strata of the Upper Quintuco Formation were not completely eroded and were unconformably

STRATIGRAPHIC UNITS

- Centenario + Rayoso groups
- Neuquén Group
- Quintuco Fm
- Vaca Muerta Fm
- Lotena Fm
- Cuyo Group
- Pre-Cuyo Group
- Basement

Figure 3.8. Uninterpreted (A) and interpreted (B) seismic sections through Sierra Barrosa inversion structure. Sections are oriented perpendicular to the main bounding fault of this inversion structure. Significant erosion on structure's crest at the top of Cuyo Group. See Figure 3.6B for location.

overlain by basal strata of the Centenario and Rayoso formations, which are slightly folded over the structure's crest. The Intra-Senonian unconformity is roughly horizontal.

Aguada Toledo Structure

The Aguada Toledo Structure (Ploszkiewicz et al., 1984; Hechem and Veiga, 2002) is an E-W oriented, 10-km long and 3-km wide anticline (Figure 3.6B). The structure is bounded to the south by a reverse-reactivated fault. Inversion caused this fault to propagate upsection until it ultimately terminated within Lower Cuyo post-rift strata. Folding associated with fault reactivation, however, affects the entire post-rift section, with intensity decreasing above the Intra-Valanginian unconformity. The structural style of the inversion structure is characterized by mild internal deformation and buttressing within the syn-rift wedge, with some associated backthrusting and reverse reactivation of secondary syn-rift normal faults (Figure 3.9). The eastern and western flanks of this double-plunging anticline are affected by syn-inversion extensional faults with N-S orientation, which are associated with internal deformation of the hangingwall.

The Intra-Callovian and Intra-Malm unconformities are expressed by mild truncation of Upper Cuyo and Lotena strata, respectively, with minor thinning of these intervals over the structure's crest. Vaca Muerta, Lower Quintuco, and the basal portion of Upper Quintuco strata, however, have uniform thickness over the structure. Truncation of Upper Quintuco strata along the Intra-Valanginian unconformity is readily

Figure 3.9. Uninterpreted (A) and interpreted (B) seismic sections through Aguada Toledo inversion structure. Sections are oriented perpendicular to the main bounding fault of this inversion structure. Significant erosion on structure's crest at the top of Cuyo Group (Intra-Callovian unconformity) and top of Quintuco Fm. (Intra-Valanginian unconformity). Minor thickness variations within Lower Quintuco Fm. See Figure 3.6B for location.

observed (Figure 3.9). The Intra-Senonian unconformity is slightly folded, with minor truncation of upper Rayoso strata.

El Cordón Structure

A fragmented, E-W oriented inversion anticline, informally referred to here as El Cordón Structure, is located ~15 km northeast of the Aguada Toledo Structure (Figure 3.6B). This inversion structure consists of a relatively small syn-rift wedge bounded by a steep northward-dipping normal fault that was reverse-reactivated during inversion. Inversion caused the fault to propagate upward within Lower Cuyo strata and folded the entire overlying section up to the top of Rayoso Group level. Intensity of deformation is markedly less than for inversion structures to the south.

The syn-rift wedge is only mildly-deformed with no observable backthrusting or buttressing. Syn-inversion normal faults perpendicular to the master fault cut post-rift strata (Figure 3.6B). Antithetic syn-inversion normal faults developed around the structure's crest (Figure 3.10).

Strata above and below the main unconformities across the structure are essentially subparallel, with only minor truncation at the top of the Cuyo Group (Intra-Callovian unconformity). The entire Quintuco Formation, however, has uniform thickness over the structure, with no internal stratal geometries indicating syn-inversion deposition. The Inter-Senonian unconformity is folded over the structure's crest.
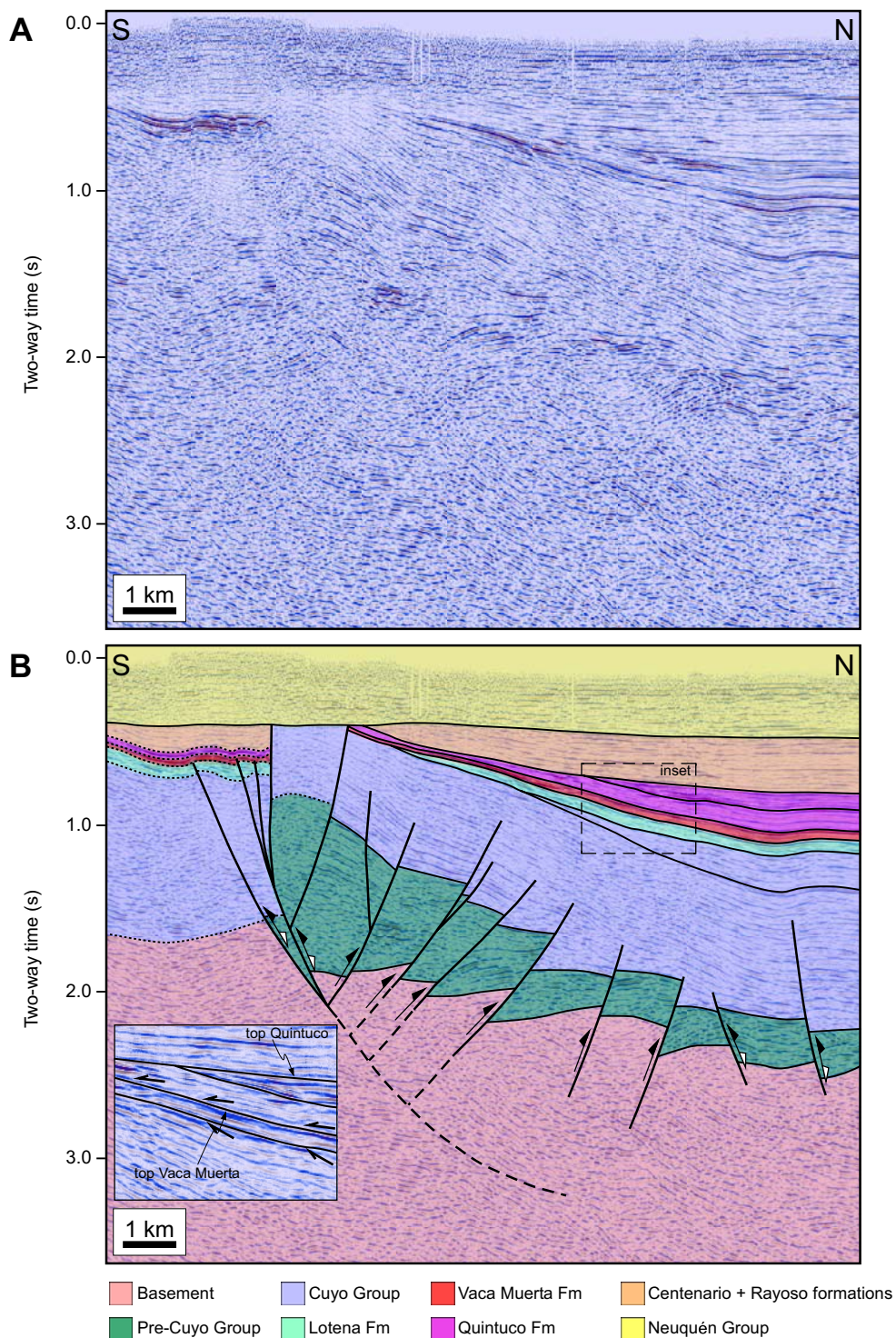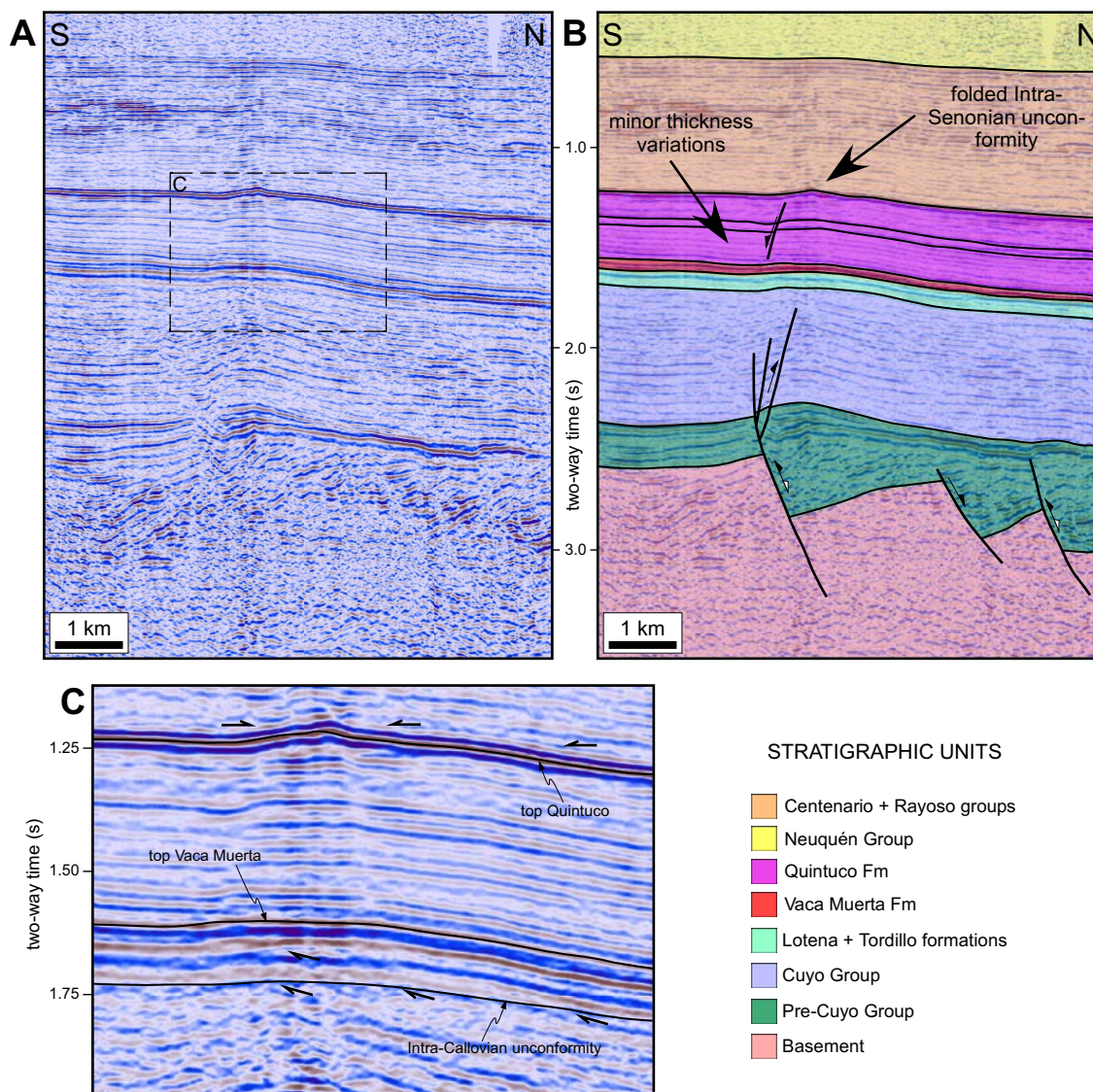
Figure 3.10. Uninterpreted (A) and interpreted (B) seismic sections through El Cordón inversion structure. Sections are oriented perpendicular to the main bounding fault of this inversion structure. Significant erosion is observed on structure's crest at the top of Cuyo Group (Intra-Callovian unconformity) and top of Quintuco Fm. (Intra-Valanginian unconformity). Lower Quintuco strata has uniform thickness over the inversion anticline. Intra-Senonian unconformity is folded. See Figure 3.6B for location.

Sauzal Bonito Structure

The Sauzal Bonito Structure is an important, but poorly understood high in the central Northern Sub-basin (Jalfin and Laffitte, 1996; Hechem and Veiga, 2002; Verzi et al., 2002). The Sauzal Bonito Structure formed, at least partly, during the Intra-Cenomanian (Mirano) inversion phase, although its present structural style has been interpreted to be affected by Cenozoic (Andean) tectonics (Hechem and Veiga, 2002).

The Sauzal Bonito Structure is an E-W oriented anticline that formed by inversion of a syn-rift wedge along a high-angle reverse-reactivated normal fault that bounds the southern flank of the structure (Figures 3.6B, 3.11). The reactivated fault cut to the level of the Lower Cuyo Group. Inversion caused fault propagation within Lower Cuyo Group and folded of the overlying section up to the Neuquén Group level.

The core of the structure is a slightly-inverted syn-rift wedge with no significant internal deformation. A low-displacement shortcut fault accommodates part of the shortening that occurred during inversion. Pre-Cuyo and Lowest Cuyo strata were deformed during inversion. Syn-inversion antithetic normal faults developed around the structure's crest (Figure 3.11).

All stratigraphic intervals have apparent conformable contacts, except for some mild truncation at the top of the Cuyo Group (i.e., along the Intra-Callovian unconformity). In addition, the Quintuco Formation has uniform thickness across the structure's crest and parallel to subparallel reflections internally. Upper Cretaceous strata and the Intra-Senonian unconformity are folded (Figure 3.11).
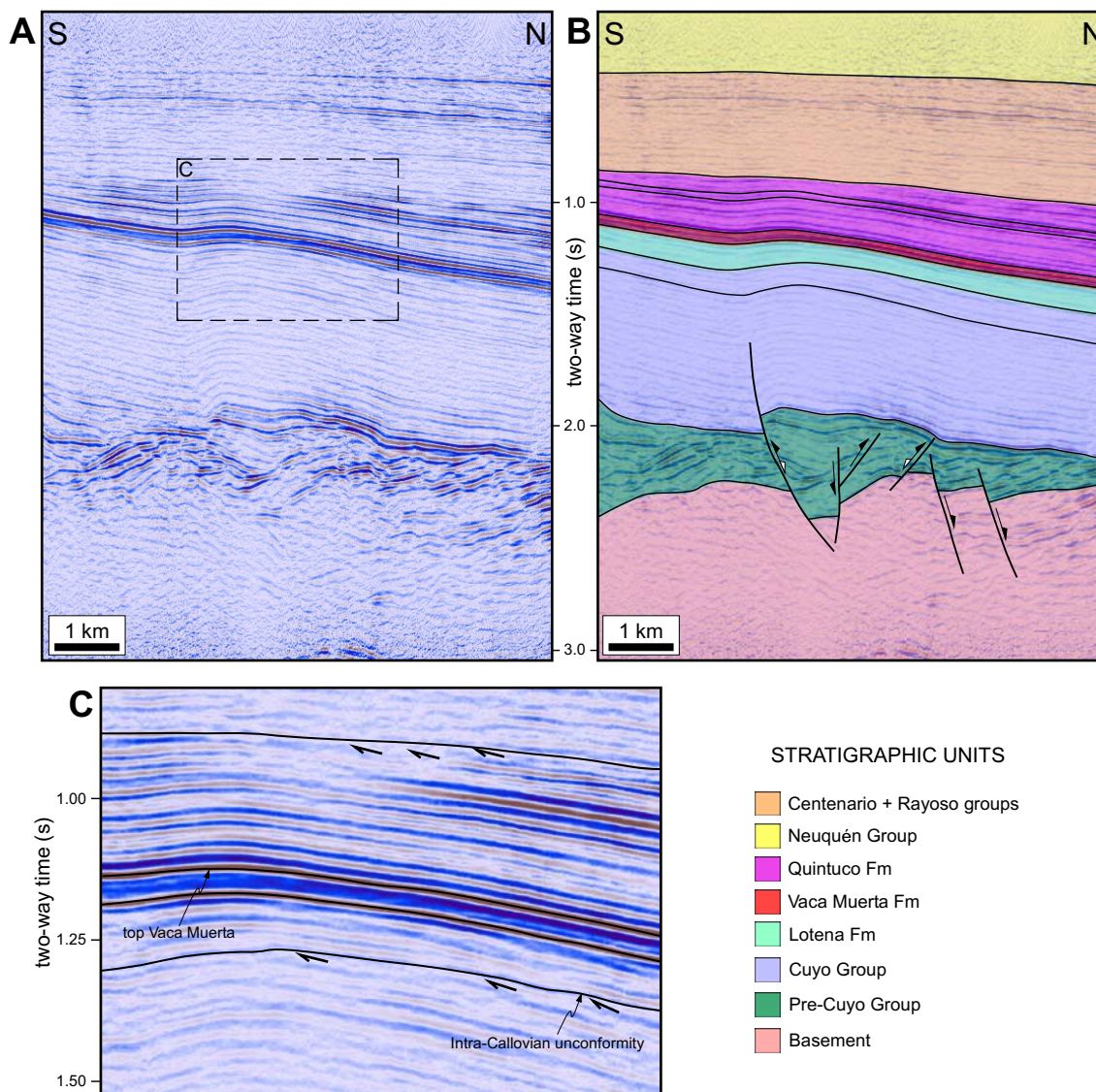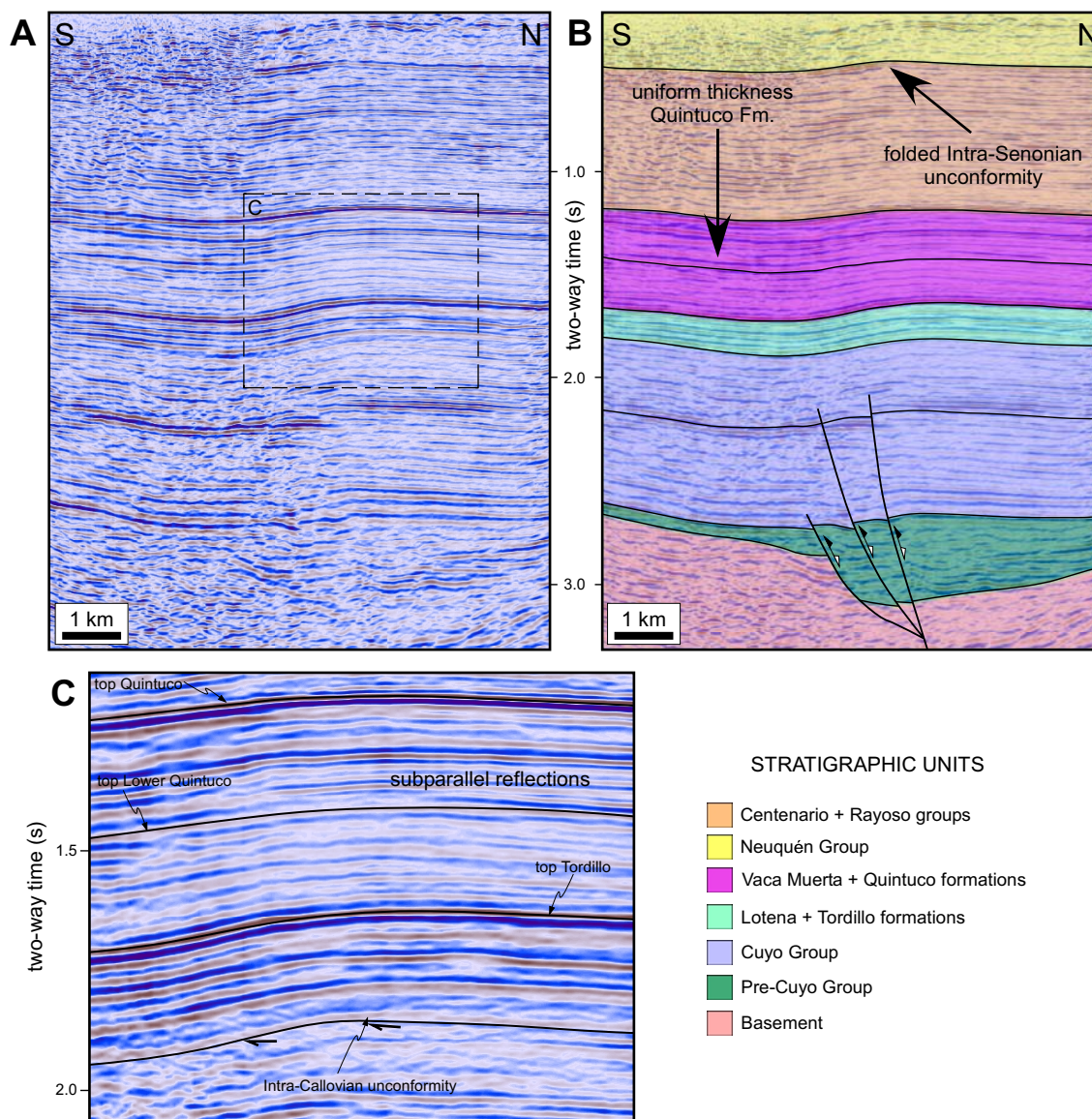
Figure 3.11. Uninterpreted (A) and interpreted (B) seismic sections through Sauzal Bonito inversion structure. Section is oriented perpendicular to the main bounding fault of this inversion structure. The top of the Cuyo Group is slightly eroded across the crest of the inversion structure (Intra-Callovian unconformity). Quintuco strata have uniform thickness over the inversion anticline. Intra-Senonian unconformity is folded. See Figure 3.6B for location.

Regional tectono-stratigraphic relationships

Inversion structures across the study area contain important patterns of unconformity development, growth stratal geometries, and deformation of the overlying section. These regional patterns can be summarized as: (1) Size of syn-rift wedges and intensity of inversion decrease markedly from south to north, with proximity to the Huincul Arch; (2) syn-inversion growth strata within the Quintuco Formation become progressively younger from south to north; (3) shortening, as expressed by folding of the Intra-Senonian unconformity and younger strata, increases slightly from south to north; (4) structures closer to the Huincul Arch exhibit significant stratal angularity along the main unconformities. The amount of missing section and angular stratal patterns along the main unconformities diminishes from south to north, although the amount of section eroded along the Intra-Callovian unconformity seems fairly similar across all of the inversion structures examined during this study.

DISCUSSION

Inversion patterns in the Northern Sub-basin

The convex-to-the-north shape of a restraining bend along the Huincul Arch caused the westward-moving block to act as a buttress or "mini indentor" that produced a localized compressive stress field across the southern part of the central Neuquén Basin. This N-S to NW-SE directed compressive stress resulted in significant tectonic inversion across the Northern Sub-basin for a distance of at least 70 km north of the

Huincul Arch's principal displacement zone. The area affected by inversion is at least

7000 km^2, based on inversion structures identified in this study and others reported in the

literature (Figure 3.12; Vergani et al., 1995; de la Colina, 1997; Berdini et al., 2002;

Gómez Omil et al., 2002; Hechem and Veiga, 2002; Mosquera, 2002). Given that the

total area of the extra-Andean (i.e., located east of the fold-and-thrust belt front)

Northern Sub-Basin is ~24,000 km^2, nearly one third of the Northern Sub-basin was

affected by Huincul Arch-related Mesozoic inversion.

Inversion structures observed in this study have similar structural styles and are

bounded by major faults with general E-W orientations. In contrast, rift depocenters with

NW-SE bounding faults (e.g., Entre Lomas and Bajada Vidal depocenters; Figure 3.12)

did not undergo inversion. These structures apparently were unfavorably oriented with

respect to the local compressive stress field across the Northern Sub-basin during Middle

Jurassic to Late Cretaceous time.

The axial part of the Northern Sub-basin is portrayed in the literature as lacking

significant Late Triassic syn-rift faulting (Figure 3.12), although basement structure

along the deepest areas of the basin are poorly imaged on seismic profiles. The inversion

structures along the southern flank of the Northern Sub-basin, however, suggest that

significant tectonic inversion should be expected along the deepest parts of the basin.

The Huincul Arch is a complex strike-slip shear zone with evidence for large inverted

rift basins. The size of inverted rift-depocenters in the Northern Sub-basin also seems to

decrease with distance from the Huincul Arch. These trends suggest that the Huincul

Arch may have been the zone of greater extension within the Neuquén Basin.
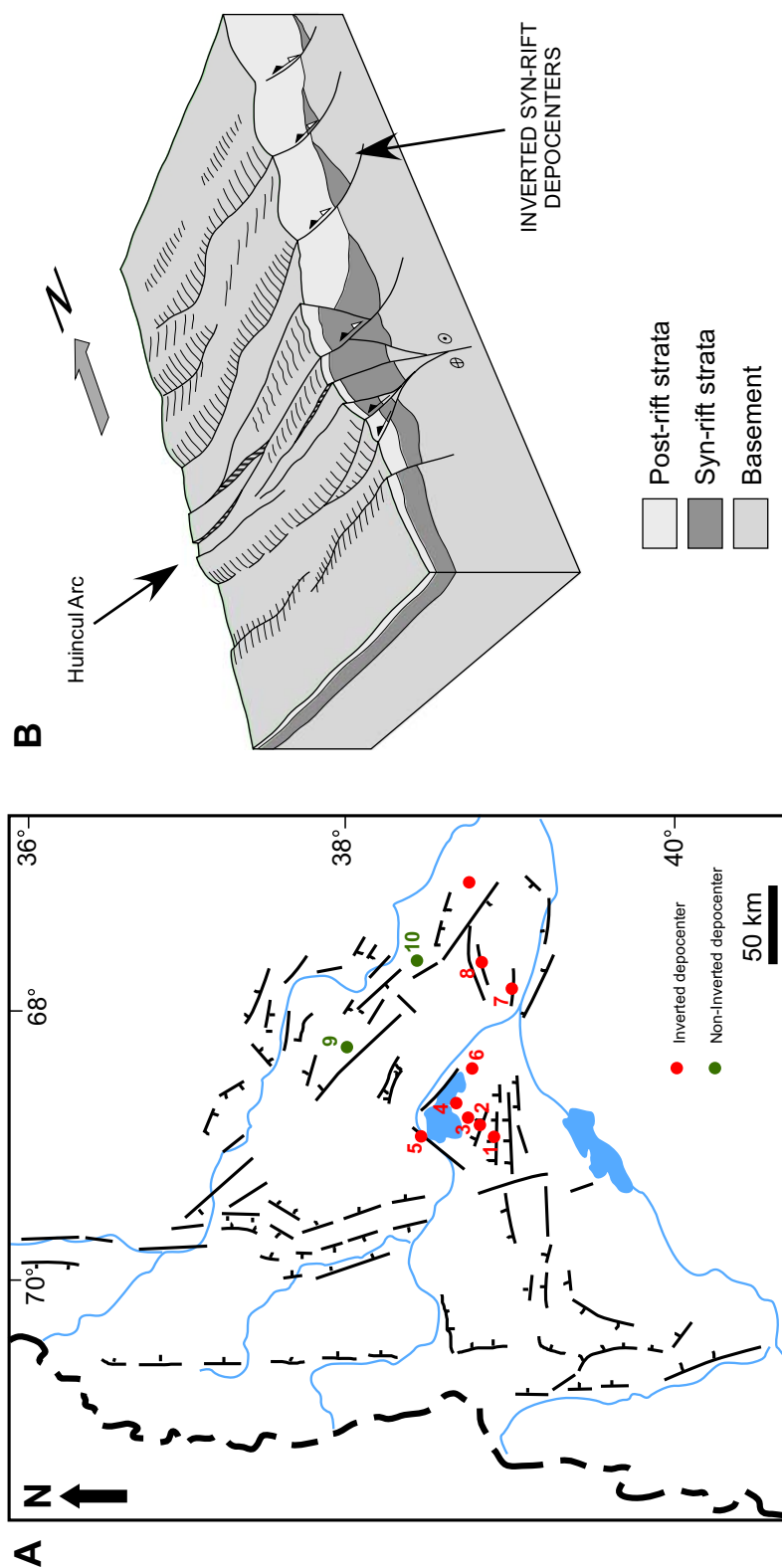
Figure 3.12. Distribution of inversion structures across the central Neuquén Basin. (A) Mesozoic inversion structures from the Neuquén Northern Sub-basin identified in this study and described in the literature. 1: Aguada Baguales; 2: Sierra Barrosa; 3: AguadaToledo; 4: El Cordon; 5: Sauzal Bonito; 6: Lindero Atravesado; 7: Río Neuquén; 8: Estancia Vieja; 9: Entre Lomas; 10: Bajada Vidal (After Vergani et al., 1995; de la Colina, 1997; Berdini et al., 2002; Gómez Omil et al., 2002; Hechem and Veiga, 2002; Mosquera, 2002). B: Schematic diagram showing the Huincul Arch principal displacement zone (PDZ) and inverted syn-rift depocenters on its northern flank.

Model for Mesozoic inversion propagation in the Northern Sub-basin

The structural and stratigraphic relationships observed in inversion structures across the Northern Sub-basin of the Neuquén Basin can be combined into a unifying conceptual model for inversion propagation and strain distribution (Figure 3.13). This model implies that distance from the Huincul Arch is the dominant control on fault reactivation and basin inversion.

An early stage of inversion occurred across the study area during early Callovian time after deposition of the post-rift Cuyo Group. Inversion was nearly synchronous across the study area as indicated by the presence of the angular Intra-Callovian unconformity in all inversion structures (Figure 3.13B-D). A period of relative quiescence and continued subsidence during late Callovian and Oxfordian time resulted in deposition of the Lotena Group, which contains strata that onlap and cover inversion highs but do not show syn-inversion growth stratal patterns (Figure 3.13D). Subsequent tectonic phases along the Huincul Arch during Kimmeridgian, Valanginian, and Cenomanian time are recorded as angular unconformities that are mostly restricted to the crest of each inversion structure. The amount of stratal truncation and angularity along these unconformities diminishes from south to north. This trend can be simply attributed to the decrease in deformation intensity away from the stress source.

The diachronous character of growth strata within the Quintuco Formation (Figures 3.7 to 3.11) and the slight northward increase in deformation of younger strata, however, suggest that younger inversion-related strain progressively migrated northward as successive structures "locked up" and shortening was transferred to inversion
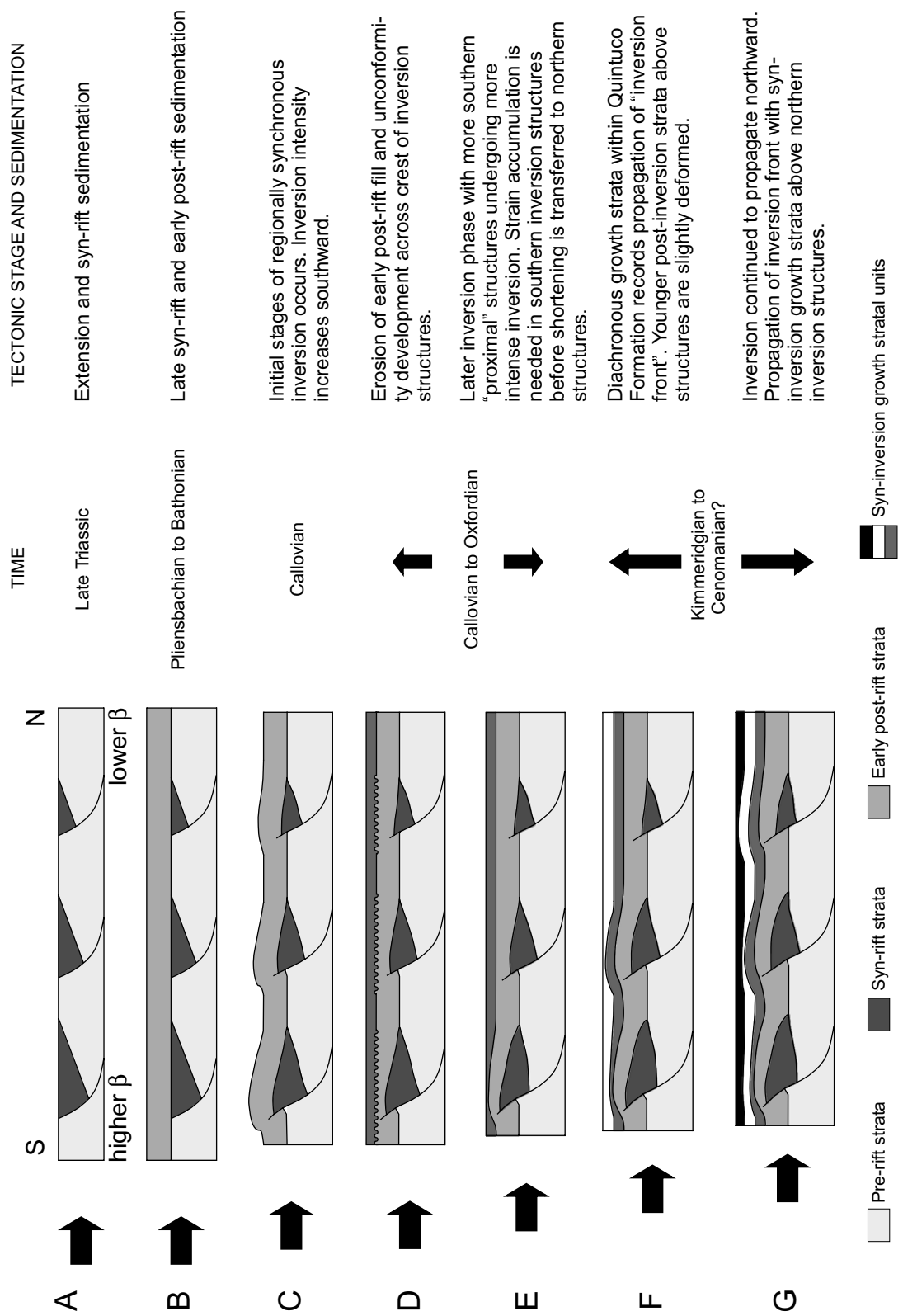
Figure 3.13. Conceptual model for inversion propagation patterns in the Neuquén Northern Sub-basin.

structures farther north from the Huincul Arch (Figure 3.13E-G). Even though minor shortening continued in inversion structures that are more "proximal" to the Huincul Arch, greater amounts of shortening clearly occurred in more "distal" structures (i.e., farther north from the Huincul Arch) during Early Cretaceous time. These patterns of northward propagation of inversion are mostly recorded by complex growth stratal patterns within the Quintuco Formation and by northward-increasing folding of younger post-Quintuco strata.

Mechanical considerations

The style of tectonic inversion in the Neuquén Northern Sub-basin suggests a strong control by pre-existing crustal discontinuities (i.e., faults) on the localization of intraplate shortening. The listric character and variable depths of detachment of the original rift faults (Figures 3.7-3.11) may have resulted in an increasing ease of compressional reactivation with depth (Figure 3.14; Sibson, 1995). That is, flat segments of basin-bounding, listric-shaped rift faults were first reactivated because of their subhorizontal attitude, and detachments at deeper crustal levels were more easily reactivated than shallower detachments. In this context, the synchroneity of fault reactivation across the Northern Sub-basin basin during the initial Callovian inversion event can be attributed to efficient transmission of N-S oriented compressive stress, which caused relatively easy reverse-reactivation of flat to low-dip segments of the original extensional faults. Relatively small amounts of shortening probably accumulated in "proximal" inversion structures before shortening was transferred to

more distal faults, resulting in almost synchronous fault reactivation of favorably-

oriented faults over a large area.
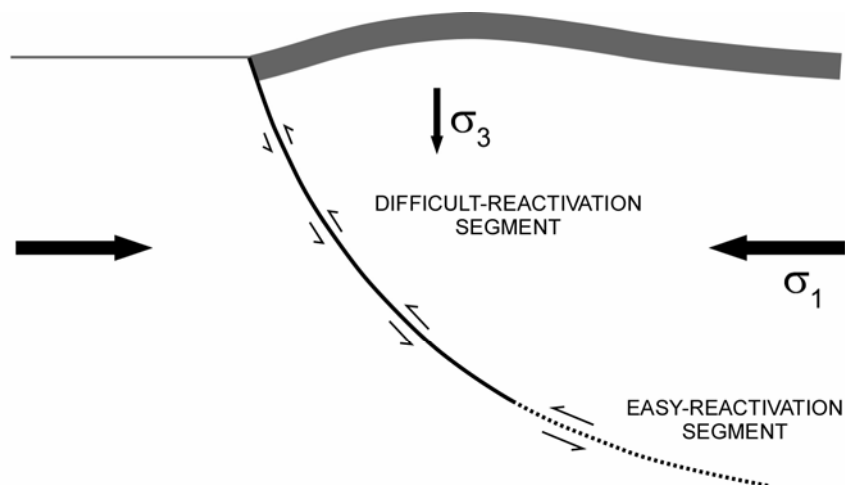
Figure 3.14. Schematic representation of a listric fault with easy- and difficult-reactivation segments. Under horizontal compressive stress the low-dip segment of the fault will be preferentially reactivated. Once significant reverse displacement along this segment has been accommodated, reactivation may occur along the more steeply dipping, shallower segment. After Sibson (1995).

During later inversion events (Kimmeridgian to Cenomanian), however, fault

reactivation was more difficult, which determined that structures more proximal to the

Huincul Arch underwent significant inversion before shortening was transferred to more

distal structures. In essence, the easy work had been done on all flat to gently-dipping

fault segments early on. Shortening during later inversion events had to be accomplished

along more steeply dipping fault segments. This more difficult shortening apparently

occurred first on more proximal inversion structures before it could be transferred to

more distal structures.

The multi-stage inversion propagation patterns can also be attributed to thermally-driven temporal variations in lithospheric mechanical behavior. Age estimations for Late Triassic rifting in the central Neuquén Basin range from 210 Ma (Rhaetian) to 190 Ma (Pliensbachian) (Digregorio and Uliana, 1980; Gulisano et al., 1984; Legarreta and Gulisano, 1989; Gulisano and Gutiérrez Pleimling, 1994). This suggests that the lithosphere was still thermally weakened at the onset of the initial Callovian phase of inversion, which occurred ~30 Myr after the end of rifting (Sandiford, 1999). Thus, initial Callovian inversion may also reflect a still warm and low-viscosity lithosphere that allowed stress to be transmitted over a broad region due to decreased shear resistance at detachment levels, resulting in widespread synchronous inversion. Subsequent inversion events at ~40, 55, and 95 Myr after rifting, affected a more thermally mature, and therefore more viscous, lithosphere. This caused significant contractional strain to accumulate within more proximal inversion structures before they locked up and transferred shortening northward to more distal structures.

The mechanisms described here may have acted concurrently and therefore it is difficult to establish the predominance of one over the other. The qualitative elaborations presented here, however, may comprise the basis for conducting numerical models of half-graben inversion propagation (cf. Buiter and Pfiffner, 2003).

CONCLUSIONS

This study contained an analysis of temporal and spatial patterns of Mesozoic tectonic inversion across the central Neuquén Basin. A model for the propagation of

inversion is proposed based on structural and stratigraphic relationships recognized on a series of structures imaged on 2D and 3D seismic data. Mechanical aspects of the proposed model were discussed. The main conclusions resulting from this study are:

1) Right-lateral Mesozoic transpression along a restraining bend in the Huincul Arch produced a localized compressive stress field across the southern part of the central Neuquén Basin. The westward-moving block acted as a buttress or "mini indentor" that produced N-S to NW-SE compression and caused a series of half-graben bounding faults to undergo reverse reactivation across the Northern Sub-basin. Inversion structures show a general E-W orientation, which is similar to original rift-depocenter orientations. Similar faults bounding syn-rift depocenters that are oriented NW to SE were not reactivated.

2) Inversion extended across almost one third of the Northern Sub-basin's area. Thus, deformation related to the tectonic evolution of the Huincul Arch was not restricted to a narrow zone of deformation close to the principal displacement zone, but affected the structural and stratigraphic evolution of a large part of the Neuquén Basin.

3) Inverted structures show similarities in styles of inversion and resulting stratigraphic patterns. There is, however, a northward decrease in size of inverted depocenters and in intensity of inversion. This trend is probably related to variations in rift-depocenter size, which decrease with distance from the Huincul Arch, suggesting the existence of an ancient rift axis along the now uplifted arch.

4) A two-stage conceptual model for Mesozoic inversion propagation across the central Neuquén Basin is proposed. According to the model, an initial stage of inversion during Callovian time produced synchronous uplift of inversion anticlines across the Northern Sub-basin. Later inversion events (during Kimmeridgian, Valanginian, and Cenomanian time) show a more diachronous timing. The "inversion front" advanced northward over time as more proximal structures accumulated strain, locked up, and transferred shortening to the next, more distal structure.

5) Synchroneity of fault reactivation during the Callovian inversion event may be related to efficient stress transmission north of the Huincul Arch, which can, in turn, be attributed to relatively easy reactivation of low-dip listric fault segments. This required little strain accumulation along "proximal" inversion structures before shortening was transferred to more distal structures. Later inversion events found harder-to-reactivate fault segments, resulting in proximal structures undergoing significant inversion before transferring shortening.

6) The amount of time elapsed since the end of rifting may also have been an important factor for explaining the multi-stage inversion. Lithosphere was still thermally weakened at the onset of the initial Callovian inversion phase. A low-viscosity lithosphere allowed stress to be transmitted efficiently over a large distance from the Huincul Arch, causing synchronous Callovian inversion across the basin. Later inversion events affected a colder and more viscous lithosphere.

Significant strain needed to accumulate along proximal inversion structures before shortening could be transferred to more distal parts of the basin.

CHAPTER IV

PLATE-SCALE SIGNIFICANCE OF THE HUINCUL ARCH

INTRODUCTION

The timing and spatial patterns of Mesozoic inversion in the central Neuquén Basin presented in Chapter III suggest a direct link with the evolution of the Huincul Arch. This unique structural feature, therefore, may be fundamental for the tectonic evolution of the basin and perhaps all of southern South America.

The Huincul Arch is a puzzling structural feature. It is a plate-scale, transcurrent shear zone that is oriented nearly perpendicular to the western margin of the South American Plate (Figure 4.1). It may be an important stress guide that was involved in the intense compression and inversion across central Neuquén Basin during a time when the rest of southern South America was undergoing pervasive extension. In addition, the Neuquén Basin is the only basin in the Argentine foreland with Jurassic and Early Cretaceous tectonic inversion, which contrasts with the more widespread Cenozoic structural reactivation that occurred later.

The tectono-stratigraphic significance of the Huincul Arch was first recognized in outcrops from western parts of the Neuquén Basin, where Upper Cretaceous red beds of the Neuquén Group are in angular unconformity with, and successively onlapped by, Upper, Middle, and Lower Jurassic strata (Windhausen, 1914; Keidel, 1925; de Ferrariis, 1947; Suero, 1951). The Huincul Arch was initially interpreted as a normal-fault-bounded basement high (de Ferrariis, 1947; Ramos, 1978; Digregorio and Uliana, 1980), but acquisition of extensive subsurface data (well logs and seismic) by the petroleum

industry showed that the Huincul Arch consists of a series of transpressional uplifts that are associated with a right-lateral strike-slip fault zone (Figures 3.3, 3.12B; Orchuela et al., 1981; Ploszkiewicz et al., 1984). The arch continues eastward into the subsurface of northern Patagonia where it becomes dominantly transtensional and is known as the Río Negro fault zone.
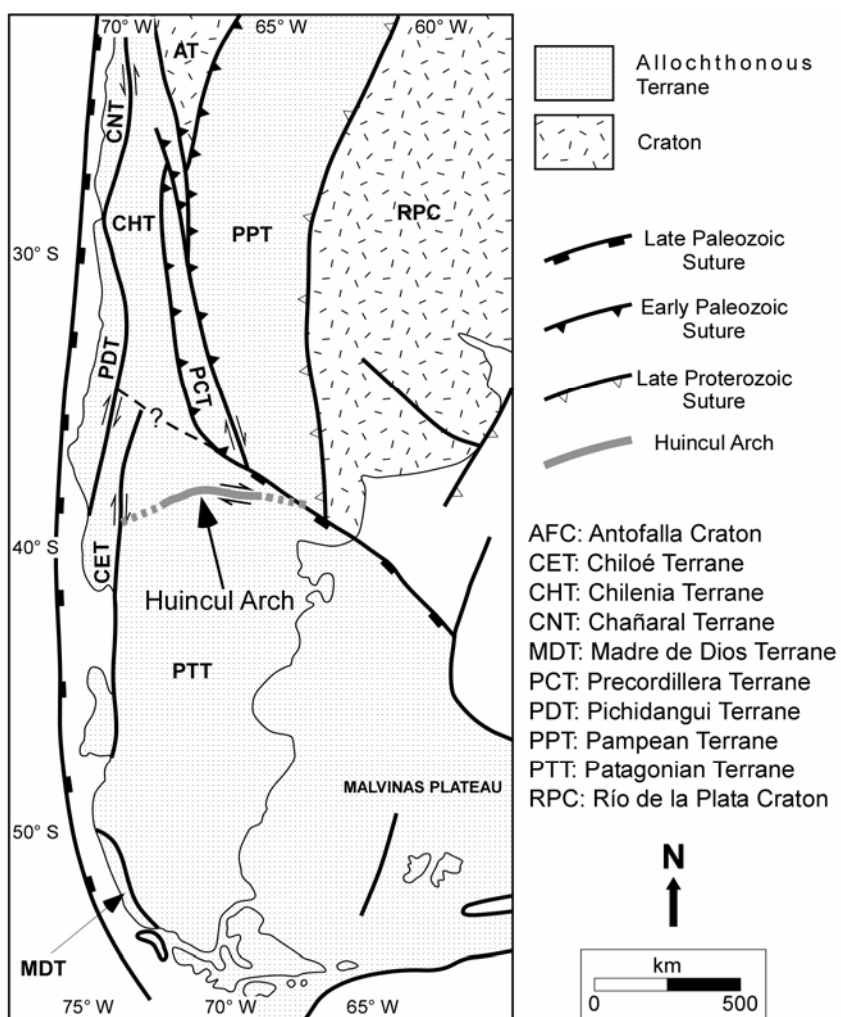
Figure 4.1. Main allochthonous terranes and cratonic block of southern South America with location of the Huincul Arch. Modified from Kley et al. (1999), Mpodozis and Ramos (1989), Ramos (1988), and Ramos and Aleman (2000).

The scale of the basement-involved deformation caused many workers to suggest that the Huincul Arch is a major crustal discontinuity of plate-scale significance (Turner and Baldis, 1978; Digregorio and Uliana, 1980; Baldis and Febrer, 1983; Orchuela and Ploszkiewicz, 1984; Franzese et al., 2003; Macdonald et al., 2003). Some authors argued that the Huincul Arch is the inboard continental projection of fracture zones within the South Atlantic (Unternehr et al., 1988; Uliana et al., 1989; Uliana et al., 1995). No attempts have been made, however, to explain the mechanism that caused displacement along the Huincul Arch or how the timing of deformation along the arch relates to plate-scale tectonic events. In this chapter we investigate the possible link between the evolution of the Huincul Arch and displacement along an adjacent intracontinental megashear zone to the south, which is known as the Gastre Fault System.

PALEOZOIC STRUCTURAL FABRIC OF SOUTHERN SOUTH AMERICA

The evolution of southern South America was strongly influenced by the antecedent tectonic grain that resulted in significant along-strike changes in structural style within the Andean thrust belt and foreland (Mpodozis and Ramos, 1990; Zalán et al., 1990; Tankard et al., 1995; Franzese et al., 2003; Jacques, 2003a; Macdonald et al., 2003). The inherited tectonic fabrics resulted from the amalgamation of continental blocks and terranes that where accreted during Late Proterozoic to early Paleozoic time (Figure 4.1; Ramos, 1988; Urien et al., 1995; Campos Neto, 2000; Cordani et al., 2000; Milani and Thomaz Filho, 2000; Aceñolaza et al., 2002). At least nine major terranes can be recognized in the Argentine foreland (Figure 4.1; Mpodozis and Ramos, 1990;

Kley et al., 1999). Within this context, the Huincul Arch is located between the Chilenia,

Precordillera, and Pampean terranes to the north, and the Patagonian terrane to the south.

The precise location of inter-terrane boundaries in northwestern Patagonia is poorly

known. Therefore, the possibility of the Huincul Arch coinciding with one or more

terrane these boundaries cannot be ignored.
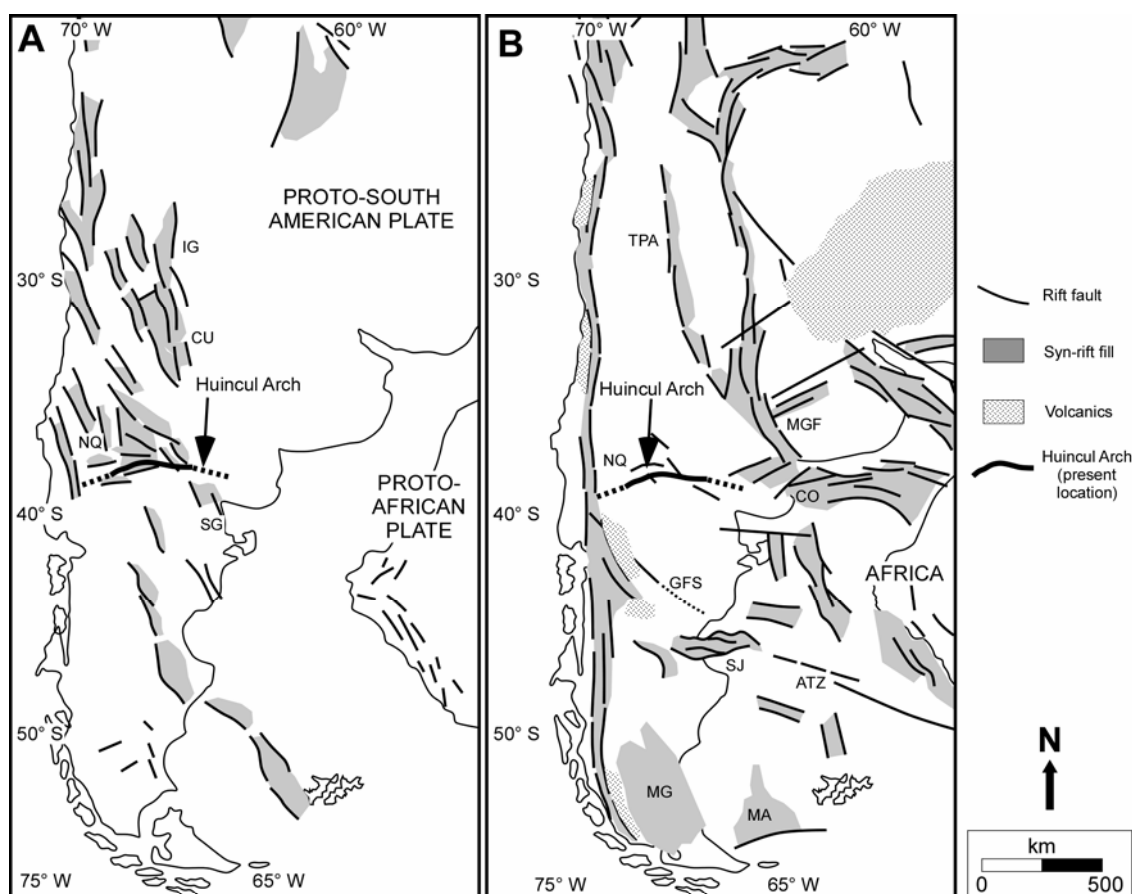
Figure 4.2. Mesozoic extension events throughout southern South America. (A) Late Jurassic - Early Cretaceous extension closely follows the Paleozoic structural fabric. (B) Late Jurassic - Early Cretaceous extensional fault systems and depocenters of increasing areal extent and complexity. Kinematic elements associated with the opening of the South Atlantic. After Uliana et al. (1989), Ramos and Aleman (2000), and Tankard et al. (1995). ATZ: Agulhas Transform Zone; CO: Colorado Basin; CU: Cuyo Basin; GFZ: Gastre Fault System; IG: Ischigualasto Basin; MA: Malvinas Basin; MG: Magallanes Basin; MGF: Martín García Fault Zone; NQ: Neuquén Basin; SG: Sierra Grande; SJ: Golfo San Jorge Basin; TDA: Trans-Pampean Arch.

TIMING OF TECTONIC EVENTS

South America underwent significant extension during Late Triassic and Early

Jurassic time, which has been attributed to the collapse of a late Paleozoic orogenic belt

(Uliana et al., 1989). Rift basins within the accreted basement provinces have dominant

fault orientations that suggest reactivation of antecedent structures (Figure 4.2A).

Extensional phases with increasing areal extent and complexity followed during Middle

and Late Jurassic time (Figure 4.2B; Uliana et al., 1989). Both Late Triassic to Early

Jurassic and Middle- to Late Jurassic extensional events are generally thought to be

precursors of the opening of the South Atlantic Ocean (Ramos and Aleman, 2000). In

that regard, pulses of increased extension are proposed for Late Jurassic (Kimmeridgian)

and Early Cretaceous (Valanginian) time, with the later pulse coincident with continental

breakup at ~130 Ma (Rabinowitz and LaBrecque, 1979; Tankard et al., 1995; Vergani et

al., 1995).

Along the Huincul Arch, Ploszkiewicz et al. (1984), Orchuela et al. (1981), and

Bettini (1984) recognized four main unconformities that can be related to Mesozoic

transpressive tectonic events. These are the Intra-Callovian (~155 Ma), Intra-Malm

(~140 Ma), Intra-Valanginian (~135 Ma), and Intra-Senonian (~100 Ma)

unconformitites. Coeval inversion events were described in Chapter III for the central

Neuquén Basin. Most studies point to a climax of inversion along the arch during

Kimmeridgian time (Orchuela et al., 1981; Tankard et al., 1995; Vergani et al., 1995).

Freije et al. (2002) and Zavala and Freije (2002), however, conducted field work in the

western part of the arch and concluded that the main deformation phase for that segment

occurred during Bathonian time. Other studies that utilized seismic data assign a Pliensbachian age (~190 Ma) to the first transpressive movements along the main axis of the arch (Mosquera, 2002).

THE HUINCUL-GASTRE CONNECTION

The synchroneity between main tectonic events along the Huincul Arch (e.g., Intra-Malm and Intra-Valanginian events) and events related to opening of the South Atlantic suggests a connection between the evolution of the arch and breakup of Gondwanaland. The kinematic link between Huincul-related inversion and South Atlantic extension is interpreted to be along the Gastre Fault System (Coira et al., 1975), a prominent NW-SE shear zone to the southeast of the Huincul Arch (Figure 4.3). The Gastre Fault System has been proposed as a large-scale South American onshore projection of the Agulhas-Falklands Fracture Zone (Figure 4.3; Rapela et al., 1991; Rapela and Pankhurst, 1992). This intracontinental shear zone was associated with the emplacement of major granite intrusions during Late Triassic to Middle Jurassic time (Rapela and Pankhurst, 1992) and crustal block rotations during Early Cretaceous (Valanginian) time (Ben-Avraham et al., 1993; Marshall, 1994; Thomson, 1998; Geuna et al., 2000).

The northwestern part of the Gastre Fault System coincides with a series of interpreted NW-SE lineaments at ~38°S, close to the Chile-Argentina border (Rapela and Pankhurst, 1992) and at the westernmost manifestations of the Huincul Arch. Both

shear zones intersect at this point and are characterized by right-lateral shear motion (Figure 4.4).

The onset of significant compressional deformation along the Huincul Arch's principal displacement zone occurred during earliest Jurassic time (Zavala, 1996; Cruz et al., 1999; Freije et al., 2002; Gómez Omil et al., 2002; Mosquera, 2002; Zavala, 2002; Zavala and Freije, 2002). It is argued here that earliest to Middle Jurassic deformation along the Huincul Arch and development of the Intra-Callovian unconformity on inversion structures' crests across the Northern Sub-basin may be related to initial displacement along the Gastre Fault System.
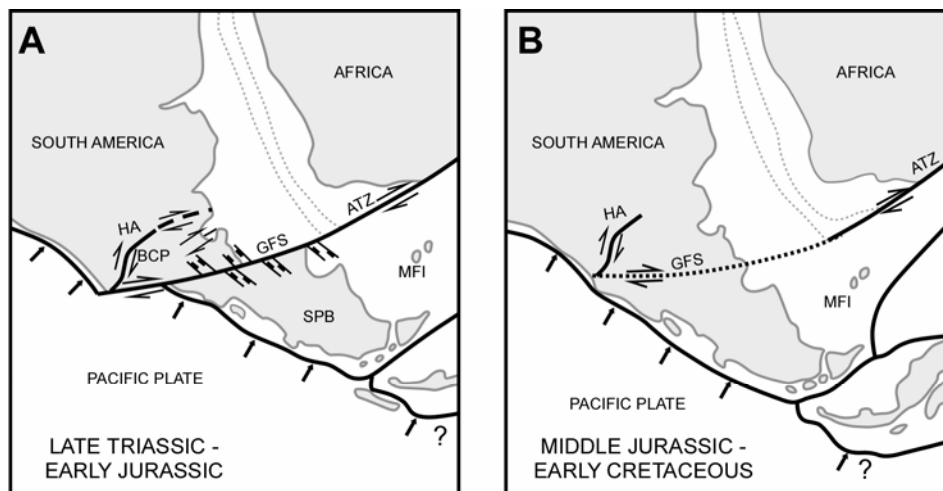
Figure 4.3. Kinematic model proposed by Rapela and Pankhurst (1992) linking the evolution of the Gastre Fault System (GFS) associated with displacement along the Agulhas-Falklands Fracture Zone. (A) Late Triassic-Early Jurassic pre-breakup paleogeography prior to major right-lateral displacement along the GFS. (B) Configuration at the onset of continental breakup during Early Cretaceous time. The Huincul Arch and its probable eastward projection are shown. ATZ: Agulhas Transform Zone; BCP: Batholith of Central Patagonia; GFS: Gastre Fault System; HA: Huincul Arch; MFI: Malvinas-Falkland Islands; SPB: Southern Patagonian Block. Modified from Rapela and Pankhurst (1992).
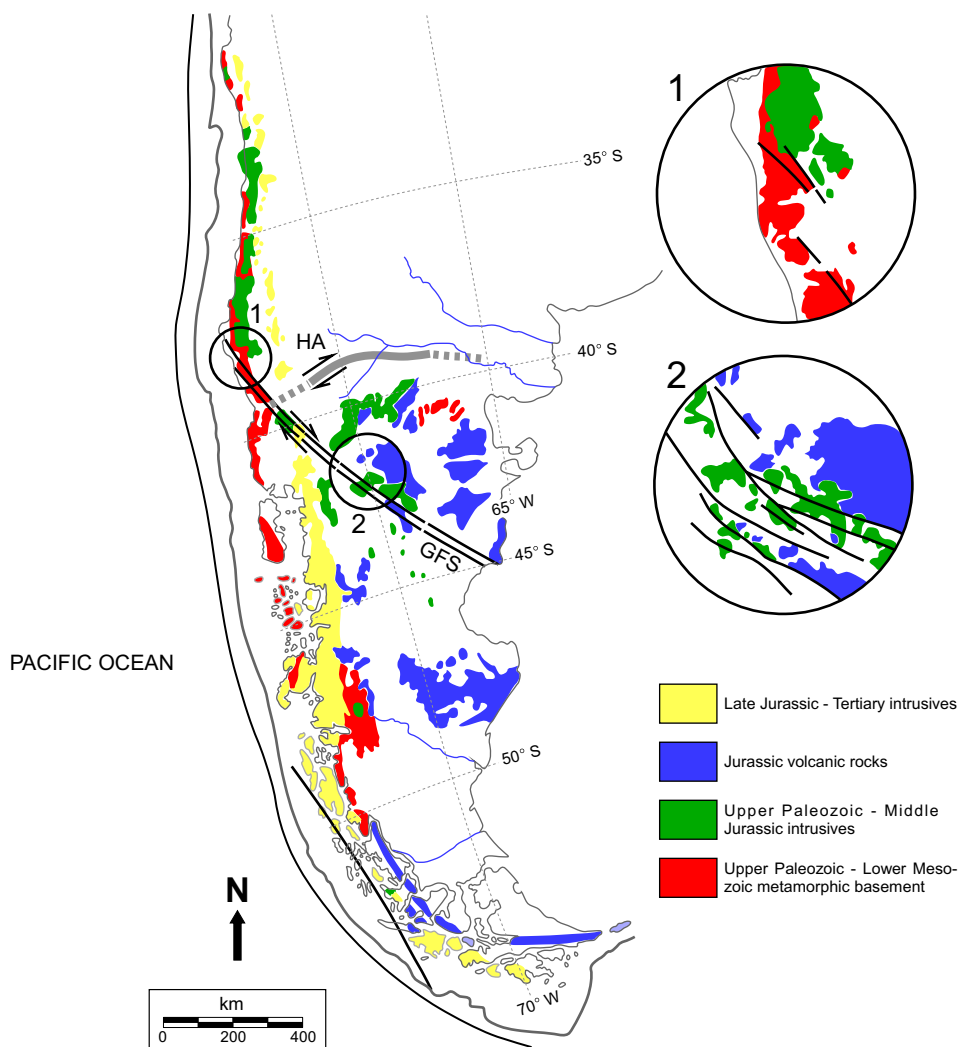
Figure 4.4. Geological map of southern South America showing the location of the Huincul Arch and the Gastre Fault System. Insets show details of the structural and igneous relationships along the present coast of Chile and in north-central Patagonia. The Huincul Arch and the Gastre Fault System may have linked at the present latitude of ~ 38° S. The Huincul Arch is interpreted to be a synthetic shear to the Gastre Fault System, which in turn is thought to be a precursor of the Agulhas Fracture Zone. Distribution of Late Paleozoic to Tertiary igneous rocks are also shown. GFS: Gastre Fault System; HA: Huincul Arch. Modified from Rapela and Pankhurst (1992).

Last stages of Mesozoic inversion in the Northern Sub-basin caused folding of post-Valanginian strata (Figure 3.9-3.12) and may have been driven by waning displacement along the Gastre Fault System during late Mesozoic and Cenozoic time (Rapela, 1997). Alternatively, inversion could have been triggered by increased mechanical coupling between the subducting and overriding plates caused by a higher convergence rate after Pangea breakup at ~130 Ma (Rabinowitz and LaBrecque, 1979), which induced compression across the Argentine foreland starting during Late Cretaceous time (Jacques, 2003b). The second interpretation is favored because the opening of the South Atlantic started being dominated by simple divergence of two rigid plates at ~84 Ma (Nürnberg and Müller, 1991), which could have prevented the Gastre Fault System from showing significant activity after that time.

CONCLUSIONS

The Huincul Arch is located in an area of significant structural complexity, which in part reflects the Paleozoic terrane amalgamation. Therefore, the Huincul Arch may coincide with one or more ancient terrane boundaries.

Timing relationships between tectonic events along the Huincul Arch and across the eastern margin of the proto-South American plate suggest a link between the evolution of the arch, breakup of Gondwanaland, and opening of the South Atlantic Ocean. The Huincul Arch is interpreted to be a synthetic shear to the Gastre Fault System linking at ~38°S close to the western continental margin, although accurate linkage location is obscured by Andean-related deformation.

CHAPTER V

CONCLUSIONS

Tectonic inversion is an important intracontinental deformation process. The complexity of structural styles that result from basin inversion is significant. This requires, therefore, detailed structural and stratigraphic mapping and analysis. This task is best achieved using 3D seismic data, for it provides the lateral continuity of coverage that neither 2D seismic nor outcrop exposures have.

Chapter II documents the structural style and stratigraphic relationships of inversion structures in the central Neuquén Basin. Interpretations are based on detailed mapping of 3D seismic, fault orientation analysis, and structural restorations. The study focuses of the analysis of Sierra Barrosa (SBS) and Aguada Toledo (ATS) anticlines, which are some of the most prominent subsurface features in the Northern Sub-basin.

The SBS inversion structure has two main fault systems. A deep fault system that affected basement and syn-rift strata was selectively reactivated during inversion. Larger faults that formed during extension were preferentially reverse-reactivated during inversion, whereas smaller faults were typically not reactivated during inversion. A shallow fault system consists of syn-inversion normal faults formed at high angle to the master fault of the SBS during inversion. These faults affected both post-rift and syn-inversion strata in the SBS. The map patterns, location, and kinematic history of these faults indicate that the hangingwall of the SBS expanded upon uplift and internally deformed as it accommodated to the shape of the curved footwall during oblique inversion. Similar structures are not reported in analog-model studies, which suggests

the need to incorporate more complex deformation scenarios into scaled-model experiments, like oblique inversion of curved (in plan view) faults allowing for hangingwall internal deformation.

Extensional fault segments bounding the SBS half-graben depocenter were reverse-reactivated and propagated upsection during inversion, resulting in a single through-going but curved fault that defines the structure's southern boundary at the post-rift level. Fault systems in former accommodation zones that formed during extension became linked into a through-going reverse fault during inversion.

Pulsed inversion along the SBS and ATS may have caused significant control on sediment dispersal from Early Jurassic to Late Cretaceous time. This is best documented for the latest Jurassic – Early Cretaceous time period, during which growth strata were deposited between late Tithonian and early Valanginian time on the flanks and crests of the SBS and ATS. The dispersal of carbonate turbidite facies that were described for the lowest Quintuco Formation in this part of the basin may have been affected by the bathymetry produced by the growing structures. The growth strata suggest a folding mechanism controlled by limb rotation with no significant kin-band migration.

Structural restorations of the SBS at different stratigraphic levels show that folding and internal deformation were probably the dominant mechanisms that accommodated contraction during the SBS's early and late stages of development. Initial fault "lock-up" at shallower stratigraphic and structural levels was due to the steep dips of the master fault at these levels, which is not conducive to reactivation. As internal syn-rift wedge deformation was "consumed", the half-graben bounding fault became

reverse-reactivated and propagated upsection. By Berriasian to early Valanginian time, the weight of the overburden inhibited additional fault displacement and folding became the main mechanism that accommodated shortening until late Cretaceous time.

Chapter III contains an analysis of the tectonic inversion problem from a regional perspective that resulted in the identification of temporal and spatial patterns of Mesozoic tectonic inversion across the central Neuquén Basin.

Mesozoic transpression along the Huincul Arch, resolved as local N-S to NW-SE compression by strain partitioning along a restraining bend, inverted a series of half-graben bounding faults across the Northern Sub-basin. Inversion structures show a general E-W orientation, whereas similar faults bounding syn-rift depocenters oriented NW to SE were not reverse-reactivated. This suggests a first-order selection mechanism for fault reactivation based on orientation.

The intensity of inversion decreases markedly from south to north with distance to the Huincul Arch. Inversion, however, is not restricted to a narrow zone of deformation close to the principal displacement zone, but covers almost one third of the Northern Sub-basin's area. This evidences that Huincul Arch-related deformation affected the structural and stratigraphic configuration of a large part of the Neuquén Basin during Early Jurassic to Late Cretaceous time.

Timing relationships derived from the stratigraphic record preserved over different inversion structures allowed the proposal of a conceptual model for Mesozoic inversion propagation across the central Neuquén Basin. According to the model, an initial stage of inversion during Middle Jurassic (Callovian) time produces synchronous

uplift of inversion anticlines across the basin. Later inversion events that occurred from Late Jurassic to Late Cretaceous (Kimmeridgian, Valanginian, and Cenomanian) time show a more diachronous character. These events are expressed as an "inversion front" that advances toward the north as structures accumulate strain, lock up, and transfer shortening to the next distal structure. Differences in inversion propagation patterns between inversion stages are attributed to the initial preferential reverse-reactivation of flat to low-dip listric fault segments. Alternatively, an initially warm and weak lithosphere may have caused efficient stress transmission over a broad area during the early inversion event, resulting in synchronous Callovian inversion across the basin. Later inversion stages, however, may have affected a colder and more viscous lithosphere, therefore significant strain needed to accumulate along proximal inversion structures before shortening could be transferred to more distal parts of the basin.

In Chapter IV we discuss the plate-scale significance of the Huincul Arch. At a mega-regional scale, timing of deformation events along the Northern Sub-basin suggest that Huincul-Arch tectonics and associated inversion structures may be controlled by right-lateral displacement motion along the Gastre Fault Zone to which the arch seems to be kinematically linked as a synthetic shear. This intracontinental megashear is thought to be related to Late Triassic-Early Cretaceous extension events that affected most southern South America previous to the opening of the South Atlantic Ocean.

REFERENCES CITED

Aceñolaza, F. G., H. Miller, and A. J. Toselli, 2002, Proterozoic-Early Paleozoic evolution in western South America - a discussion: Tectonophysics, v. 354, p. 121-137.

Assumpção, M., 1992, The regional intraplate stress field in South America: Journal of Geophysical Research, v. 97, p. 11889-11903.

Assumpção, M., 1998, Focal mechanisms of small earthquakes in the southeastern Brazilian shield: a test of stress models of the South American plate: Geophysical Journal International, v. 133, p. 430-498.

Badley, M. E., J. D. Price, and L. C. Backshall, 1989, Inversion, reactivated faults and related structures: seismic examples from the southern North Sea, *in* M. A. Cooper, and G. D. Williams, eds., Inversion Tectonics: Geological Society Special Publication 44, p. 201-219.

Bailey, C. M., S. Giorgis, and L. Coiner, 2002, Tectonic inversion and basement buttressing: an example from the central Appalachian Blue Ridge province: Journal of Structural Geology, v. 24, p. 925-936.

Baldis, B. A. J., and J. Febrer, 1983, Geodynamics of the Argentine Andean Arc and related regions, *in* R. Cabré, ed., Geodynamics of the Eastern Pacific Region, Caribbean and Scotia Arcs: American Geophysical Union Geodynamic Series 9, p. 127-135.

Barrio, C. A., 1990, Paleogeographic control of Upper Cretaceous tidal deposits, Neuquén Basin, Argentina: Journal of South American Earth Sciences, v. 3, p. 31-49.

Beauchamp, W., 2004, Superposed folding resulting from inversion of a synrift accommodation zone, Atlas Mountains, Morocco, *in* K. R. McClay, ed., Thrust tectonics and hydrocarbon systems: AAPG Memoir 82, p. 635-646.

Beauchamp, W., M. Barazangi, A. Demnati, and M. El Alji, 1996, Intracontinental rifting and inversion: Missour Basin and Atlas Mountains, Morocco: AAPG Bulletin, v. 80, p. 1459-1482.

Beauchamp, W., M. Barazangi, A. Demnati, and M. El Alji, 1997, Inversion of synrift normal faults on the High Atlas Mountains, Morocco: The Leading Edge, v. 16, p. 1171-1175.

Ben-Avraham, Z., C. J. H. Hartnady, and J. A. Malan, 1993, Early tectonic extension between the Agulhas Bank and the Falkland Plateau due to the rotation of the Lafonia microplate: Earth and Planetary Science Letters, v. 117, p. 43-58.

Berdini, O., C. D. Arregui, and M. Pimentel Mendes, 2002, Evolución tecto-sedimentaria de la estructura Río Neuquén, Cuenca Neuquina, República Argentina: XV Congreso Geológico Argentino. Actas v. 3, p. 187-192.

Bernal, A., and S. Hardy, 2002, Syn-tectonic sedimentation associated with three-dimensional fault-bend fold structures: a numerical approach: Journal of Structural Geology, v. 24, p. 609-635.

Bernal, A., S. Hardy, R. Gawthorpe, and E. Finch, 2004, Stratigraphic expression of the lateral propagation and growth of isolated fault-related uplifts: Basin Research, v. 16, p. 219-233.

Bettini, F. H., 1984, Pautas sobre cronología estructural en el área del Cerro Lotena, Cerro granito y su implicancia en el significado de la Dorsal del Neuquén, Provincia del Neuquén: 9 Congreso Geológico Argentino. Actas v. 2, p. 342-361.

Betts, P. G., 2001, Three-dimensional structure along the inverted Palaeoproterozoic Fiery Creek Fault System, Mount Isa terrane, Australia: Journal of Structural Geology, v. 23, p. 1953-1969.

Bjorklund, T., and K. Burke, 2002, Four-dimensional analysis of the inversion of a half-graben to form the Whittier fold-fault system of the Los Angeles basin: Journal of Structural Geology, v. 24, p. 1369-1387.

Bracaccini, O. I., 1970, Rasgos tectónicos de las acumulaciones Mesozoicas en las provincias de Mendoza y Neuquén, República Argentina: Asociación Geológica Argentina, Revista, v. 25, p. 275-284.

Brodie, J., and N. White, 1995, The link between sedimentary basin inversion and igneous underplating, *in* J. G. Buchanan, and P. G. Buchanan, eds., Basin Inversion: Geological Society Special Publication 88, p. 21-38.

Brun, J.-P., and T. Nalpas, 1996, Graben inversion in nature and experiments: Tectonics, v. 15, p. 677-687.

Buchanan, P. G., 1991, Geometries and kinematic analysis of inversion tectonics from analogue model studies: Ph.D. dissertation, Royal Holloway and Bedford New College, University of London, London, UK.

Buchanan, P. G., and K. R. McClay, 1991, Sandbox experiments of inverted listric and planar fault systems: Tectonophysics, v. 188, p. 97-115.

Buchanan, P. G., and K. R. McClay, 1992, Experiments on basin inversion above reactivated domino faults: Marine and Petroleum Geology, v. 9, p. 486-500.

Buiter, S. J. H., and O. A. Pfiffner, 2003, Numerical models of the inversion of half-graben basins: Tectonics, v. 22, p. NO. 5, 1057, doi:10.1029/2002TC001417.

Bulnes, M., and K. McClay, 1999, Benefits and limitations of different 2D algorithms used in cross-section restoration of inverted extensional faults: application to physical experiments: Tectonophysics, v. 312, p. 175-189.

Bulnes, M., and K. R. McClay, 1998, Structural analysis and kinematic evolution of the inverted central South Celtic Sea Basin: Marine and Petroleum Geology, v. 15, p. 667-687.

Burbank, D., A. Meigs, and N. Brozovic, 1996, Interactions of growing folds and coeval depositional systems: Basin Research, v. 8, p. 199-223.

Butler, R. W. H., 1989, The influence of pre-existing basin structure on thrust systems evolution in the Western Alps, *in* M. A. Cooper, and G. D. Williams, eds., Inversion Tectonics: Geological Society Special Publication 44, p. 105-122.

Campos Neto, M. C., 2000, Orogenic Systems from Southwestern Gondwana. An approach to Brasiliano-Pan African cycle and orogenic collage in southeastern Brazil, *in* U. G. Cordani, E. J. Milani, A. Thomaz Filho, and D. A. Campos, eds., Tectonic Evolution of South America, 31st International Geological Congress: Rio de Janeiro, Brazil, p. 335-365.

Cartwright, J. A., 1989, The kinematics of inversion in the Danish Central Graben, *in* M. A. Cooper, and G. D. Williams, eds., Inversion Tectonics: Geological Society Special Publication 44, p. 153-175.

Casas-Sainz, A. M., A. L. Cortes, and A. Maestro, 2002, Sequential limb rotation and kink-band migration recorded by growth strata, Almazan Basin, North Spain: Sedimentary Geology, v. 146, p. 25-45.

Chambers, J. L. C., I. Carter, I. R. Cloke, J. Craig, S. J. Moss, and D. W. Paterson, 2004, Thin-skinned and thick-skinned inversion-related thrusting - A structural model for the Kutai Basin, Kalimantan, Indonesia, *in* K. R. McClay, ed., Thrust tectonics and hydrocarbon systems: AAPG Memoir 82, p. 614-634.

Champel, B., P. van der Beek, J. L. Mugnier, and P. Leturmy, 2002, Growth and lateral propagation of fault-related folds in the Siwaliks of western Nepal: rates, mechanisms, and geomorphic signature: Journal of Geophysical Research, v. 107, B6, 2111, 10.1029/2001JB000578.

Chapman, T. J., 1989, The Permian to Cretaceous structural evolution of the Western Approaches Basin (Melville sub-basin), UK, *in* M. A. Cooper, and G. D. Williams, eds., Inversion Tectonics: Geological Society Special Publication 44, p. 177-200.

Chebli, G. A., M. E. Mozetic, E. R. Rossello, and M. Bühler, 1999, Cuencas sedimentarias de la llanura Chacopamepana, *in* R. Caminos, ed., Geología Argentina. Anales 29 (20), Servicio Geológico-Minero Argentino - Instituto de Geología y Recursos Minerales, p. 627-644.

Cobbold, P. R., and K. E. Meisling, 2001, Reactivation of an obliquely rifted margin, Campos and Santos basins, southeastern Brazil: AAPG Bulletin, v. 85, p. 1925-1944.

Cobbold, P. R., and E. A. Rossello, 2003, Aptian to Recent compressional deformation, foothills of the Neuquén Basin, Argentina: Marine and Petroleum Geology, v. 20, p. 429-443.

Coira, B., F. E. Nullo, C. Prosperpio, and V. A. Ramos, 1975, Tectónica de basamento de la región occidental del Macizo Norpatagónico: Asociación Geológica Argentina, Revista, v. 30, p. 361-383.

Cooper, G. T., 1995, Seismic structure and extensional development of the eastern Otway Basin-Torquay Embayment: The Australian Petroleum Exploration Association Journal, v. 35, p. 241-256.

Cordani, U. G., K. Sato, W. Teixeira, C. C. G. Tassinari, and M. A. S. Basei, 2000, Crustal Evolution of the South American Platform: 31st International Geological Congress, p. 19-40.

Coward, M., 1994, Inversion Tectonics, *in* L. Hancock Paul, ed., Continental Deformation: Oxford, UK, Pergamon Press, p. 289-304.

Coward, M. P., R. Gillcrist, and B. Trudgill, 1991, Extensional structures and their tectonic inversion in the Western Alps, *in* M. Roberts Alan, G. Yielding, and B. Freeman, eds., The geometry of normal faults.: Geological Society Special Publications, v. 56: London, United Kingdom, Geological Society of London, p. 93-112.

Cristallini, E., A. H. Cominguez, and V. A. Ramos, 1997, Deep structure of the Metan-Guachipas region; tectonic inversion in northwestern Argentina: Journal of South American Earth Sciences, v. 10, p. 403-421.

Cruz, C. E., A. Boll, R. Gómez Omil, E. A. Martínez, C. D. Arregui, C. A. Gulisano, G. A. Laffitte, and H. J. Villar, 2002, Hábitat de hidrocarburos y sistemas de carga

Los Molles y Vaca Muerta en el sector central de la cuenca Neuquina, Argentina (CD-ROM): V Congreso de Exploración y Desarrollo de Hidrocarburos, Trabajos Técnicos, Instituto Argentino del Petróleo y del Gas, 20 p.

Cruz, C. E., F. Robles, C. A. Sylwan, and H. J. Villar, 1999, Los sistemas petroleros Jurásicos de la Dorsal de Huincul, Cuenca Neuquina, Argentina: IV Congreso de Exploración y Desarrollo de Hidrocarburos, Instituto Argentino del Petróleo y del Gas, Actas v. 1, p. 177-195.

Davison, I., 1986, Listric normal fault profiles: calculation using bed-length balance and fault displacement: Journal of Structural Geology, v. 8, p. 209-210.

de Ferrariis, C. d., 1947, Edad del arco o dorsal antigua del Neuquén oriental de acuerdo con la estratigrafía de la zona inmediata: Revista de la Sociedad Geológica Argentina, v. 2, p. 256-283.

de la Colina, J. C., 1997, Integrated seismic stratigraphic and 2-D basin analysis of the Bajo Baguales and Los Bastos blocks, Dorsal de Huincul, Neuquén Basin, Argentina: M.S. thesis, University of Oklahoma, 203 p.

Deeks, N. R., and S. A. Thomas, 1995, Basin inversion in a strike-slip regime: the Tornquist Zone, Southern Baltic Sea, *in* J. G. Buchanan, and P. G. Buchanan, eds., Basin Inversion: Geological Society Special Publication 88, p. 319-338.

Dellapé, D., 1993, Yacimiento Río Tunuyán: XII Congreso Geológico Argentino y II Congreso de Exploración de Hidrocarburos. Actas v. 1, p. 427-430.

Dellapé, D. A., and A. Hegedus, 1995, Structural Inversion and Oil Occurrence in the Cuyo Basin of Argentina, *in* A. J. Tankard, R. Suárez S., and H. J. Welsink, eds., Petroleum basins of South America: AAPG Memoir 62, p. 359-367.

Dewey, J. F., 1988, Extensional collapse of orogens: Tectonics, v. 7, p. 1123-1139.

Digregorio, J. H., 1972, Neuquén, *in* H. A. Leanza, ed., Geología Regional Argentina: Córdoba, Argentina, Academia Nacional de Ciencias, p. 439-505.

Digregorio, J. H., 1978, Estratigrafía de las Acumulaciones Mesozoicas, *in* E. O. Rolleri, ed., VII Congreso Geológico Argentino. Geología y recursos naturales del Neuquén: Relatorio VII Congreso Geológico Argentino, p. 37-65.

Digregorio, J. H., and M. A. Uliana, 1980, Cuenca Neuquina, Simposio de Geología Regional Argentina, v. 2, Academia Nacional de Ciencias de Córdoba, p. 985-1032.

Digregorio, R. E., C. A. Gulisano, A. R. Gutiérrez Pleimling, and S. A. Minniti, 1984, Esquema de la evolución geodinámica de la Cuenca Neuquina y sus implicancias paleogeográficas: IX Congreso Geológico Argentino. Actas v. 2, p. 147-162.

Dorobek, S. L., S. K. Reid, and M. Elrick, 1991, Antler foreland stratigraphy of Montana and Idaho; the stratigraphic record of eustatic fluctuations and episodic tectonic events, *in* D. Cooper John, and H. Stevens Calvin, eds., Paleozoic paleogeography of the Western United States II: Field Trip Guidebook 67-SEPM Pacific Section, p. 487-507.

Dubois, A., F. Odonne, G. Massonnat, T. Lebourg, and R. Fabre, 2002, Analogue modelling of fault reactivation: tectonic inversion and oblique remobilisation of grabens: Journal of Structural Geology, v. 24, p. 1741-1752.

Dula, W. F., 1991, Geometric Models of Listric Normal Faults and Rollover Folds: AAPG Bulletin, v. 75, p. 1609-1625.

Echavarría, L., and R. W. Allmendinger, 2002, Diagramas de separación vertical: una herramienta para reconocer estratos de crecimiento: XV Congreso Geológico Argentino. Actas v. 3, p. 242-245.

Eisenstadt, G., and M. O. Withjack, 1995, Estimating inversion: results from clay models, *in* J. G. Buchanan, and P. G. Buchanan, eds., Basin Inversion: Geological Society Special Publication 88, p. 119-136.

Erslev, E. A., 1991, Trishear fault-propagation folding: Geology, v. 19, p. 617-620.

Etheridge, M. A., 1986, On the reactivation of extensional fault systems: Philosophical Transactions of the Royal Society of London. Series A, Mathematical and Physical Sciences, v. A317, p. 179-194.

Ford, M., E. A. Williams, and A. Artoni, 1997, Progressive evolution of a fault-related fold pair from growth strata geometries, Sant Llorenc de Morunys, SE Pyrenees: Journal of Structural Geology, v. 19, p. 413-441.

Franzese, J., L. Spalletti, I. Gómez Pérez, and D. Macdonald, 2003, Tectonic and paleoenvironmental evolution of Mesozoic sedimentary basins along the Andean foothills of Argentina (32°-54°S): Journal of South American Earth Sciences, v. 16, p. 81-90.

Franzese, J. R., and L. A. Spalletti, 2001, Late Triassic - early Jurassic continental extension in southwestern Gondwana: Tectonic segmentation and pre-break-up rifting: Journal of South American Earth Sciences, v. 14, p. 257-270.

Freije, H., G. Azúa, R. González, J. J. Ponce, and C. Zavala, 2002, Actividad tectónica sinsedimentaria en el Jurásico sur de la cuenca Neuquina (CD-ROM): V Congreso de Exploración y Desarrollo de Hidrocarburos, Trabajos Técnicos, Instituto Argentino del Petróleo y del Gas, 17 p.

Geuna, S. E., R. Somoza, H. Vizan, E. G. Figari, and C. A. Rinaldi, 2000, Paleomagnetism of Jurassic and Cretaceous rocks in central Patagonia: a key to constrain the timing of rotations during the breakup of southwestern Gondwana?: Earth and Planetary Science Letters, v. 181, p. 145-160.

Gibbs, A. D., 1983, Balanced cross-section construction from seismic sections in areas of extensional tectonics: Journal of Structural Geology, v. 5, p. 153-160.

Gillcrist, R., M. Coward, and J. L. Mugnier, 1987, Structural inversion and its controls: examples from the Alpine Foreland and the French Alps: Geodinamica Acta, v. 1, p. 5-34.

Gómez Omil, R., J. Schmithalter, A. Cangini, L. Albariño, and A. Corsi, 2002, El grupo Cuyo en la Dorsal de Huincul. Consideraciones estratigráficas, tectónicas y petroleras. Cuenca Neuquina (CD-ROM): V Congreso de Exploración y Desarrollo de Hidrocarburos, Trabajos Técnicos, Instituto Argentino del Petróleo y del Gas, 22 p.

Gulisano, C. A., and A. R. Gutiérrez Pleimling, 1994, Field Guide - The Jurassic of the Neuquén Basin - a) Neuquén Province, Secretaría de Minería de la Nación - Asociación Geológica Argentina, 111 p.

Gulisano, C. A., A. R. Gutiérrez Pleimling, and R. E. Digregorio, 1984, Esquema estratigráfico de la secuencia Jurásica del oeste de la provincia del Neuquén: IX Congreso Geológico Argentino. Actas v. 1, p. 236-259.

Gulisano, C. A., and L. Legarreta, 1987, Análisis secuencial del Jurásico, Cretácico y Eoterciario de la Cuenca Neuquina, Argentina: X Congreso Geológico Argentino, Actas v. 5, p. 16-17.

Gulisano, C. A., and G. A. Pando, 1981, Estratigrafía y facies de los depósitos jurásicos entre Piedra del Águila y Sañicó, departamento Collón Curá, provincia del Neuquén: VIII Congreso Geológico Argentino, Actas v. 3, p. 553-577.

Harding, T. P., 1985, Seismic characteristics and identification of negative flower structures, positive flower structures, and positive structural inversion: AAPG Bulletin, v. 69, p. 582-600.

Hardy, S., and M. Ford, 1997, Numerical modeling of trishear fault propagation folding: Tectonics, v. 16, p. 841-854.

Hardy, S., and J. Poblet, 1994, Geometric and numerical model of progressive limb rotation in detachment folds: Geology, v. 22, p. 371-374.

Hayward, A. B., and R. H. Graham, 1989, Some geometrical characteristics of inversion, *in* M. A. Cooper, and G. D. Williams, eds., Inversion Tectonics: Geological Society Special Publication 44, p. 17-39.

Hechem, J. J., and R. Veiga, 2002, Loma la Lata, enseñanzas del pasado y algunas preguntas para el futuro (CD-ROM): V Congreso de Exploración y Desarrollo de Hidrocarburos, Trabajos Técnicos, Instituto Argentino del Petróleo y del Gas, 14 p.

Hill, K. C., and G. T. Cooper, 1996, A strategy for palinspastic restoration of inverted basins: thermal and structural analyses in SE Australia, *in* P. G. Buchanan, and D. A. Nieuwland, eds., Modern Developments in Structural Interpretation, Validation and Modeling: Geological Society Special Publication 99: London, UK, p. 99-115.

Hinterwimmer, G. A., and J. M. Jáuregui, 1985, Análisis de facies de los depósitos de turbiditas de la F. Los Molles en el sondeo Barda Colorada Este, provincia del Neuquén: IX Congreso Geológico Argentino, Actas v. 5, p. 124-135.

Homovc, J. F., G. A. Conforto, P. A. Lafourcade, and L. A. Chelotti, 1995, Fold belt in the San Jorge Basin, Argentina: an example of tectonic inversion, *in* J. G. Buchanan, and P. G. Buchanan, eds., Basin Inversion: Geological Society Special Publication 88, p. 235-248.

Hooper, R. J., L. S. Goh, and F. Dewey, 1995, The inversion history of the northeastern margin of the Broad Fourteens Basin, *in* J. G. Buchanan, and P. G. Buchanan, eds., Basin Inversion: Geological Society Special Publication 88, p. 307-317.

Hurley, N. F., H. C. Tanner, and C. Barcat, 1995, Unconformity-related porosity development in the Quintuco Formation (Lower Cretaceous), Neuquén Basin, Argentina, *in* D. A. Budd, A. H. Saller, and P. M. Harris, eds., Unconformities and porosity in carbonate strata.: AAPG Memoir 63: Tulsa, OK, United States, p. 159-175.

Jacques, J. M., 2003a, A tectonostratigraphic synthesis of the Sub-Andean basins: implications for the geotectonic segmentation of the Andean Belt: Journal of the Geological Society of London, v. 160, p. 687-701.

Jacques, J. M., 2003b, A tectonostratigraphic synthesis of the Sub-Andean basins: inferences on the position of South American intraplate accommodation zones and their control on South Atlantic opening: Journal of the Geological Society of London, v. 160, p. 703-717.

Jalfin, A. G., and G. A. Laffitte, 1996, Loma La Lata giant gas field from a petroleum paleosystem, Neuquén Basin, Argentina (abs.), AAPG International Conference and Exhibition: AAPG Bulletin, v. 80, p. 1298.

Keidel, J., 1925, Sobre la estructura tectónica de las capas petrolíferas en el oriente del territorio del Neuquén: República Argentina. Dirección General de Minas, Geología e Hidrología, v. 8: Buenos Aires, Argentina, Ministerio de Agricultura de la Nación, 67 p.

Keller, J. V. A., and K. R. McClay, 1995, 3D sandbox models of positive inversion, *in* J. G. Buchanan, and P. G. Buchanan, eds., Basin Inversion: Geological Society Special Publication 88, p. 137-146.

Kelly, P. G., D. C. P. Peacock, D. J. Sanderson, and A. C. McGurk, 1999, Selective reverse-reactivation of normal faults, and deformation around reverse-reactivated faults in the Mesozoic of the Somerset coast: Journal of Structural Geology, v. 21, p. 493-509.

Kim, Y.-S., and D. J. Sanderson, 2005, The relationship between displacement and length of faults: a review: Earth-Science Reviews, v. 68, p. 317-334.

Kley, J., and C. Monaldi, 2002, Tectonic inversion in the Santa Barbara System of the central Andean foreland thrust belt, northwestern Argentina: Tectonics, v. 21, p. NO. 6, 1061, doi:10.1029/2002TC902003.

Kley, J., C. R. Monaldi, and J. A. Salfity, 1999, Along-strike segmentation of the Andean foreland: causes and consequences: Tectonophysics, v. 301, p. 75-94.

Kluth, C. F., 1986, Plate tectonics of the ancestral Rocky Mountains, *in* A. Peterson James, ed., Paleotectonics and sedimentation in the Rocky Mountain region, United States.: AAPG Memoir 41, p. 353-369.

Kluth, C. F., 1991, Inversion and reinversion of the Sangre de Cristo-Rio Grande Rift area, southern Colorado and northern New Mexico, *in* W. Geissman John, E. Elston Wolfgang, and G. R. Keller, eds., Geological Society of America, Rocky Mountain Section: Abstracts with Programs, v. 23, p. 39.

Kluth, C. F., 1994, Deformation of the footwall by "shortcut faults" during inversion; examples from Europe and the Sangre de Cristo Mountains, Colorado, AAPG Annual Convention Abstracts, p. 189.

Kluth, C. F., and P. J. Coney, 1981, Plate tectonics of the ancestral Rocky Mountains: Geology, v. 9, p. 10-15.

Kluth, C. F., H. Ye, L. H. Royden, C. Burchfiel, and M. Schuepbach, 1998, Late Paleozoic deformation of interior North America; the greater ancestral Rocky Mountains; discussion and reply: AAPG Bulletin, v. 82, p. 2272-2279.

Koopman, A., A. Speksnijder, and W. T. Horsfield, 1987, Sandbox model studies of inversion tectonics: Tectonophysics, v. 137, p. 379-388.

Kress, P. R., 1995, Tectonic Inversion of the Subandean Foreland - a Combined Geophysical and Geological Approach: Ph.D. thesis, Freien Universität Berlin, Berlin, 120 p.

Legarreta, L., 2002, Eventos de desecación en la cuenca Neuquina: depósitos continentales y distribución de hidrocarburos (CD-ROM): V Congreso de Exploración y Desarrollo de Hidrocarburos, Trabajos Técnicos, Instituto Argentino del Petróleo y del Gas, 20 p.

Legarreta, L., and C. A. Gulisano, 1989, Análisis estratigráfico secuencial de la Cuenca Neuquina (Triásico superior-Terciario inferior), *in* G. A. Chebli, and L. A. Spalletti, eds., Cuencas sedimentarias argentinas: Serie Correlación Geológica, v. 6, Programa Internacional de Correlación Geológica Proyecto 192, Desarrollo del Cámbrico y Ordovícico de Latinoamérica, p. 221-243.

Legarreta, L., C. A. Gulisano, and M. A. Uliana, 1993, Las secuencias sedimentarias jurásico-cretácicas: XII Congreso Geológico Argentino y II Congreso de Exploración de Hidrocarburos, Actas v. 1, p. 87-114.

Legarreta, L., G. Laffitte, and S. A. Minniti, 1999, Cuenca Neuquina: Múltiples posibilidades en las series Jurásico-Cretácicas del depocentro periandino: IV Congreso de Exploración y Desarrollo de Hidrocarburos, Instituto Argentino del Petróleo y del Gas, Actas v. 1, p. 145-175.

Legarreta, L., and M. A. Uliana, 1991, Jurassic-Cretaceous marine oscillations and geometry of back-arc basin fill, central Argentine Andes, *in* D. I. M. Macdonald, ed., Sedimentation, Tectonics and Eustasy. Sea-level Changes at Active Margins: Special Publication of the International Association of Sedimentologists, v. 12, p. 429-450.

Legarreta, L., and M. A. Uliana, 1996, The Jurassic succession in west-central Argentina; stratal patterns, sequences and paleogeographic evolution: Palaeogeography, Palaeoclimatology, Palaeoecology, v. 120, p. 303-330.

Letouzey, J., 1990, Fault reactivation, inversion and fold-thrust belt, *in* J. Letouzey, ed., Petroleum and Tectonics in Mobile Belts, Éditions Technip, p. 101-128.

Letouzey, J., P. Werner, and A. Marty, 1990, Fault reactivation and structural inversion. Backarc and intraplate compressive deformations. Example of the eastern Sunda shelf (Indonesia): Tectonophysics, v. 183, p. 341-362.

Light, M. P. R., M. L. Keeley, M. P. Maslanyj, and C. M. Urien, 1993, The tectonostratigraphic development of Patagonia, and its relevance to hydrocarbon exploration: Journal of Petroleum Geology, v. 16, p. 465-481.

Lima, C. C., 2000, Ongoing compression across intraplate South America: observations and some implications for petroleum exploitation and exploration: Revista Braseileira de Geociências, v. 30, p. 203-207.

Lima, C. C., 2003, Ongoing compression across South American plate: Observations, numerical modelling and some implications for petroleum geology, *in* S. Ameen Mohammed, ed., Fracture and in-situ stress characterization of hydrocarbon reservoirs: Geological Society Special Publication 209, p. 87-100.

Lowell, J. D., 1995, Mechanics of basin inversion from worldwide examples, *in* J. G. Buchanan, and P. G. Buchanan, eds., Basin Inversion: Geological Society Special Publication 88, p. 39-57.

Macdonald, D., I. Gomez-Perez, J. Franzese, L. Spalletti, L. Lawver, L. Gahagan, I. Dalziel, C. Thomas, N. Trewin, M. Hole, and D. Paton, 2003, Mesozoic break-up of SW Gondwana: implications for regional hydrocarbon potential of the southern South Atlantic: Marine and Petroleum Geology, v. 20, p. 287-308.

Manceda, R., and D. Figueroa, 1995, Inversion of the Mesozoic Neuquén Rift in the Malargüe fold and thrust belt, Mendoza, Argentina, *in* A. J. Tankard, R. S. Soruco, and H. J. Welsink, eds., Petroleum basins of South America: AAPG Memoir 62: Tulsa, OK, United States, p. 369-382.

Maretto, H. and M. E. Lara, 2002, Discontinuidades estratigráficas, distribución de fluidos y calidad de reservorio: un ejemplo de la Formación Tordillo en Loma la Lata (CD-ROM): V Congreso de Exploración y Desarrollo de Hidrocarburos, Trabajos Técnicos, Instituto Argentino del Petróleo y del Gas, 14 p.

Marone, C., 1995, Fault zone strength and failure criteria: Geophysical Research Letters, v. 22, p. 723-726.

Marshak, S., K. E. Karlstrom, and J. M. Timmons, 2000, Inversion of Proterozoic extensional faults; an explanation for the pattern of Laramide and ancestral Rockies intracratonic deformation, United States: Geology, v. 28, p. 735-738.

Marshak, S., W. J. Nelson, and J. H. McBride, 2003, Phanerozoic strike-slip faulting in the continental interior platform of the United States: examples from the

Laramide Orogen, Midcontinent, and Ancestral Rocky Mountains, *in* F. Storti, E. Holdsworth Robert, and F. Salvini, eds., Intraplate strike-slip deformation belts: Geological Society Special Publication 210, p. 159-184.

Marshall, J. E. A., 1994, The Falkland Islands: A key element in Gondwana paleogeography: Tectonics, v. 13, p. 499-514.

McClay, K., 1989, Analogue models of inversion tectonics, *in* M. A. Cooper, and G. D. Williams, eds., Inversion Tectonics: Geological Society Special Publication 44, p. 41-59.

McClay, K. R., 1995, The geometries and kinematics of inverted fault systems: a review of analogue model studies, *in* J. G. Buchanan, and P. G. Buchanan, eds., Basin Inversion: Geological Society Special Publication 88, p. 97-118.

Milani, E. J., and A. Thomaz Filho, 2000, Sedimentary Basins of South America, *in* U. G. Cordani, E. J. Milani, and A. Thomaz Filho, eds., Tectonic Evolution of South America, 31st International Geological Congress: Rio de Janeiro, Brazil, p. 389-449.

Mitchum, R. M., Jr., and M. A. Uliana, 1985, Seismic Stratigraphy of Carbonate Depositional Sequences, Upper Jurassic-Lower Cretaceous, Neuquén Basin, Argentina, *in* O. R. Berg, and D. G. Woolverton, eds., Seismic stratigraphy II: an integrated approach to hydrocarbon exploration.: AAPG Memoir 39, p. 255-274.

Mitra, S., 1993, Geometric and kinematic evolution of inversion structures: AAPG Bulletin, v. 77, p. 1159-1191.

Mitra, S., and Q. T. Islam, 1994, Experimental (clay) models of inversion structures: Tectonophysics, v. 230, p. 211-222.

Morley, C. K., 1995, Developments in the structural geology of rifts over the last decade and their impact on hydrocarbon exploration, *in* J. J. Lambiase, ed., Hydrocarbon Habitat in Rift Basins: Geological Society Special Publication 80, p. 1-32.

Mosquera, A., 2002, Inversión tectónica Jurásico inferior en el sector central de la Dorsal de Huincul, área Los Bastos (CD-ROM): V Congreso de Exploración y Desarrollo de Hidrocarburos, Trabajos Técnicos, Instituto Argentino del Petróleo y del Gas, 11 p.

Mpodozis, C., and V. A. Ramos, 1990, The Andes of Chile and Argentina, *in* G. Ericksen, E., M. T. Cañas Pinochet, and J. A. Reinemund, eds., Geology of the Andes and its relation to hydrocarbon and mineral resources: Circum-Pacific Council for Energy and Mineral Resources, Earth Science Series, p. 59-90.

Nadin, P. A., N. J. Kusznir, and J. Toth, 1995, Transient regional uplift in the Early Tertiary of the northern North Sea and the development of the Iceland Plume: Journal of the Geological Society, v. 152, p. 953-958.

Nalpas, T., S. Le Douaran, J.-P. Brun, P. Unternehr, and J.-P. Richert, 1995, Inversion of the Broad Fourteens Basin (offshore Netherlands), a small-scale model investigation: Sedimentary Geology, v. 95, p. 237-250.

Nielsen, S. B., and D. L. Hansen, 2000, Physical explanation of the formation and evolution of inversion zones and marginal troughs: Geology, v. 28, p. 875-878.

Nürnberg, D., and R. D. Müller, 1991, The tectonic evolution of the South Atlantic from Late Jurassic to present: Tectonophysics, v. 191, p. 27-53.

Olson, C., 2001, Timing and tectonic implications of basin inversion in the Nam Con Son Basin and adjacent areas, southern South China Sea: M.S. thesis, Texas A&M University, College Station, TX, 176 p.

Orchuela, I. A., and V. J. Ploszkiewicz, 1984, La Cuenca Neuquina, *in* V. A. Ramos, ed., Geología y Recursos Naturales de Río Negro, IX Congreso Geológico Argentino, Relatorio, p. 163-183.

Orchuela, I. A., V. J. Ploszkiewicz, and R. F. Viñes, 1981, Reinterpretación estructural de la denominada "Dorsal Neuquina": VII Congreso Geológico Argentino, Actas v. 3, p. 281-293.

Pando, G. A., S. G. Del Vó, G. Laffitte, and M. Arguijo, 1984, Posibilidades oleogenéticas, migración y entrampamiento en las sedimentitas Jurásicas (Lias-Dogger) de la región centro-meridional de la Cuenca Neuquina: IX Congreso Geológico Argentino, Actas v. 7, p. 52-67.

Pángaro, F., and P. Bruveris, 1999, Reactivación tectónica multiepisódica de sistemas extensionales, Cuenca Neuquina, Argentina: XIV Congreso Geológico Argentino, Actas v. 1, p. 231-234.

Peroni, G. O., A. Hegedus, J. J. Cerdan, L. Legarreta, M. A. Uliana, and G. A. Laffitte, 1995, Hydrocarbon Accumulation in an Inverted Segment of the Andean Foreland: San Bernardo Belt, Central Patagonia, *in* A. J. Tankard, R. Suárez S., and H. J. Welsink, eds., Petroleum Basins of South America, v. AAPG Memoir 62, p. 403-419.

Platt, J. P., and P. C. England, 1993, Convective removal of lithosphere beneath mountain belts: thermal and mechanical consequences: American Journal of Science, v. 293, p. 307-336.

Ploszkiewicz, J. V., I. A. Orchuela, J. C. Vaillard, and R. F. Vines, 1984, Compresión y desplazamiento lateral en la Zona de Falla Huincul, estructuras asociadas, Provincia del Neuquén: IX Congreso Geológico Argentino, Actas v.2, p. 163-169.

Poblet, J., K. McClay, F. Storti, and J. A. Munoz, 1997, Geometries of syntectonic sediments associated with single-layer detachment folds: Journal of Structural Geology, v. 19, p. 369-381.

Rabinowitz, P. D., and J. L. LaBrecque, 1979, The Mesozoic South Atlantic Ocean and evolution of its continental margins: Journal of Geophysical Research, v. 84, p. 5973-6002.

Ramos, V. A., 1978, Estructura, *in* E. O. Rolleri, ed., Geología y recursos naturales del Neuquén: Relatorio VII Congreso Geológico Argentino: Buenos Aires, Argentina, p. 99-118.

Ramos, V. A., 1988, Late Proterozoic-Early Paleozoic of South America - A collisional history: Episodes, v. 11, p. 168-174.

Ramos, V. A., and A. Aleman, 2000, Tectonic Evolution of the Andes, *in* U. G. Cordani, E. J. Milani, A. Thomaz Filho, and D. A. Campos, eds., Tectonic Evolution of South America, 31st International Geological Congress: Rio de Janeiro, Brazil, p. 635-685.

Rapela, C. W., 1997, El sistema de fallas de Gastre: e pur si muove: Asociación Geológica Argentina, Revista, v. 52, p. 219-222.

Rapela, C. W., G. F. Dias, J. R. Franzese, G. Alonso, and A. R. Benvenuto, 1991, El Batolito de la Patagonia central; evidencias de un magmatismo Triásico-Jurásico asociado a fallas transcurrentes: Revista Geológica de Chile, v. 18, p. 121-138.

Rapela, C. W., and R. J. Pankhurst, 1992, The granites of northern Patagonia and the Gastre Fault System in relation to the break-up of Gondwana, *in* B. C. Storey, T. Alabaster, and R. J. Pankhurst, eds., Magmatism and the causes of continental break-up: Geological Society Special Publication 68, p. 209-220.

Riba, O., 1976, Syntectonic unconformities of the Alto Cardener, Spanish Pyrenees: a genetic interpretation: Sedimentary Geology, v. 15, p. 213-233.

Rodríguez, J. F. R., and R. Littke, 2001, Petroleum generation and accumulation in the Golfo San Jorge Basin, Argentina: a basin modeling study: Marine and Petroleum Geology, v. 18, p. 995-1028.

Roure, F., J.-P. Brun, B. Colletta, and J. Van Den Driessche, 1992, Geometry and kinematics of extensional structures in the alpine foreland basin of southeastern France: Journal of Structural Geology, v. 14, p. 503-519.

Salvini, F., and F. Storti, 2002, Three-dimensional architecture of growth strata associated to fault-bend, fault-propagation, and decollement anticlines in non-erosional environments: Sedimentary Geology, v. 146, p. 57-73.

Sandiford, M., 1999, Mechanics of basin inversion: Tectonophysics, v. 305, p. 109-120.

Sandiford, M., S. Frederiksen, and J. Braun, 2003, The long-term thermal consequences of rifting: implications for basin reactivation: Basin Research, v. 15, p. 23-43.

Schiuma, M., C. Saavedra, P. Malone, M. Cevallos, L. Rebori, and G. Vergani, 2002, Cuenca Neuquina. Los Reservorios del Grupo Lotena, Rocas Reservorio de las Cuencas Productivas de la Argentina, Instituto Argentino del Petróleo y del Gas, p. 314-320.

Schlische, R. W., and M. H. Anders, 1996, Stratigraphic effects and tectonic implications of the growth of normal faults and extensional basins, *in* K. K. Beratan, ed., Reconstructing the history of Basin and Range extension using sedimentology and stratigraphy: Geological Society of America Special Paper 303, p. 183-203.

Schmidt, C. J., R. A. Astini, C. H. Costa, C. E. Gardini, and P. E. Kraemer, 1995, Cretaceous rifting, alluvial fan sedimentation, and Neogene inversion, Southern Sierras Pampeanas, Argentina, *in* A. J. Tankard, R. Suárez S., and H. J. Welsink, eds., Petroleum basins of South America: AAPG Memoir 62, p. 341-358.

Scott, D. L., J. Braun, and M. A. Etheridge, 1994, Dip analysis as a tool for estimating regional kinematics in extensional terranes: Journal of Structural Geology, v. 16, p. 393-401.

Scott, D. L., M. A. Etheridge, and B. R. Rosendahl, 1992, Oblique-slip deformation in extensional terranes: a case study from the Lakes Tanganyika and Malawi rift zones, East Africa: Tectonics, v. 11, p. 998-1009.

Shaw, J. H., E. Novoa, and C. D. Connors, 2004, Structural controls on growth stratigraphy in contractional fault-related folds, *in* K. R. McClay, ed., Thrust tectonics and hydrocarbon systems: AAPG Memoir 82, p. 400-412.

Sibson, R. H., 1985, A note on fault reactivation: Journal of Structural Geology, v. 7, p. 751-754.

Sibson, R. H., 1990, Rupture nucleation on unfavorably oriented faults: Bulletin of the Seismological Society of America, v. 80, p. 1580-1604.

Sibson, R. H., 1995, Selective fault reactivation during basin inversion: potential for fluid redistribution through fault-valve action, *in* J. G. Buchanan, and P. G. Buchanan, eds., Basin Inversion: Geological Society Special Publication 88, p. 3-19.

Sibson, R. H., and G. Xie, 1998, Dip range for intracontinental reverse fault ruptures: Truth not stranger than friction?: Bulletin of the Seismological Society of America, v. 88, p. 1014-1022.

Smith, W. H. F., and D. T. Sandwell, 1997, Global seafloor topography from satellite altimetry. World Wide Web electronic publication. http://topex.ucsd.edu/www_html/mar_topo.html [accessed 10 April 2003].

Song, T., 1997, Inversion styles in the Songliao basin (northeast China) and estimation of the degree of inversion: Tectonophysics, v. 283, p. 173-188.

Storti, F., and J. Poblet, 1997, Growth stratal architectures associated to decollement folds and fault-propagation folds. Inferences on fold kinematics: Tectonophysics, v. 282, p. 353-373.

Strayer, L. M., S. G. Erickson, and J. Suppe, 2004, Influence of growth strata on the evolution of fault-related folds - distinct-element models, *in* K. R. McClay, ed., Thrust tectonics and hydrocarbon systems: AAPG Memoir 82, p. 413-437.

Suero, T., 1951, Descripción geológica de la Hoja 36c, Cerro Lotena (Provincia del Neuquén): Dirección Nacional de Minería, Buenos Aires, Boletín, v. 76, 1-91 p.

Suppe, J., G. T. Chou, and S. C. Hook, 1992, Rates of folding and faulting determined from growth strata, *in* K. McClay, ed., Thrust Tectonics: London, Chapman & Hall, p. 105-121.

Suppe, J., and A. Medwedeff, 1990, Geometry and kinematics of fault-propagation folding: Eclogae geologicae Helvetiae, v. 83, p. 409-454.

Tankard, A. J., M. A. Uliana, H. J. Welsink, V. A. Ramos, M. Turic, A. B. Franca, E. J. Milani, B. B. de Brito Neves, N. Eyles, J. Skarmeta, H. Santa Ana, F. Wiens, M. Cibrián, O. López Paulsen, G. J. B. Germs, M. J. De Wit, T. Machacha, and R. M. Miller, 1995, Structural and tectonic controls of basin evolution in Southwestern Gondwana during the Phanerozoic, *in* A. J. Tankard, R. Suárez S., and H. J. Welsink, eds., Petroleum basins of South America: AAPG Memoir 62, p. 5-52.

Thomas, D. W., and M. P. Coward, 1995, Late Jurassic-Early Cretaceous inversion in the northern East Shetland Basin, northern North Sea, *in* J. G. Buchanan, and P. G. Buchanan, eds., Basin inversion: Geological Society Special Publication 88: London, UK, p. 275-306.

Thomson, K., 1998, When did the Falklands rotate?: Marine and Petroleum Geology, v. 15, p. 723-736.

Turner, J. C. M., and B. A. J. Baldis, 1978, La estructura transcontinental del limite septentrional de la Patagonia: VII Congreso Geológico Argentino, Actas v. 2, p. 225-238.

Turner, J. P., and G. A. Williams, 2004, Sedimentary basin inversion and intra-plate shortening: Earth-Science Reviews, v. 65, p. 277-304.

Uliana, M. A., M. E. Arteaga, L. Legarreta, J. J. Cerdan, and G. O. Peroni, 1995, Inversion structures and hydrocarbon occurrence in Argentina, *in* J. G. Buchanan, and P. G. Buchanan, eds., Basin inversion: Geological Society Special Publication 88, p. 211-233.

Uliana, M. A., K. T. Biddle, and J. Cerdan, 1989, Mesozoic extension and the formation of Argentine sedimentary basins, *in* A. J. Tankard, and H. R. Balkwill, eds., Extensional tectonics and stratigraphy of the North Atlantic margins: AAPG Memoir 46, p. 599-614.

Uliana, M. A., D. A. Dellapé, and G. A. Pando, 1975, Estratigrafía de las sedimentitas rayosianas (Cretácico inferior de las Provincias de Neuquén y Mendoza): II Congreso Ibero-Americano de geología económica. La geología en el desarrollo de los pueblos. Actas v. 1, p. 177-196.

Uliana, M. A., and L. Legarreta, 1993, Hydrocarbons habitat in a Triassic-to-Cretaceous sub-Andean setting; Neuquén Basin, Argentina: Journal of Petroleum Geology, v. 16, p. 397-420.

Unternehr, P., D. Curie, J. L. Olivet, J. Goslin, and P. Beuzart, 1988, South Atlantic fits and intraplate boundaries in Africa and South America: Tectonophysics, v. 155, p. 169-179.

Urien, C. M., and J. J. Zambrano, 1994, Petroleum systems in the Neuquén Basin, Argentina, *in* L. B. Magoon, and W. G. Dow, eds., The petroleum system - from source to trap: AAPG Memoir 60, p. 513-534.

Urien, C. M., J. J. Zambrano, and M. R. Yrigoyen, 1995, Petroleum basins of southern South America: An Overview, *in* A. J. Tankard, R. Suárez S., and H. J. Welsink, eds., Petroleum basins of southern South America: AAPG Memoir 62, p. 63-77.

van der Beek, P., B. Champel, and J.-L. Mugnier, 2002, Control of detachment dip on drainage development in regions of active fault-propagation folding: Geology, v. 30, p. 471-474.

van Wees, J. D., and F. Beekman, 2000, Lithosphere rheology during intraplate basin extension and inversion: Inferences from automated modeling of four basins in western Europe: Tectonophysics, v. 320, p. 219-242.

Vanbrabant, Y., J. Braun, and D. Jongmans, 2002, Models of passive margin inversion: implications for the Rhenohercynian fold-and-thrust belt, Belgium and Germany: Earth and Planetary Science Letters, v. 202, p. 15-29.

Veiga, R., 2002, Migración de hidrocarburos y sistemas petroleros cuyanos en el ámbito central de la cuenca Neuquina - Argentina (CD-ROM): V Congreso de Exploración y Desarrollo de Hidrocarburos, Trabajos Técnicos, Instituto Argentino del Petróleo y del Gas, 20 p.

Vergani, G. D., A. J. Tankard, H. J. Belotti, and H. J. Welsink, 1995, Tectonic evolution and paleogeography of the Neuquén Basin, Argentina, *in* A. J. Tankard, R. S. Soruco, and H. J. Welsink, eds., Petroleum basins of South America: AAPG Memoir 62, p. 383-402.

Verzi, H., M. Fernández, H. Maretto, and J. J. Hechem, 2002, Miembro inferior de la Formación Quintuco, análisis sismoestratigráfico. Loma la Lata, Neuquén, Argentina (CD-ROM): V Congreso de Exploración y Desarrollo de Hidrocarburos, Trabajos Técnicos, Instituto Argentino del Petróleo y del Gas, 6 p.

Ware, P. D., and J. P. Turner, 2002, Sonic velocity analysis of the Tertiary denudation of the Irish Sea basin, *in* A. G. Doré, J. A. Cartwright, M. S. Stoker, J. P. Turner, and N. White, eds., Exhumation of the North Atlantic margin: Timing, mechanisms and implications for petroleum exploration: Geological Society Special Publications 196, p. 355-370.

Welsink, H. J., E. Martinez, O. Aranibar, and J. Jarandilla, 1995, Structural inversion of a Cretaceous rift basin, Southern Altiplano, Bolivia, *in* A. J. Tankard, R. Suárez S., and H. J. Welsink, eds., Petroleum basins of South America: AAPG Memoir 62, p. 305-324.

Williams, G. D., C. M. Powell, and M. A. Cooper, 1989, Geometry and kinematics of inversion tectonics, *in* M. A. Cooper, and G. D. Williams, eds., Inversion Tectonics: Geological Society Special Publication 44, v. 44, p. 3-15.

Windhausen, A., 1914, Contribución al conocimiento geológico de los territorios del Río Negro y Neuquén, con su estudio de la región petrolífera de la parte central del

Neuquén, Ministerio de Agricultura, Sección Geología, Mineralogía y Minería, Anales, v. 10: Buenos Aires, p. 1-60.

Withjack, M. O., and E. T. Peterson, 1993, Prediction of normal-fault geometries - A sensitivity analysis: AAPG Bulletin, v. 77, p. 1860-1873.

Woodward, N. B., S. E. Boyer, and J. Suppe, 1989, Balanced geological cross-sections: An essential technique in geological research and exploration: Short Course in Geology, v. 6: Washington, DC, American Geophysical Union, 128 p.

Yamada, Y., and K. McClay, 2003a, Application of geometric models to inverted listric fault systems in sandbox experiments. Paper 1: 2D hanging wall deformation and section restoration: Journal of Structural Geology, v. 25, p. 1551-1560.

Yamada, Y., and K. McClay, 2003b, Application of geometric models to inverted listric fault systems in sandbox experiments. Paper 2: insights for possible along strike migration of material during 3D hanging wall deformation: Journal of Structural Geology, v. 25, p. 1331-1336.

Yamada, Y., and K. R. McClay, 2004, 3-D Analog modeling of inversion thrust structures, *in* K. R. McClay, ed., Thrust tectonics and hydrocarbon systems: AAPG Memoir 82, p. 276-301.

Yang, K.-M., and S. L. Dorobek, 1995, The Permian Basin of West Texas and New Mexico: Tectonic history of a "composite" foreland basin and its effects on stratigraphic development, *in* S. L. Dorobek, and G. M. Ross, eds., Stratigraphic Evolution of Foreland Basins: SEPM Special Publication 52, p. 149-174.

Ye, H., L. H. Royden, B. C. Burchfiel, and M. Schuepbach, 1996, Late Paleozoic deformation of interior North America: The Greater Ancestral Rocky Mountains: AAPG Bulletin, v. 80, p. 1397-1432.

Yrigoyen, M. R., A. Ortiz, and R. Manoni, 1989, Cuencas Sedimentarias de San Luis, *in* G. A. Chebli, and L. A. Spalletti, eds., Simposio Cuencas Sedimentarias Argentinas. X Congreso Geológico Argentino, Serie Correlación Geológica v. 6, p. 203-219.

Zalán, P. V., S. Wolff, M. A. M. Astolfi, I. S. Vieira, J. C. J. Concelção, V. T. Appi, E. V. S. Neto, J. R. Cerqueira, and A. Marques, 1990, The Paraná Basin, Brazil, *in* M. W. Leighton, D. R. Kolata, D. F. Otlz, and J. J. Eidel, eds., Interior Cratonic Basins: AAPG Memoir 51, p. 681-708.

Zavala, C., 1996, High-resolution sequence stratigraphy in the Middle Jurassic Cuyo Group, South Neuquén Basin, Argentina, *in* A. C. Riccardi, ed., Advances in Jurassic research: GeoResearch Forum, v. 1-2, p. 295-304.

Zavala, C., 2002, El contacto entre los grupos Cuyo y Lotena (Jurásico) en la Sierra de la Vaca Muerta. Cuenca Neuquina, Argentina.: XV Congreso Geológico Argentino, Actas v.1, p. 711-715.

Zavala, C., and H. Freije, 2002, Cuñas clásticas Jurásicas vinculadas a la Dorsal de Huincul. Un ejemplo del área de Picún Leufú. Cuenca Neuquina, Argentina (CD-ROM). V Congreso de Exploración y Desarrollo de Hidrocarburos, Trabajos Técnicos, Instituto Argentino del Petróleo y del Gas, 14 p.

Ziegler, P. A., 1987, Late Cretaceous and Cenozoic intra-plate compressional deformations in the Alpine foreland--a geodynamic model: Tectonophysics, v. 137, p. 389-420.

Ziegler, P. A., 1989, Geodynamic model for Alpine intra-plate compressional deformation in Western and Central Europe, *in* M. A. Cooper, and G. D. Williams, eds., Inversion Tectonics: Geological Society Special Publication 44, p. 63-85.

Ziegler, P. A., S. Cloetingh, and J.-D. van Wees, 1995, Dynamics of intra-plate compressional deformation: the Alpine foreland and other examples: Tectonophysics, v. 252, p. 7-59.

Ziegler, P. A., J.-D. van Wees, and S. Cloetingh, 1998, Mechanical controls on collision-related compressional intraplate deformation: Tectonophysics, v. 300, p. 103-129.

Zilli, N., I. Orchuela, D. Dellapé, and R. Otano, 1979, Análisis de las formaciones Quintuco y Loma Montosa en el sector centro oriental de la cuenca Neuquina: VII Congreso Geológico Argentino, Actas v.1, p. 609-615.

VITA

GABRIEL ORLANDO GRIMALDI CASTRO

Born: June 26, 1965, Buenos Aires, Argentina

gabrielgrimaldi@gmail.com

Currently at: Chevron Corporation
Energy Technology Company
1500 Louisiana St.
Houston, TX 77002

Education

Universidad Nacional de Córdoba, Argentina, B.S., Geology, 1989
Texas A&M University, College Station, TX, USA, M.S., Geology, 1999
Texas A&M University, College Station, TX, USA, Ph.D., Geology, 2005

Professional experience

BP America Production Company, Houston, TX
Summer Intern, 2003

ChevronTexaco Exploration & Production Technology Co., San Ramon, CA
Summer Intern, 2002

Texas A&M University, Dept. of Geology & Geophysics, College Station, TX
Teaching Assistant, 2001-2004

Natural Survey Consulting S.A., Buenos Aires, Argentina
Environmental Consultant, 1999-2000

National Secretariat of Energy, Buenos Aires, Argentina
Environmental Advisor, 1995-1996

Roggio S.A., Buenos Aires, Argentina
Staff Geologist, 1991-1995